OCT 11 1957
UNIVERSITY OF MICHIGAN
OCT 1957
PHYSICS LIBRARY

Journal of Research

of the

National Bureau of Standards

SEPTEMBER 1957

VOLUME 59 NUMBER 3

U. S. DEPARTMENT OF COMMERCE
Sinclair Weeks, Secretary
NATIONAL BUREAU OF STANDARDS
A. V. Astin, Director

SEPTEMBER • 1957
VOLUME • 59
NUMBER • 3

JOURNAL OF RESEARCH
of the
NATIONAL BUREAU OF STANDARDS

The National Bureau of Standards

Functions and Activities

The functions of the National Bureau of Standards are set forth in the Act of Congress, March 3, 1901, as amended by Congress in Public Law 619, 1950. These include the development and maintenance of the national standards of measurement and the provision of means and methods for making measurements consistent with these standards; the determination of physical constants and properties of materials; the development of methods and instruments for testing materials, devices, and structures; advisory services to Government Agencies on scientific and technical problems; invention and development of devices to serve special needs of the Government; and the development of standard practices, codes, and specifications. The work includes basic and applied research, development, engineering, instrumentation, testing, evaluation, calibration services, and various consultation and information services. A major portion of the Bureau's work is performed for other Government Agencies, particularly the Department of Defense and the Atomic Energy Commission. The scope of activities is suggested by the listing of divisions and sections on the inside of the back cover.

Publications

The results of the Bureau's work take the form of either actual equipment and devices or published papers. These papers appear either in the Bureau's own series of publications or in the journals of professional and scientific societies. The Bureau itself publishes three monthly periodicals, available from the Government Printing Office: The Journal of Research, which presents complete papers reporting technical investigations; the Technical News Bulletin, which presents summary and preliminary reports on work in progress; and Basic Radio Propagation Predictions, which provides data for determining the best frequencies to use for radio communications throughout the world. There are also five series of nonperiodical publications: The Applied Mathematics Series, Circulars, Handbooks, Building Materials and Structures Reports, and Miscellaneous Publications.

Information on the Bureau's publications can be found in NBS Circular 460, Publications of the National Bureau of Standards ($1.25) and its Supplement ($0.75), available from the Superintendent of Documents, Government Printing Office, Washington 25, D. C.

Order all publications from the Superintendent of Documents
U. S. Government Printing Office, Washington 25, D. C.

The use of funds for printing this publication approved by the Director of the Bureau of the Budget (May 4, 1956).

Journal of Research of the National Bureau of Standards Vol. 59, No. 3, September 1957 Research Paper 2783

A Computation of Cyclic Cubic Units[1]

Harvey Cohn and Saul Gorn[2]

The paper is a report on a tabulation of units performed on the EDVAC at the U. S. Army Proving Grounds in Aberdeen, Maryland. The algebraic number fields involved were 45 cyclic cubic fields of discriminant l^2, where l is one of the primes of form $3m+1$ from 7 through 499. The object of the search was the discovery of units through a specific method, an algorithm based on Minkowski's geometric number theory but particularly amenable to a stored-program computer. In the computation, combined use was made of integral arithmetic and decimal arithmetic but with careful error analysis.

1. Introduction

An essential part of the lure of algebraic number theory consists of tabulations of almost unpredictable irregularity. The advanced theory has somehow surpassed the scope of numerical data without perceptibly improving the power to predict such data. As a result, for a small calculation an algebraic number theorist would not forego the personal satisfaction that results from the many ingenious, fortuitous, and deeply meaningful combinations of integers that he would encounter. Yet to really appreciate these vital irregularities he needs longer tabulations, with the inevitable requirements of uniformity and efficiency. Here the modern electronic digital computer can be used profitably.

The discussion of the problem that follows will be primarily from the point of view of the computer program rather than from its theoretical development. Thus, for instance, the field will have to be regarded not as a set of elements satisfying certain axioms, etc., in the manner of Dedekind and Steinitz, but as an algebra with a definite basis and definite "structure constants" for multiplications. As a matter of historical fact the exhibiting of a basis was generally far from trivial and lagged considerably behind existence theorems [*1*, *10*][3]

2. Description of Fields

For any prime $l(=3m+1)$ a cyclic cubic field will be defined. Our interest centers around *algebraic integers* of such a field, written as follows (owing to the presence of the so-called normal basis):

$$\xi=a\omega_1+b\omega_2+c\omega_3=(a,b,c). \tag{1}$$

Here a, b, c are rational integers (or coordinates), and ω_1, ω_2, ω_3 (or the normal basis) are the three roots of the defining (normal) equation [*8*].

$$F(\omega)=\omega^3+\omega^2-m\omega-n=0. \tag{2}$$

Here n is defined as follows: First, $4l$ is decomposed (uniquely) into the combination

$$4l=A^2+27g^2, \tag{3}$$

where the signs of A and g are specified by the conditions (in integral k)

$$A=3k+1, \qquad g>0. \tag{4a}$$

---

[1] The computing time was provided under contract DA-028-ORD-12332 with the United States Army Office of Ordnance Research. The first named author was then at Wayne University, Detroit, Mich., and the second named author was at the Ballistics Research Laboratory, Aberdeen, Md. The first named author is currently at Washington University, St. Louis, Mo.

The preliminary report (reference [*5*]), was cleared for publication by the Ballistics Research Laboratory on April 26, 1956. The background description, the illustrative examples, and the final tabulation were prepared at the National Bureau of Standards. This work has formed the basis for a further calculation currently on the SEAC.

[2] Now at Moore School of Electrical Engineering, Philadelphia, Pa.

[3] Italicized figures in brackets indicate the literature references at the end of this paper.

Then, finally an integer n always exists, for which

$$27n=(A+3)l-1. \tag{4b}$$

All algebraic integers under discussion are *real*.

The most general *basis* of the field would be given by an integral unimodular combination $\zeta_i=\sum a_{ij}\omega_j \quad i,j=1,2,3$, $\det|a_{ij}|=\pm 1$. There is essentially no other basis [9].

The particular designation of roots is standardized as

$$\omega_1>\omega_2>\omega_3. \tag{5}$$

Thus we can distinguish among conjugates ξ (given above), and ξ', ξ'' given by

$$\xi'=c\omega_1+a\omega_2+b\omega_3=(c,a,b) \tag{6a}$$

$$\xi''=b\omega_1+c\omega_2+a\omega_3=(b,c,a) \tag{6b}$$

(formed by cyclic permutation of ω_1, ω_2, ω_3), so that $\xi'''=\xi$, etc. As a matter of notation, the subscripts denote conjugates only in reference to the basis ω_i. Later on ξ_i shall denote (unrelated) integers of the field.

It was mentioned earlier that the discriminant of the field or the determinant

$$\begin{vmatrix} \omega_1 & \omega_2 & \omega_3 \\ \omega_2 & \omega_3 & \omega_1 \\ \omega_3 & \omega_1 & \omega_2 \end{vmatrix}^2 \tag{7}$$

has the value l^2. This fact (which can be verified directly from eq (1)) is not used directly in the machine computation but uniquely identifies the field in question [6].

The multiplication of any two numbers in the field can be expressed in integral arithmetic; e. g.,

$$\xi_1=(a_1,b_1,c_1), \qquad \xi_2=(a_2,b_2,c_2), \tag{8}$$

then one can find the explicit representation of $\xi_1\xi_2$ in terms of the normal basis by means of the structure constants α_1, β_1, γ_1, α_2, β_2, γ_2, defined by

$$\omega_1^2=\alpha_1\omega_1+\beta_1\omega_2+\gamma_1\omega_3$$

and

$$\omega_2\omega_3=\alpha_2\omega_1+\beta_2\omega_2+\gamma_2\omega_3.$$

The explicit formula is, then, e. g.,

$$\xi_1\xi_2=(A,B,C), \tag{9a}$$

where

$$\left.\begin{aligned} A&=\alpha_1a_1a_2+\gamma_1b_1b_2+\beta_1c_1c_2+\beta_2(a_1b_2+a_2b_1)+\alpha_2(b_1c_2+b_2c_1)+\gamma_2(c_1a_2+c_2a_1),\\ B&=\beta_1a_1a_2+\alpha_1b_1b_2+\gamma_1c_1c_2+\gamma_2(a_1b_2+a_2b_1)+\beta_2(b_1c_2+b_2c_1)+\alpha_2(c_1a_2+c_2a_1),\\ C&=\gamma_1a_1a_2+\beta_1b_1b_2+\alpha_1c_1c_2+\alpha_2(a_1b_2+a_2b_1)+\gamma_2(b_1c_2+b_2c_1)+\beta_2(c_1a_2+c_2a_1). \end{aligned}\right\} \tag{9b}$$

This product can therefore be computed in the following tabular form:

a_1a_2	α_1	β_1	γ_1
b_1b_2	γ_1	α_1	β_1
c_1c_2	β_1	γ_1	α_1
$a_1b_2+a_2b_1$	β_2	γ_2	α_2
$b_1c_2+b_2c_1$	α_2	β_2	γ_2
$c_1a_2+a_1c_2$	γ_2	α_2	β_2
	$(A$	B	$C).$

These structure constants are given explicitly by the formulas:

$$\left.\begin{aligned} \alpha_2&=\frac{m+k+1}{3}, & \beta_2&=\frac{g+m-\alpha_2}{2}, & \gamma_2&=\frac{-g+m-\alpha_2}{2},\\ \alpha_1&=\alpha_2-m+1, & \beta_1&=\frac{g-m-\alpha_2}{2}, & \gamma_1&=\frac{-g-m-\alpha_2}{2}. \end{aligned}\right\} \tag{9c}$$

They are listed in table 2 (see p. 166).

In particular, the norm of ξ is defined for (1) by the integer

$$N(\xi)=\xi\xi'\xi''=-n(a+b+c)^3-l\{(k-g+1)\Sigma a^2b/2+(k+g+1)\Sigma ab^2/2+abc\}, \tag{10a}$$

and the trace is defined by

$$t(\xi)=\xi+\xi'+\xi''=-(a+b+c), \tag{10b}$$

so that the defining equation of ξ, ξ', or ξ'' is

$$\xi^3-t(\xi)\xi^2+\tilde{t}(\xi\xi')\xi-N(\xi)=0, \tag{10}$$

with the further designation

$$\tilde{t}(\xi)=t(\xi\xi')=-m(a+b+c)^2+l\Sigma ab. \tag{10c}$$

Note that if $a+b+c=0$, then $N(\xi)$ is divisible by l. Thus, applying this information to

$$\xi-\xi'=((a-c),(b-c),(c-a)),$$

we find $N(\xi-\xi')=(\xi-\xi')(\xi'-\xi'')(\xi''-\xi)$ is an integer divisible by l.

3. Units

Units are algebraic integers of norm equal to ± 1. They are written as

$$\eta=u_1\omega_1+u_2\omega_2+u_3\omega_3=(u_1,u_2,u_3), \tag{11}$$

where, as before, u_1, u_2, u_3 are integers. The most general unit has the form $\pm\eta_o^a\eta_o'^b$, where a and b are (positive, negative, or zero) integers, whereas η_0 is a specially designated *fundamental* unit [6, p. 19]. The only *fundamental* units are $\pm\eta_o^{\pm 1}$, $\pm(\eta_o')^{\pm 1}$, $\pm(\eta_o'')^{\pm 1}$. In what follows, units will be normalized (by a change of sign) to have, conveniently, only norm $+1$.

If we take eq (10a) and set $N(\xi)=1$ and $(a,b,c)=(u_1,u_2,u_3)$, we obtain a cubic equation in these three latter unknowns, which we are in effect solving. Now such an equation (unlike, say, the Pell equation), has very little intrinsic interest. The interest in units is derived entirely from their role in *unique factorization*.

To give an example, when $l=19$, one finds (as a byproduct of the main calculation) that

$$N(\omega_1)=N(2\omega_1-\omega_2)=7. \tag{12}$$

This does *not* mean that 7 has two different factorizations, although seemingly

$$7=\omega_1\omega_2\omega_3=(2\omega_1-\omega_2)(2\omega_2-\omega_3)(2\omega_3-\omega_1). \tag{12a}$$

The reason, of course, is that the factors can pair off as *associates*, or

$$(2\omega_2-\omega_3)/\omega_1=(-\omega_1-2\omega_2), \tag{12b}$$

a unit of the field. To see this, in (12a) calling one set of factors ξ, ξ_1', ξ_1'' and the other ξ_2, ξ_2', ξ_2'', respectively, we must verify that one of the ratios ξ_2/ξ_1, ξ_2'/ξ_1, ξ_2''/ξ_1 is a unit. Thus for example, in accordance with the rules of section 2, we compute

$$\frac{\xi_2'}{\xi_1}=\frac{\xi_2'\xi_1'\xi_1''}{\xi_1\xi_1'\xi_1''}=\frac{(A^*,B^*,C^*)}{N(\xi_1)} \tag{13}$$

and find that A^*, B^*, and C^* are now divisible by $N(\xi_1)$. In practice, the whole computation would be performed modulo $N(\xi_1)(=7$ here), using the structure constants of table 2.

Thus the preliminary step in understanding factorization in fields becomes the recognition of units. Traditionally, one creates, by trial and error, combinations such as (12a), and one hunts for units, usually with better luck than one can completely explain [4].

The method used here will be very systematic. It is an algorithm for creating a surfeit of algebraic integers with small norms (including norm unity). In the process, a unit, indeed a fundamental unit, is inevitably produced. (Unfortunately, machine limitations forced the weakening of the method, as is explained in section 6.)

4. The Sign-Discrimination Algorithm

One operates with so-called *reduced* 3×4 matrices of algebraic integers [2, section 4]:

$$\phi=\begin{pmatrix}\xi_1 & \xi_2 & \xi_3 & \xi_4\\ \xi_1' & \xi_2' & \xi_3' & \xi_4'\\ \xi_1'' & \xi_2'' & \xi_3'' & \xi_4''\end{pmatrix}. \tag{14a}$$

The columns represent conjugates of algebraic integers of sum zero

$$\xi_1+\xi_2+\xi_3+\xi_4=0 \tag{14b}$$

and such that any three of the four ξ_i form a basis. The further, and most vital, condition is that the sign pattern be

$$\operatorname{sgn}\phi=\begin{pmatrix}+ & - & - & +\\ - & + & - & +\\ - & - & + & +\end{pmatrix} \tag{14c}$$

either as ϕ now stands or under some rearrangement of columns.

The algorithm is a method of generating such matrices in chains. A matrix ϕ_1 is said to be a *neighbor* of ϕ if it is formed by adding one column of ϕ to another column of ϕ and at the same time subtracting it from a third column of ϕ (the three columns being different). Thus there are 4! possibilities to consider corresponding to the distinct triples $(j_1j_2j_3)$, where $1\leq j\leq4$. For instance, the operation

$$\phi[341]\phi_1 \tag{15a}$$

can be understood to mean that the "third column of ϕ is increased by the fourth column, which in turn diminishes the first," or, writing just the first rows,

$$\left.\begin{aligned}\phi&=(\xi_1,\ \xi_2,\ \xi_3,\ \xi_4)\\ \phi_1&=(\xi_1-\xi_4,\ \xi_2,\ \xi_3+\xi_4,\ \xi_4).\end{aligned}\right\} \tag{15b}$$

(The relation (15a) can be read *backward* as an operation on ϕ_1.) Of the 4! possible neighbors, either 3, 4, 5, or 6 will be reduced, depending on inequalities satisfied by the elements [2, section 10].

We next define the conjugate ϕ' of a matrix ϕ to be the matrix formed by replacing the first row ξ_i by its conjugate ξ_i' and forming the remaining rows from ξ_i' instead of ξ_i. The conjugate ϕ' will not be reduced as it stands, but a rearrangement of the columns (in this case the interchange of first and second) will render it reduced. Likewise, we define ϕ''. Note $\phi'''=\phi$ again. Finally, two matrices ϕ_1 and ϕ_2 are said to be *proportional* to one another if, for $\phi_1^*=\phi_1$, ϕ_1', or ϕ_1'', and numbers η, η', η'',

$$\phi_2 = \begin{pmatrix} \eta & 0 & 0 \\ 0 & \eta' & 0 \\ 0 & 0 & \eta'' \end{pmatrix} \phi_1^* . \tag{16}$$

It is easily seen that η, η', η'' are necessarily the conjugates of a unit, possibly 1, having norm $+1$. (In some cases ϕ_1 is proportional to itself, leading to interesting possibilities related to ramified primes but beyond the scope of the present discussion [2, section 22].) In all cases, proportional matrices will have the same set of norms (possibly under rearrangement).

The algorithm operates as follows: The initial matrix is taken for convenience (writing only the first row) as

$$\phi_0 = (\omega_1, \omega_3, \omega_2, 1), \qquad n > 0, \tag{17a}$$

with norms respectively

$$(n, n, n, 1), \tag{17b}$$

or as

$$\phi_0 = (\omega_1 + \omega_2, \omega_3 + \omega_1, -\omega_1, 1) \qquad n < 0 \tag{17c}$$

with norms respectively

$$(-n+m, -n+m, -n, 1). \tag{17d}$$

Branching out from ϕ_0, one forms all reduced neighbors of matrices present, terminating a branch when the matrix is proportional to one already present. Indeed, the number of reduced matrices is finite to within proportionalities [2, section 8]. The factors of proportionality η are units among which can always be found the fundamental unit [2, section 18].

5. Modified Algorithm

The original algorithm, as just described, is a branching algorithm in which each ϕ may have more than one successor, and each ϕ is compared with all those preceding. Because each ϕ contains 12 components and there could be more than 50 produced, the internal storage of the EDVAC would be taxed before the algorithm had gone very far. The branching algorithm was therefore modified to a form in which only one successor is chosen for each ϕ, and the comparison (16) is always between ϕ_0 and the most recent ϕ.

The modification consisted in trying only one-third of the 4! possible neighbors, namely,

$$[123], [132], [423], [432], [214], [241], [314], [341] \tag{18}$$

characterized by the fact that the second and third indices are either 2,3 or 1,4 in some order. Either one or two neighbors of this type occur, but the EDVAC takes only the first that occurs in the program, thus we have a chain-type algorithm rather than a branching algorithm, with the further property that $\sum_1^4 |\xi_i|$ decreases at each step [2, section 17], whereas the corresponding sums for the second and third row (conjugates) increase or remain the same. This assures us that when the inevitable proportionality occurs, the unit will not be 1 (but it need not be a fundamental unit either).

As an illustration (see table 1) [4] the matrix sequence ϕ_i is reproduced for $l = 19$. It is

$\phi_0[241]$ $\phi_1[132]$ $\phi_2[314]$ $\phi_3[314]$ $\phi_4[314]$ $\phi_5[423]$ $\phi_6[341]$ $\phi_7[123]$ $\phi_8[123]$ $\phi_9[123]$ $\phi_{10}[432]$ $\phi_{11}[214]$ ϕ_{12}.

The EDVAC discovered that ϕ_0 is proportional to (some rearrangement of) ϕ_{12}. The specific numerical values are of some interest. We therefore calculate

[4] A full explanation of table 1 is given in section 7.

$$\omega_1 = \ \ 2.507\ 018\ 643$$
$$\omega_2 = -1.221\ 876\ 162$$
$$\omega_3 = -2.285\ 142\ 481,$$

which (except for minor modifications in section 7) is the accuracy presented by the EDVAC. Thus

$$\phi_0 = \quad ((1,0,0) \qquad (0,1,0) \qquad (0,0,1) \qquad (-1,-1,-1))$$

or

$$\phi_0 = \begin{pmatrix} 2.507\ 018\ 643 & -2.285\ 142\ 481 & -1.221\ 876\ 162 & 1 \\ -1.221\ 876\ 162 & 2.507\ 018\ 643 & -2.285\ 142\ 481 & 1 \\ -2.285\ 142\ 481 & -1.221\ 876\ 162 & 2.507\ 018\ 643 & 1 \end{pmatrix}$$

$$\phi_{12} = \quad ((7,5,5) \qquad (4,-3,6) \qquad (2,6,-1) \qquad (-13,-8,-10))$$

or

$$\phi_{12} = \begin{pmatrix} 0.014\ 037\ 286 & -0.017\ 151\ 828 & -0.032\ 077\ 205 & 0.035\ 191\ 747 \\ -7.443\ 752\ 324 & 17.010\ 034\ 653 & -18.661\ 625\ 853 & 9.095\ 343\ 524 \\ -9.570\ 284\ 962 & -23.992\ 882\ 825 & 11.693\ 703\ 058 & 21.869\ 464\ 729 \end{pmatrix}$$

The EDVAC then "recognized" that the first column would serve as a proportionality factor, i. e., if we rearrange the columns of ϕ_{12} to form

$$\phi_{12}^* = ((-13,-8,-10),\ (2,6,-1),\ (4,-3,6),\ (7,5,5)),$$

then

$$\phi_{12}^* = \begin{pmatrix} \eta & 0 & 0 \\ 0 & \eta' & 0 \\ 0 & 0 & \eta'' \end{pmatrix} \phi_0,$$

where $\eta = 0.014\ 037\ 286$, $\eta' = -7.443\ 752\ 34$, and $\eta'' = -9.570\ 284\ 962$. In this case the decimal accuracy would be easily sufficient for "recognition," but integral arithmetic was used (see section 8).

The unit produced, $\eta = (7,5,5)$, is not fundamental, but, early in the course of the computation, for ϕ_1, ξ_2 happened to come out as $\eta_0 = (-1,-1,0)$, a fundamental unit (see section 10). Actually,

$$\eta = (\eta_0'')^2/\eta_0'.$$

This can be easily verified from the multiplication scheme (9), e. g., $(\eta_0'')^2 = (-6,-3,-5)$, $(\eta_0')^{-1} = (2,2,1)$.

6. Numerical Accuracy

As the algorithm was first conceived and applied in experiment [2, section 11], decimal accuracy seemed sufficient because the symmetric functions could be correctly evaluated by the nearest integer when necessary. In a long computation, however, the algorithm can go astray in many ways:

(a) The algorithm may incorrectly discriminate the reduced neighbors from the others. This is bound to happen because the subset of the reduced neighbors chosen by the modified algorithm just mentioned has $\sum_1^4 |\xi_i|$ approaching zero monotonically. The error in the quantities ξ_i can soon be bigger than the quantities themselves, making a simple discrimination in sign untrustworthy.

(b) It may make uncertain the decision as to whether ϕ and ϕ^* are proportional; for example, it may have to be decided that (using an obvious notation), $\xi_1/\xi_1^* = \xi_2/\xi_2^* = \xi_3/\xi_3^* = \xi_4/\xi_4^*$, in which all the quantities involved are in error.

(c) It may of course make the approximations to the all-important resulting units untrustworthy; for these are the ratios discussed in (b).

A vital and desirable modification, to control the accuracy of the computations, consisted in carrying out all arithmetic operations exactly by using integral arithmetic; (explicit formulas for the integral arithmetic operations on two such integers are given in section 2). Furthermore, all quotients were removed from the algorithm (see section 8).

It would also have been quite easy in principle to have handled the sign discriminations in integral arithmetic. For instance, to tell if two algebraic numbers ξ_1 and ξ_2 agree in sign, all we need have done is test to see if the three conjugates $\xi_1\xi_2$, $\xi_1'\xi_2'$, and $\xi_1''\xi_2''$ are each positive (total positiveness), which, by Descartes' law of signs, is a matter of seeing that the defining eq (10) for $(\xi_1\xi_2)$ has (integral) coefficients with alternating sign. At the time, however, the EDVAC internal storage was not sufficient to handle the enormous integers, so that an automatic error analysis was used instead. This was the only departure from integral arithmetic.

7. Input-Output and Error Controls

With the exception of the following operations, the problem was run completely internally, with no human intervention:

(a) For each l, the structure constants in table 2 were computed in advance by hand (merely to save space in the memory) through the α_2 column. (The entire table is given for convenience of hand checking.)

(b) For each l, the zeros (and maximum errors) of the polynomial (2) were computed in advance by machine. The polynomial was scaled by dividing its zeros by m and carrying through the computation in fixed point. The root-finding method for the scaled polynomial,

$$f(\omega)=\left(\frac{\omega}{m}\right)^3+\frac{1}{m}\left(\frac{\omega}{m}\right)^2-\frac{1}{m}\left(\frac{\omega}{m}\right)-\frac{n}{m^3}, \tag{19}$$

is the bisection method (Horner's method in binary), for appropriate isolating intervals. The maximum error in the coefficients of the scaled polynomial, for EDVAC, is 2^{-44}, whence the maximum error in evaluating the scaled polynomial is 7×2^{-44}; if, then, we use $\epsilon=2^{-41}$, the machine will provide an automatic error analysis in solving for ω_i by finding the zeros r_i^+ of $f(\omega)+2\epsilon$, r_i^- of $f(\omega)-2\epsilon$, and setting

$$\frac{\omega_i}{m}=\frac{r_i^+ + r_i^-}{2}, \qquad \epsilon_1=\frac{r_i^+ - r_i^-}{2}.$$

Because the numerical values of the zeros ω_i are only used in the main algorithm to discriminate the signs of linear homogeneous expressions, $a\omega_1+b\omega_2+c\omega_3$, the scaled values ω_i/m and their error bounds ϵ_i were used directly.

(c) The input and output of the algorithm itself was by means of IBM cards, in decimal. (This required internal conversion on input and output because the EDVAC arithmetic is binary.) For each l two IBM cards were read in. One contained the integers l, m, g, α_2, n. The other contained the integer l together with the (10-digit) decimals ω_1/m, ω_2/m, ω_3/m, and the errors in ω_1, ω_2, ω_3.

The output cards were as follows: First, there were copies of the two input cards; second, for each ϕ_i, as soon as it was produced, four cards were punched with $j=1,2,3,4$, respectively, indicating the column of ϕ_i (prior to possible rearrangement) being described. The algebraic integer ξ_j was described by the integers l, i, j, a_j, b_j, c_j, $N(\xi)$, $t(\xi)$, $\bar{t}(\xi)$, where N, t, $\bar{t}$ refer to the defining eq (10) and

$$\xi_j=a_j\omega_1+b_j\omega_2+c_j\omega_3.$$

Third, there would be a card containing the integers (see (11)) l, i, $j(=5)$, u_1, u_2, u_j, $N(\xi)(=1)$, $t(\xi)$, $\bar{t}(\xi)$ if the algorithm runs to completion to produce a ϕ_i proportional to ϕ_0 with factor η.

TABLE 1. *Input-output cards*

The material in this table is presented in the form in which it is printed out by EDVAC.

INPUT CARDS									
Structure constants	l				m	g	k	α_2	n
	19				6	1	2	3	7
Roots and errors ($\times 10^{-10}$)	l			ω_1/m	ω_2/m	ω_3/m	Error ω_1/m	Error ω_2/m	Error ω_3/m
	19			4178364406	−2036460270	−3808570802	1	1	1

OUTPUT CARDS									
Matrix cards	l	Matrix number	Column number	$(\xi_i = a_i\omega_1 + b_i\omega_2 + c_i\omega_3)$			$N(\xi_i)$	$t(\xi_i)$	$\bar{t}(\xi_i)$
				a_i	b_i	c_i			
(ξ_1)	19	0	1	1	0	0	7	−1	−6
(ξ_2)	19	0	2	0	0	1	7	−1	−6
(ξ_3)	19	0	3	0	1	0	7	−1	−6
(ξ_4)	19	0	4	−1	−1	−1	1	3	3
(ξ_1)	19	1	1	2	1	1	11	−4	−1
(ξ_2)	19	1	2	−1	−1	0	1	2	−5
(ξ_3)	19	1	3	0	1	0	7	−1	−6
(ξ_4)	19	1	4	−1	−1	−1	1	3	3
(ξ_1)	19	2	1	2	2	1	1	−5	2
(ξ_2)	19	2	2	−1	−2	0	1	3	−16
(ξ_3)	19	2	3	0	1	0	7	−1	−6
(ξ_4)	19	2	4	−1	−1	−1	1	3	3
(ξ_1)	19	3	1	2	2	1	1	−5	2
(ξ_2)	19	3	2	−1	−2	0	1	3	−16
(ξ_3)	19	3	3	2	3	1	11	−6	−7
(ξ_4)	19	3	4	−3	−3	−2	7	8	15
(ξ_1)	19	4	1	2	2	1	1	−5	2
(ξ_2)	19	4	2	−1	−2	0	1	3	−16
(ξ_3)	19	4	3	4	5	2	7	−11	−4
(ξ_4)	19	4	4	−5	−5	−3	11	13	31
(ξ_1)	19	5	1	2	2	1	1	−5	2
(ξ_2)	19	5	2	−1	−2	0	1	3	−16
(ξ_3)	19	5	3	6	7	3	1	−16	3
(ξ_4)	19	5	4	−7	−7	−4	7	18	51
(ξ_1)	19	6	1	2	2	1	1	−5	2
(ξ_2)	19	6	2	−1	−2	0	1	3	−16
(ξ_3)	19	6	3	7	9	3	19	−19	−57
(ξ_4)	19	6	4	−8	−9	−4	1	21	14

TABLE 1. *Input-output cards*—Continued

OUTPUT CARDS—continued

Matrix cards	l	Matrix number	Column number	$(\xi_i = a_i\omega_1 + b_i\omega_2 + c_i\omega_3)$			$N(\xi_i)$	$t(\xi_i)$	$\bar{t}(\xi_i)$
				a_i	b_i	c_i			
(ξ_1)	19	7	1	10	11	5	7	−26	29
(ξ_2)	19	7	2	−1	−2	0	1	3	−16
(ξ_3)	19	7	3	−1	0	−1	1	2	−5
(ξ_4)	19	7	4	−8	−9	−4	1	21	14
(ξ_1)	19	8	1	9	9	5	11	−23	75
(ξ_2)	19	8	2	−1	−2	0	1	3	−16
(ξ_3)	19	8	3	0	2	−1	7	−1	−44
(ξ_4)	19	8	4	−8	−9	−4	1	21	14
(ξ_1)	19	9	1	8	7	5	7	−20	89
(ξ_2)	19	9	2	−1	−2	0	1	3	−16
(ξ_3)	19	9	3	1	4	−1	11	−4	−115
(ξ_4)	19	9	4	−8	−9	−4	1	21	14
(ξ_1)	19	10	1	7	5	5	1	−17	71
(ξ_2)	19	10	2	−1	−2	0	1	3	−16
(ξ_3)	19	10	3	2	6	−1	7	−7	−218
(ξ_4)	19	10	4	−8	−9	−4	1	21	14
(ξ_1)	19	11	1	7	5	5	1	−17	71
(ξ_2)	19	11	2	−3	−8	1	11	10	−353
(ξ_3)	19	11	3	2	6	−1	7	−7	−218
(ξ_4)	19	11	4	−6	−3	−5	1	14	21
(ξ_1)	19	12	1	7	5	5	1	−17	71
(ξ_2)	19	12	2	4	−3	6	7	−7	−408
(ξ_3)	19	12	3	2	6	−1	7	−7	−218
(ξ_4)	19	12	4	−13	−8	−10	7	31	200

Unit card	l	Matrix	Indicator	$(\eta = u_1\omega_1 + u_2\omega_2 + u_3\omega_3)$			$N(\eta)$	$t(\eta)$	$\bar{t}(\eta)$
				u_1	u_2	u_3			
	19	12	5	5	7	5	1	−17	71

The algorithm is then applied to the next case automatically. A complete set of input-output cards is listed in table 1 for $l = 19$.

On the other hand, *error controls* could stop a case (or the current value of l) before it has run to completion in the following ways:

(a) The first error control computes the numerical approximations to ξ_1, ξ_2, ξ_3, ξ_4 from their components a_j, b_j, c_j and values of ω_i. Thus the maximum error in $\xi_j = a_j\omega_1 + b_j\omega_2 + c_j\omega_3$ is $\epsilon = |a_j|\epsilon_1 + |b_j|\epsilon_2 + |c_j|\epsilon_3$, so that the (scaled) condition $\epsilon_i/m < \epsilon$ would mark the sign discrimination on ξ_i as untrustworthy. In this case an extra card was printed containing l, i, 5, ξ_1^*, ξ_2^*, ξ^*, ξ_4^*, with ξ_j^* being the numerical approximation. The computation proceeded to the next l automatically.

(b) The second error control checked each computed norm to stop the machine if any negative norms appeared or if any ϕ_t failed to have one of the eight neighbors (18). (None did.)

(c) The third error control checked the imminence of overflow by testing to see if the largest term appearing in the norm calculation, $n(a+b+c)^3$, becomes too large ($>2^{44}$) to fit in the registers. In case of this eventuality, the machine proceeded to the next case, printing no signal card. These controls required very little storage.

8. Neighbor Formation and Comparison

What remains is now to describe the portion of the program that is strictly internal, and which, by itself, would not come to the attention of the machine operator. The two main steps of the algorithm are neighbor formation and comparison.

The neighbor formation consists of the formation of ϕ_{t+1} from ϕ_t and, ultimately, the replacement of ϕ_t by ϕ_{t+1}. Here, essentially, each neighbor operation of type (18) was tried in succession on ϕ_t, and the sign discriminations were made to test if the pattern (14c) were valid. Here the numerical estimates were kept in double precision, the integral and fractional parts being stored separately (each consisting of at most about 13 decimal digits).

The comparison of ϕ_0 and ϕ_t is more complex. First of all, the cases $l=7$ and 13 were excluded by virtue of the fact that $|n|=1$ (so that $+\omega_1$ or $-\omega_1$ is a unit anyway). In the other cases ($l\geq 19$), the set of norms in ω_0 (see eq (17b,d)) contains exactly one norm of value 1. Thus a ϕ_t is not conceivably proportional to ϕ_1 unless some column in ϕ_t is a unit (say) η. A further necessary condition is that all the norms in ϕ_t match those of ϕ_0. When this was satisfied the machine multiplied the top row of ϕ_0 by η, η', and η'', in turn (using (9a,b)) testing at each stage to see if ϕ_t or a conjugate was obtained. (In this last step, the possible column rearrangements are fewer if there is only one norm in ϕ_0 equal to 1.)

It is seen that the machine part of the algorithm at no time involved division (even such minor calculations as division by 2 were performed by shifting the binary numbers).

9. Supplementary Hand Computations

The restriction that the whole process be contained in a memory of 1,024 cells proved to be very great. As a result, in the EDVAC program provision was made only for double precision numerical estimates (the integral part and the fractional part being stored separately) and single precision integers. Thus only a few cases ran to completion, but only 18 cases failed to produce at least one unit in some ϕ_t (with or without giving rise to proportionality). In these cases a hand computation produced units from the algebraic numbers automatically computed. The general scheme for these hand computations was the following: Suppose the machine has produced two nonconjugate numbers ξ_1, ξ_2 with same norm, preferably a small prime p. If p is uniquely factorable in the field, then ξ_1 must be associated with a conjugate of ξ_2, as we can test in the manner described earlier in section 3, completely in integral arithmetic. If the norm is not prime, more complicated combinations must be tried, but they are no different in principle.

At least half the hand-computed units were obtained quickly in this fashion. The cases that did not yield to this method directly did so when more than two integers were used in proper combination.

10. Fundamental Units

In each case those units η were noted for which

$$\max t(\eta),\bar{t}(\eta) \tag{20}$$

over all units *produced in the algorithm* was a minimum. In accordance with arguments given by Hasse [6], this would be the fundamental unit if one were present in the list.

By a remarkable coincidence, almost simultaneously with the completion of the runs (Aug. 1954) Peter Swinnerton-Dyer kindly communicated an independent table giving the

traces t, $\bar{t}$ of the fundamental units for $7 \leq l < 300$. A comparison of the tables showed perfect agreement except in the three cases, $l = 373, 379, 463$. In just these cases the (hand) computed units had positive traces for t and $\bar{t}$, which should have suggested that the units computed from the EDVAC output are squares.

In the listing in table 2, the components and traces of both a unit and its reciprocal are shown in each case (here $t(\eta) = \bar{t}(1/\eta)$). In those cases where the units were computed by hand, (*) is shown. In general, regardless of how the units were produced or derived, the symbol "f" indicates the fundamental unit (and reciprocal) and "ff" is reserved for cases where both fundamental unit and reciprocal were produced by machine. In the three exceptional cases, the units, denoted by "s", are squares of fundamental units.

In order, however, to give some kind of reasonable impression of the amount of labor, particularly in view of 13-digit coordinates (!), we should point out that the number of trials in testing fundamental units is easily

$$O\{\log[\max \bar{t}(\eta), t(\eta)]/\log l\}^2. \tag{21}$$

To see this very quickly, note that if η is *not* a fundamental unit, we can write (recalling $\eta\eta'\eta'' = 1$),

$$\left.\begin{aligned} \eta &= \eta_0^a (\eta_0')^b \\ \eta' &= (\eta_0')^a (\eta_0'')^b = \eta_0^{-b} (\eta_0')^{a-b} \\ \eta'' &= (\eta_0'')^a \eta_0^b = \eta_0^{-b-a} (\eta_0')^{-a} \end{aligned}\right\}, \tag{22}$$

where η_0 is some (as yet unknown) fundamental unit, and a and b are rational integers. By taking reciprocals, or conjugates if necessary, we can assure ourselves that $a \geq b \geq 0$. Then

$$\eta^b (\eta')^a = \eta_0^M, \tag{22a}$$

where

$$M = a^2 - ab + b^2. \tag{22b}$$

Letting $\max(|\eta|, |\eta'|, |\eta''|) = \mathrm{H}$, $\max(|\eta_0|, |\eta_0'|, |\eta_0''|) = \mathrm{H}_0$, we find

$$\mathrm{H}^{a+b} > \mathrm{H}_0^M, \tag{23a}$$

or since $(a+b)/M \leq 2a/M \leq 2a/(4a^2/3) = 3/(2a)$,

$$\mathrm{H}_0 \leq \mathrm{H}^{(3/2a)}. \tag{23b}$$

But, by the concluding remarks of section 2,

$$l \leq |\eta_0 - \eta_0'||\eta_0' - \eta_0''||\eta_0'' - \eta_0| < 8\mathrm{H}^3$$

and

$$\mathrm{H}^2 < \eta^2 + (\eta')^2 + (\eta'')^2 = t(\eta)^2 - 2\bar{t}(\eta);$$

thus

$$0 \leq b \leq a \leq \frac{3 \log \mathrm{H}}{2 \log \mathrm{H}_0} \leq 18 \frac{\log 2\,[\max |t(\eta)|, |\bar{t}(\eta)|]}{\log [l/8]}.$$

This verifies the order of magnitude (21).[5]

The problem of showing the units η to be fundamental now resolves itself to checking on whether any of the units $\eta^b(\eta')^a$ is a perfect M power, where a and b come from the finite set (24). But this check is somewhat laborious, even to program for the EDVAC, and owing to the convenience of Swinnerton-Dyer's table, it was never carried out.

---

[5] Much stronger inequalities are given by Hasse [6] using more specialized notation and information.

TABLE 2. *Structure constants and units*

Prime	Structure Constants										Result of algorithm		Components of unit produced: $\eta_r^{-1} = u_1\omega_1 + u_2\omega_2 + u_3\omega_3$			Trace of units, $t(\eta)$, $t(\eta^{-1})$
l	m	k	g	n	α_2	β_2	γ_2	α_1	β_1	γ_1	No. of matrices	No. of units	u_1	u_2	u_3	
7	2	0	1	1	1	1	0	−2	−1	−2	special	special	1	0	0	−1
13	4	−2	1	−1	1	2	1	−4	−2	−3	special	special	1	1	0	−2
19	6	2	1	7	3	2	1	−4	−4	−5	12 comp	7ff	−1	0	0	1
31	10	1	2	8	4	4	2	−7	−6	−8	30 comp	3f	1	2	1	−4
37	12	−4	1	−11	3	5	4	−10	−7	−8	13 comp	3ff	−1	−1	0	2
43	14	−3	2	−8	4	6	4	−11	−8	−10	32 over	1f	2	1	2	−5
61	20	0	3	9	7	8	5	−14	−12	−15	32 over	2f	−5	−7	−3	15
67	22	−2	3	−5	7	9	6	−16	−13	−16	19 comp	1f	11	17	21	−49
73	24	2	3	27	9	9	6	−16	−15	−18	34 over	2f	−1	−2	−1	4
79	26	−6	1	−41	7	10	9	−20	−16	−17	39 over	9f	2	2	3	−7
97	32	6	1	79	13	10	9	−20	−22	−23	50 over	13f	9	9	7	−25
103	34	4	3	61	13	12	9	−22	−22	−25	46 disc	3f	−39	−47	−65	151
109	36	−1	4	4	12	14	10	−25	−22	−26	37 disc	1f	−13	−16	−10	39
127	42	−7	2	−80	12	16	14	−31	−26	−28	43 over	1f	11	14	17	−42
139	46	−8	1	−103	13	17	16	−34	−29	−30	36 over	8f	−6	−9	−5	20
151	50	6	3	123	19	17	14	−32	−33	−36	45 disc	1f	52	51	54	−157
157	52	−5	4	−64	16	20	16	−37	−32	−36	36 over	1f*	17	19	13	−49
165	54	8	1	169	21	17	16	−34	−37	−38	46 disc	8f	−31	−41	−47	119
181	60	2	5	67	21	22	17	−40	−38	−43	22 over	1f	−2	−3	−2	7
193	64	−8	3	−143	19	24	21	−46	−40	−43	43 disc	1f	3	3	4	−10
													−3	−3	−2	8
													4	3	4	−11
													−12	−14	−9	35
													66	85	93	−244
													521	373	443	−1337
													449	533	627	−1609
													−131	−81	−99	311
													14565	15367	19277	−49209
													−3	−4	−3	10
													4	4	5	−13
													20	17	18	−55
													−184	−229	−243	656
													−10557	−8071	−8883	27511
													2683	2953	3509	−9145
													−4	−4	−3	11
													5	4	5	−14
													12	15	10	−37
													199	233	258	−690
													142	171	135	−448
													1030	1086	1299	−3415

193	64	−8	3	−143	19	24	21	−46	−40	−43	43 disc	1f				
													199	255	258	−690
													142	171	135	−448
													1030	1086	1299	−3415
199	66	−4	5	−59	21	25	20	−46	−41	−46	33 over	2f	−45	−35	−39	119
													95	105	121	−321
211	70	4	5	125	25	25	20	−46	−45	−50	63 over	1f	17	12	16	−45
													233	275	296	−802
223	74	9	2	256	28	24	22	−47	−50	−52	35 over	1f*	−117735	−120801	−96959	335495
													61785	49591	60217	−171593
229	76	7	4	212	28	26	22	−49	−50	−54	23 over	1f*	5673	6737	7111	−19521
													162609	129785	154103	−446497
241	80	−6	5	−125	25	30	25	−56	−50	−55	27 over	1f	−107	−86	−93	286
													87	94	108	−289
271	90	−10	3	−261	27	33	30	−64	−57	−60	30 over	1f*	−37	−19	−28	84
													6029	6254	7316	−19599
277	92	−9	4	−236	28	34	30	−65	−58	−62	34 over	1f	−27	−21	−23	71
													277	291	337	−905
283	94	−11	2	−304	28	34	32	−67	−60	−62	33 over	1f*	14945	17561	14607	−47113
													−38735	−39631	−46569	124935
307	102	5	6	216	36	36	30	−67	−66	−72	30 disc	1f*	−3988957	−4265923	−3500815	11755695
													1233880499	1405925741	1503532433	−4143338673
313	104	−12	1	−371	31	37	36	−74	−67	−68	39 over	4ff	−5	−6	−5	16
													6	6	7	−19
331	110	0	7	49	37	40	33	−74	−70	−77	30 disc	1f	−31	−34	−28	93
													29	32	35	−96
337	112	−2	7	−25	37	41	34	−76	−71	−78	39 over	1f*	127	144	116	−387
													5189	5685	6266	−17140
349	116	12	1	517	45	37	36	−74	−79	−80	57 over	7ff	−6	−6	−5	17
													7	6	7	−20
367	122	−12	3	−435	37	44	41	−86	−78	−81	43 over	1f*	10967	12600	10682	−34249
													654389	671994	771641	−2098024
373	124	4	7	221	43	44	37	−82	−80	−87	35 over	1s*	−863424	−924319	−772262	2560005
													−771297	−862345	−923164	2556806
379	126	−10	5	−365	39	46	41	−88	−80	−85	38 over	1s*	−269376	−304892	−257481	831749
													−258046	−269967	−305561	833574
397	132	11	4	544	48	44	40	−85	−88	−92	60 disc	1f	37	33	35	−105
													−627	−719	−741	2087
409	136	10	5	515	49	46	41	−88	−90	−95	31 disc	1f*	5133	5330	4511	−14974
													495	418	476	−1389
421	140	6	7	343	49	49	42	−92	−91	−98	31 disc	1f*	122	130	109	−361
													1167	1304	1381	−3852
433	144	−1	8	16	48	52	44	−97	−92	−100	50 disc	1f*	−111055	−120569	−102055	333679
													91329	99383	107897	−298609
439	146	9	6	504	52	50	44	−95	−96	−102	49 over	1f*	958722876509	814793743515	917779916345	−2691296536369
													−2609272963	−2939073045	−3070187671	8618533679
457	152	3	8	220	52	54	46	−101	−98	−106	47 over	1f*	−4710533	−5036695	−4281243	14028471
													2763599779	3040707889	3251216741	−9055524409
463	154	−8	7	−343	49	56	49	−106	−98	−105	44 over	1s*	−57726	−49333	−52147	159206
													−49086	−51886	−57437	158409
487	162	8	7	505	57	56	49	−106	−106	−113	33 over	1f*	10649	11170	9561	−31380
													2607	2904	3046	−8557
499	166	−11	6	−536	52	60	54	−115	−106	−112	56 over	1f*	4533791744955	5045136467209	4350456032733	−13929384244897
													−3447237	−3665999	−4104363	11217599

11. Conclusion

The EDVAC produced 176 pages of tabulations, too long to be reproduced here, including some 3,500 algebraic numbers with small norms, in less than 6 hours. With the precision provided for in the coding, only four cases ran to completion, but 25 of the 43 cases run produced at least one unit in the process (for $l=97$, 13 units were produced). The remaining 18 cases provided enough material to permit the hand computation of at least one unit. (For $l=499$, the unit required 43 decimal places to check by hand).

In every case where $g=1$ the explicitly known fundamental unit $(-(k-g+1)/2, -(k-g+1)/2, -(k-g-1)/2$ was among those produced by machine, as well as the (non-fundamental) unit $(-1,-2,0)$, except when $l=37$ and 313.

In addition to units, mentioned earlier, the number of matrices produced after ϕ_0 is shown in table 2, with the following symbols denoting the outcome of the computation (see section 7): "comp" meaning completed, "disc" meaning incomplete (by failure of sign discrimination), "over" meaning incomplete (by overflow in norm formation).

It is clear, however, that to obtain the fullest benefit of this algorithm one would require considerably greater storage, both to perform the unmodified algorithm (guaranteeing a fundamental unit) and to permit sufficient decimal (or preferably integral) precision.

12. References

[1] A. A. Albert, Normalized integral bases of algebraic number fields, Ann. of Math. **38,** 923 (1937).

[2] H. Cohn, A periodic algorithm for cubic forms, I, II, Amer. J. Math. **74,** 821–833 (1952), **76,** 904 (1954).

[3] H. Cohn, Numerical study of signature rank of cubic cyclotomic units, Math. Tables and other Aids to Comput. **47,** 186 (1954).

[4] R. Dedekind, Uber die Anzahl der Idealklassen in reinen kubischen Zahlkörpern, J. Reine Angew. Math. **121,** 123 (1900).

[5] S. Gorn, A computation with algebraic numbers, B. R. L. Report No. 963, Aberdeen Proving Ground, Maryland (1955).

[6] H. Hasse, Arithmetische Bestimmung von Grundeinheit und Klassenzahl in zyklischen kubischer und biquadratischen Zahlkörpern, Abh. Deutsch. Akad. Wiss. Berlin (Berlin, 1950).

[7] E. Hecke, Theorie der algebraischen Zahlen Akad. Verlag, Leipzig, 1923).

[8] G. B. Mathews, Theory of numbers, pt. I, p. 222 (Deighton Bell & Co., Cambridge, 1892).

[9] M. Newman and O. Taussky, On a generalization of the normal bases in abelian algebraic number fields, Comm. Pure Appl. Math. **9,** 85 (1956).

[10] L. Tornheim, Minimal basis and inessential discriminant divisors for a cubic field, Pacific J. Math. **5,** 623 (1955).

WASHINGTON, September 12, 1956.

Journal of Research of the National Bureau of Standards Vol. 59, No. 3, September 1957 Research Paper 2784

Estimation of the Frequencies of Thin Elastic Plates With Free Edges

Tosio Kato,[1] Hiroshi Fujita,[2] Yoshimoto Nakata,[2] and Morris Newman

A variational method is proposed for calculating the frequencies of thin elastic plates with free edges, with rigorous error estimates. As a numerical example, the fundamental frequency of a square plate with the Poisson ratio 0.225 is calculated with a satisfactory result, the possible relative error being less than 1/2000. Generalization to more complicated boundary conditions is straightforward.

1. Introduction

1.1. The present paper is concerned with the study of the vibration of a thin elastic plate with *free edges*. Let us consider a plate that occupies in its natural condition a plane domain D in the xy-plane bounded by a sufficiently regular contour C. It is known [1,2][3] that the problem of determining the frequencies of this plate may be reduced to the following eigenvalue problem, denoted by (Pr.), for the differential system consisting of the differential equation

$$\Delta^2 w=\left(\frac{\partial^2}{\partial x^2}+\frac{\partial^2}{\partial y^2}\right)^2 w=\lambda w \qquad \text{in } D, \tag{1}$$

with the boundary conditions

$$\left.\begin{aligned} \frac{\partial \Delta w}{\partial n}+(1-\mu)\frac{d}{ds}\frac{\partial^2 w}{\partial n \partial t}=0 \qquad & \text{on } C,\\ \mu\Delta w+(1-\mu)\frac{\partial^2 w}{\partial n^2}=0 \qquad & \text{on } C, \end{aligned}\right\} \tag{2}$$

where μ is an elastic constant, called Poisson's ratio, such that $0\leqq\mu<\frac{1}{2}$ (the mathematical theory applies for $0\leqq\mu<1$), and where s is the arc length parameter of C and $\partial/\partial n$, $\partial/\partial t$ represent respectively the derivatives in the directions of the outer normal vector n and the tangential vector t to C at the point under consideration. In the case of angular points on C, where the direction of n varies discontinuously with a jump, w is subjected to an additional boundary condition [1]: $\partial^2 w/\partial n\partial t$ at a point P on C tends to the same value as P approaches any one of the angular points from either side.

The main object is to propose a variational method that enables us to calculate approximate values of the eigenvalues with a rigorous estimate of the error; in other words, to calculate upper and lower bounds for the eigenvalues. Such a method seems interesting and important from the viewpoint of application, inasmuch as it appears, even for most elementary shapes of C, almost impossible to obtain an explicit solution of (Pr.). On the other hand, usual approximating methods applied to (Pr.) seem to suffer from the lack of error estimation. For example, the well-known method of Ritz is applicable and was actually applied to the case of a square plate [2]. Although we know empirically that his method provides us with approximate values whose accuracy is satisfactory in most cases dealt with in practice, it should be noted that they are only known to be upper bounds for the quantities in question and nothing can be said about the error bounds. See [10] for a comparative discussion of existing methods, some of which furnish lower bounds.

---

[1] University of Tokyo, American University, and National Bureau of Standards.
[2] Department of Physics, University of Tokyo.
[3] Figures in brackets indicate the literature references at the end of this paper.

1.2. Our method is based on the following theorem, proved in [3], concerning a self-adjoint operator in a Hilbert space [4] of the type T^*T, which reads, in a form slightly modified for our later convenience,

THEOREM 1.[5] *Let T be a closed linear operator with its domain dense in a Hilbert space $\mathfrak{H}$ and its range in a second Hilbert space $\mathfrak{H}'$ and let T^* be the adjoint of T. Let $\alpha^2<\lambda<\beta^2$ $(0\leqq\alpha<\beta)$ be an open interval containing at most one nondegenerate eigenvalue of the operator T^*T but no other points of its spectrum. If u and v are elements belonging to the domains of T and T^*, respectively, such that*

$$\|u\|\neq 0, \qquad \|v\|\neq 0, \qquad (Tu,v)=(u,T^*v)\geqq 0 \tag{3}$$

and

$$(\eta-\alpha)(\beta-\eta)>\epsilon^2 \tag{4}$$

hold, where

$$\eta=\frac{(Tu,v)}{\|u\|\cdot\|v\|}, \qquad \epsilon^2=\frac{1}{2}\left[\frac{\|Tu\|^2}{\|u\|^2}+\frac{\|T^*v\|^2}{\|v\|^2}\right]-\eta^2, \tag{5}$$

then there exists certainly an eigenvalue λ' of the operator T^*T in the interval (α^2,β^2) and the following inequality is valid: [6,7]

$$L\leqq\lambda'\leqq U, \tag{6}$$

where

$$L=L(u,v)=\left(\eta-\frac{\epsilon^2}{\beta-\eta}\right)^2, \qquad U=U(u,v)=\left(\eta+\frac{\epsilon^2}{\eta-\alpha}\right)^2. \tag{7}$$

In order to make this theorem applicable to (Pr.), it is required to construct the spaces $\mathfrak{H}$, $\mathfrak{H}'$ and define the operators T,T^* in such a manner that the eigenvalue problem $T^*Tw=\lambda w$ is equivalent to (Pr.) and the quantities in (5) are practically calculable, at least for the u and v chosen. (Pr.) is nothing but the eigenvalue problem for a self-adjoint operator H (in a real Hilbert space $\mathfrak{H}$ of square integrable functions on D), defined as

$$Hw=\Delta^2 w \tag{8}$$

for w subjected to the same boundary conditions as those of (Pr.), in addition to certain regularity conditions making $\Delta^2 w$ well-defined. Therefore, our problem is to reduce this preassigned operator H to the form

$$H=T^*T \tag{9}$$

with a suitable choice of $\mathfrak{H}'$, T, and T^*. Here, u and v may be called "trial functions," or possibly "trial vector functions," in estimating λ', a better choice of which will yield a better estimate. Finally, α^2 and β^2 are, loosely speaking, a rough upper bound of the next lower eigenvalue to λ' and a rough lower bound of the next upper eigenvalue, respectively. Such rough estimates will be obtained by other methods (for instance, the Ritz method for α^2), or occasionally by solving an appropriate auxiliary problem, as in the case for β^2 concerning a square plate, treated later. The decomposition of H into the form T^*T is carried out in section 2 for a general shape of C. This is followed by some supplementary remarks on theorem

[4] Concerning the theory of Hilbert space, we mostly follow the notations and terminology of Stone [4]. For operators between two Hilbert spaces, see Murray [5].

[5] An elementary proof of this theorem will be given elsewhere.

[6] Any eigenvalue of T^*T is nonnegative, because $(T^*Tw,w)=\|Tw\|^2\geqq 0$.

[7] $\eta-\frac{\epsilon^2}{\beta-\eta}>0$ and $\eta+\frac{\epsilon^2}{\eta-\alpha}>0$ follow from (4).

1 for improvement of the approximation. In section 3, confining ourselves to the case of the square plate bounded by $x=\pm 1$, $y=\pm 1$, we illustrate in detail the method of actual calculation along the lines mentioned above and give a numerical estimate of the smallest positive eigenvalue of (Pr.), taking $\mu=0.225$, with a relative error bound less than 1/1000. Section 4 is devoted to concluding remarks, with a brief reference to other methods with the same object that are applicable to (Pr.).

2. Decomposition of the Operator and Remarks on Theorem 1

The first part of this section is devoted to decomposing H, the differential operator of (Pr.) including the boundary conditions, into the form T^*T in the sense stated in the introduction, namely, to constructing T and T^* so that $H=T^*T$, i. e., $T^*Tw=\lambda w$, implies (Pr.). Strictly speaking, the differential operators appearing here as well as in the sequel must be replaced by their closed extensions with certain extended domains, or in other words, differentiations should be interpreted in a certain generalized sense. Nevertheless, detailed discussions of this situation will not be given, for they seem to be unnecessary for practical application, which is the ultimate object.

2.1. We begin with the following heuristic considerations.[8] Let T be a closed operator from $\mathfrak{H}$ into $\mathfrak{H}'$ and T^* its adjoint. Then the eigenvalue problem $T^*Tw=\lambda w$ is equivalent, at least under a suitable assumption on the spectrum of T^*T, to the variational problem

$$\delta\|Tu\|^2=0, \qquad \|u\|^2=1,$$

where δ is the first variation. Thus, T^*T is the "gradient operator" of the quadratic functional $\|Tu\|^2$ in the sense that $\delta\|Tu\|^2=2(T^*Tu,\delta u)$. On the other hand, as explained in textbooks [1, 8], (Pr.) is derived from the variational problem

$$\delta J[u]=0, \qquad \int_D u^2dxdy=1,$$

where $J[u]$, which represents (apart from a constant factor) the elastic energy of the plate, is expressed by

$$J[u]=\int_D\left[(\Delta u)^2-2(1-\mu)\left\{\frac{\partial^2u}{\partial x^2}\frac{\partial^2u}{\partial y^2}-\left(\frac{\partial^2u}{\partial x\partial y}\right)^2\right\}\right]dxdy, \tag{10}$$

that is, H is the gradient operator of $J[u]$. Accordingly, $\mathfrak{H}$ being the same as that introduced in defining H, it is reasonable to adopt $\mathfrak{H}'$ and T such that

$$\|Tu\|^2=J[u] \tag{11}$$

holds. In fact, we proceed as follows. Let $L^2(D;\rho)$ denote the real Hilbert space consisting of functions integrable (in square) on D with norm defined by

$$\|u\|^2=\rho\int_D u^2dxdy,$$

where ρ is a positive constant.

In view of (11) and the fact that $J[u]$ can be written as

$$J[u]=\int_D\left[\mu(\Delta u)^2+(1-\mu)\left\{\left(\frac{\partial^2u}{\partial x^2}\right)^2+\left(\frac{\partial^2u}{\partial y^2}\right)^2+2\left(\frac{\partial^2u}{\partial x\partial y}\right)^2\right\}\right]dxdy, \tag{12}$$

we define $\mathfrak{H}'$ by

$$\mathfrak{H}'=L^2(D;\mu)\times L^2(D;1-\mu)\times L^2(D;1-\mu)\times L^2(D;2-2\mu), \tag{13}$$

[8] Some general devices useful in such decomposition are proposed in [6].

where $\times$ represents the Cartesian product of Hilbert spaces. It should be noticed that an element v of $\mathfrak{H}'$ is a four-component vector function $v=\{v_1,v_2,v_3,v_4\}$ defined on D. Now the requirement $J[u]=\|Tu\|^2$ is evidently fulfilled by the operator T, defined by

$$Tu=Tu(x,y)=\left\{\Delta u, \frac{\partial^2 u}{\partial x^2}, \frac{\partial^2 u}{\partial y^2}, \frac{\partial^2 u}{\partial x \partial y}\right\} \in \mathfrak{H}'. \tag{14}$$

Elements u belonging to the domain $\mathfrak{D}$ of T are subjected to certain regularity conditions, but are otherwise arbitrary, i. e., free from any boundary conditions. Though these regularity conditions are too complicated to be specified explicitly in elementary terminology, it will be enough for our purposes to know that the class $\hat{C}$ of functions u, such that u, $\partial u/\partial x$, $\partial u/\partial y$ are continuous and $\partial^2 u/\partial x^2$, $\partial^2 u/\partial x \partial y$, $\partial^2 u/\partial y^2$ are piecewise continuous on $D+C$, is contained in $\mathfrak{D}$; namely, $\hat{C} \subset \mathfrak{D}$.

T^* is defined (together with its domain $\mathfrak{D}^* \subset \mathfrak{H}'$) by the condition that

$$(Tu,v)=(u,T^*v) \tag{15}$$

be valid for any $u \in \mathfrak{D}$. To determine the form of T^*, we note that

$$(Tu,v)=\int_D \left[\mu(\Delta u)v_1+(1-\mu)\frac{\partial^2 u}{\partial x^2}v_2+(1-\mu)\frac{\partial^2 u}{\partial y^2}v_3+2(1-\mu)\frac{\partial^2 u}{\partial x \partial y}v_4\right]dxdy. \tag{16}$$

In reducing the right side of (16) to the form $\int_D u \cdot T^*v \, dxdy$, we can resort to devices similar to those usually employed in deriving the differential equation and the boundary conditions of (Pr.) from the variational problem concerning $J[u]$. Before doing this, we introduce some notations, some of which appeared in section 1.

Let

s = arc length parameter,
$n=n(s)=(n_x,n_y)$ = unit outer normal vector to C,
$t=t(s)=(t_x,t_y)$ = unit tangential vector to C in the positive direction,

and note that

$$\frac{\partial}{\partial n}=n_x\frac{\partial}{\partial x}+n_y\frac{\partial}{\partial y}, \qquad \frac{\partial}{\partial t}=t_x\frac{\partial}{\partial x}+t_y\frac{\partial}{\partial y}, \tag{17}$$

and also

$$\frac{\partial}{\partial x}=n_x\frac{\partial}{\partial n}+t_x\frac{\partial}{\partial t}, \qquad \frac{\partial}{\partial y}=n_y\frac{\partial}{\partial n}+t_y\frac{\partial}{\partial t}. \tag{18}$$

Hereafter it is assumed that the components of n and t are differentiable except at possible angular points $P_1,P_2,\ldots,P_s$ with $s=s_1,s_2,\ldots,s_s$. Also it is known that, for any sufficiently regular functions $F(x,y)$, $G(x,y)$, the identities

$$\left.\begin{aligned}\int_D \frac{\partial F}{\partial x}G\,dxdy&=-\int_D F\frac{\partial G}{\partial x}\,dxdy+\int_C F\cdot Gn_x\,ds,\\ \int_D \frac{\partial F}{\partial y}G\,dxdy&=-\int_D F\frac{\partial G}{\partial y}\,dxdy+\int_C F\cdot Gn_y\,ds,\end{aligned}\right\} \tag{19}$$

are true.

Provided the components of v are sufficiently regular that all procedures used below may be justified, the expression for (Tu,v) in (16) becomes, by some small calculations that make use of (18) and (19),

$$(Tu,v)=\int_D u\cdot\left[\mu\Delta v_1+(1-\mu)\left\{\frac{\partial^2 v_2}{\partial x^2}+\frac{\partial^2 v_3}{\partial y^2}+2\frac{\partial^2 v_4}{\partial x\partial y}\right\}\right]dxdy-\int_C u\cdot P ds+\int_C\frac{\partial u}{\partial n}Q ds+\int_C\frac{\partial u}{\partial t}R ds, \tag{20}$$

where

$$\left.\begin{aligned} P=P(v,s)&=\mu\frac{\partial v_1}{\partial n}+(1-\mu)\left\{\frac{\partial v_2}{\partial x}n_x+\frac{\partial v_3}{\partial y}n_y+\frac{\partial v_4}{\partial x}n_y+\frac{\partial v_4}{\partial y}n_x\right\}\\ Q=Q(v,s)&=\mu v_1+(1-\mu)\{v_2n_x^2+v_3n_y^2+2v_4n_xn_y\},\\ R=R(v,s)&=(1-\mu)\{v_2n_xt_x+v_3n_yt_y+v_4(n_xt_y+n_yt_x)\}.\end{aligned}\right\} \tag{21}$$

Furthermore, because at a point P with $s=\sigma$ we have

$$\left(\frac{\partial u}{\partial t}\right)_P=\left(\frac{du(s)}{ds}\right)_{s=\sigma},$$

and consequently

$$\int_C\frac{\partial u}{\partial t}R ds=\int_C\frac{du}{ds}R ds,$$

we can rewrite the last term of (20) by partial integration, taking account of the fact that C is closed and that R, as well as the components of n and t, is differentiable with respect to s except at $s=s_1, \ldots, s_n$, so that

$$\int_C\frac{\partial u}{\partial t}R ds=-\int_C u\frac{dR}{ds}ds-\sum_{i=1}^{n}u(s_i)D_i, \tag{22}$$

where $D_i=\lim\limits_{s\to s_i+0}R-\lim\limits_{s\to s_i-0}R, \qquad (i=1,2,\ldots,n).$

The substitution of (22) into (20) results in

$$(Tu,v)=\int_D u\left[\mu\Delta v_1+(1-\mu)\left\{\frac{\partial^2 v_2}{\partial x^2}+\frac{\partial^2 v_3}{\partial y^2}+2\frac{\partial^2 v_4}{\partial x\partial y}\right\}\right]dxdy-\int_C u\left(P+\frac{dR}{ds}\right)ds+\int_C\frac{\partial u}{\partial n}Q ds-\sum_{i=1}^{n}u(s_i)D_i. \tag{23}$$

This expression should be equal to (u,T^*v). Because u and $\partial u/\partial n$ on C are arbitrary, we immediately conclude that this is true if and only if v satisfies the boundary conditions

$$\left.\begin{aligned} P+\frac{d}{ds}R&=0,\\ Q&=0,\\ D_i&=0, \qquad (i=1,2,\ldots,n).\end{aligned}\right\} \tag{24}$$

Then T^* is given by

$$T^*v=T^*\{v_1,v_2,v_3,v_4\}=\mu\Delta v_1+(1-\mu)\left\{\frac{\partial^2 v_2}{\partial x^2}+\frac{\partial^2 v_3}{\partial y^2}+2\frac{\partial^2 v_4}{\partial x\partial y}\right\}. \tag{25}$$

Though an element v belonging to $\mathfrak{D}^*$ must obey certain regularity conditions besides the boundary conditions (24), we will not discuss these in detail. Again it is sufficient to know that any v with components belonging to $\hat{C}$ and satisfying the boundary conditions (24) is contained in $\mathfrak{D}^*$.

The construction given above shows that the operators T and T^* are certainly the desired ones, but it may be worthwhile to verify directly the equality $H=T^*T$, i. e., the equivalence of the eigenvalue problem $T^*Tw=\lambda w$ to (Pr.).

Let w belong to the domain of T^*T. Then Tw belongs to $\mathfrak{D}^*$ and consequently is subjected to (24). But

$$P(Tw)=\mu\frac{\partial\Delta w}{\partial n}+(1-\mu)\left\{\frac{\partial^3 w}{\partial x^3}n_x+\frac{\partial^3 w}{\partial y^3}n_y+\frac{\partial^3 w}{\partial x^2\partial y}n_y+\frac{\partial^3 w}{\partial x\partial y^2}n_x\right\}$$

$$=\mu\frac{\partial\Delta w}{\partial n}+(1-\mu)\left[\left\{\frac{\partial}{\partial x}\left(\frac{\partial^2 w}{\partial x^2}\right)n_x+\frac{\partial}{\partial y}\left(\frac{\partial^2 w}{\partial x^2}\right)n_y\right\}+\left\{\frac{\partial}{\partial x}\left(\frac{\partial^2 w}{\partial y^2}\right)n_x+\frac{\partial}{\partial y}\left(\frac{\partial^2 w}{\partial y^2}\right)n_y\right\}\right]$$

$$=\mu\frac{\partial\Delta w}{\partial n}+(1-\mu)\frac{\partial}{\partial n}\left(\frac{\partial^2 w}{\partial x^2}+\frac{\partial^2 w}{\partial y^2}\right)$$

$$=\frac{\partial}{\partial n}\Delta w$$

by virtue of (17). Similarly, we obtain

$$Q(Tw)=\mu\Delta w+(1-\mu)\left\{\frac{\partial^2 w}{\partial x^2}n_x^2+\frac{\partial^2 w}{\partial y^2}n_y^2+2\frac{\partial^2 w}{\partial x\partial y}n_xn_y\right\}$$

$$=\mu\Delta w+(1-\mu)\frac{\partial^2 w}{\partial n^2},$$

$$R(Tw)=(1-\mu)\left\{\frac{\partial^2 w}{\partial x^2}n_xt_x+\frac{\partial^2 w}{\partial y^2}n_yt_y+\frac{\partial^2 w}{\partial x\partial y}(n_xt_y+n_yt_x)\right\}$$

$$=(1-\mu)\frac{\partial^2 w}{\partial t\partial n}.$$

Thus, w satisfies all boundary conditions of H and therefore belongs to the domain of H. Conversely, by a similar argument it is seen that any element in the domain of H belongs to the domain of T^*T. Finally, we observe that

$$T^*Tw=\mu\Delta(\Delta w)+(1-\mu)\left\{\frac{\partial^2}{\partial x^2}\left(\frac{\partial^2 w}{\partial x^2}\right)+\frac{\partial^2}{\partial y^2}\left(\frac{\partial^2 w}{\partial y^2}\right)+2\frac{\partial^2}{\partial x\partial y}\left(\frac{\partial^2 w}{\partial x\partial y}\right)\right\}$$

$$=\Delta^2 w,$$

as it should be.

2.2. The following remarks on theorem 1 include some devices that would be of use in obtaining a good estimate, particularly in constructing a desirable pair u and v.

Remark 2.1. The estimates given by theorem 1 are sharp when ϵ^2 is small. But it is known [3] that ϵ^2 can be written in an alternative form,

$$\epsilon^2=\frac{1}{2}\left(\left\|\frac{1}{\|u\|}Tu-\frac{\eta}{\|v\|}v\right\|^2+\left\|\frac{1}{\|v\|}T^*v-\frac{\eta}{\|u\|}u\right\|^2\right),$$

and $\epsilon^2=0$ occurs if, and only if,

$$Tu=\frac{\|u\|}{\|v\|}\eta v \qquad \text{and} \qquad T^*v=\frac{\|v\|}{\|u\|}\eta u.$$

This implies that $T^*Tu=\eta^2 u$, so that η^2 is equal to an exact eigenvalue λ' of T^*T and u is the corresponding exact eigenfunction w. Thus we may expect a good result when u and v approximate, apart from constant factors, w and Tw closely. This interpretation of u and v should be taken into account, in particular when some knowledge concerning the behavior of w is given in some way or other, for instance from physical considerations or experimental results. As for precise discussions of the relations between u, v, and w, reference is made to the paper by Kato [3].

REMARK 2.2. If u and v are not completely preassigned but admit of some free parameters, it would be intrinsically the best way to choose those parameters first to minimize U and then maximize L. In practice, however, it appears sufficient as well as convenient for calculation to determine them by minimizing ϵ^2. A standard form for such adjustable trial functions is

$$\left.\begin{aligned} u &= \alpha_1 u^{(1)} + \alpha_2 u^{(2)} + \ \cdots\ + \alpha_m u^{(m)}, \\ v &= \beta_1 v^{(1)} + \beta_2 v^{(2)} + \ \cdots\ + \beta_n v^{(n)}, \end{aligned}\right\} \tag{26}$$

where $u^{(1)}, u^{(2)}, \cdots, u^{(m)}$ are fixed functions belonging to $\mathfrak{D}$ and $v^{(1)}, v^{(2)}, \cdots, v^{(n)}$ are fixed vector functions belonging to $\mathfrak{D}^*$, and where $\alpha_1, \alpha_2, \cdots, \alpha_m, \beta_1, \beta_2, \cdots, \beta_n$ are free parameters. If we calculate the quantities in (5) with these u and v, then $\|u\|^2$, $\|Tu\|^2$ become quadratic forms in $\{\alpha_l\}$, $\|v\|^2$, $\|T^*v\|^2$ quadratic forms in $\{\beta_k\}$, and (Tu,v) a bilinear form in $\{\alpha_l\}$ and $\{\beta_k\}$. Thus ϵ^2 becomes an algebraic expression in those parameters whose minimum is desired. There is little difficulty in the necessary computations, especially when we can resort to an automatic computer, even if m and n in (26) are not very small.

REMARK 2.3. Suppose that a closed subspace $\mathfrak{M}$ of $\mathfrak{H}$ reduces the operator $H=T^*T$, that is, let $Hw \in \mathfrak{M}$ for any w belonging to the intersection of $\mathfrak{M}$ and the domain of H. Then we can regard H as an operator in the Hilbert space $\mathfrak{M}$ denoted by $H_{\mathfrak{M}}$. It is known that eigenvalues and eigenvectors of $H_{\mathfrak{M}}$ are also eigenvalues and eigenvectors of H, so that we may speak of an eigenvalue of H in $\mathfrak{M}$. If the eigenvalue λ' of H in question turns out to be an eigenvalue of $H_{\mathfrak{M}}$, we can derive an estimate for λ' from theorem 1 more conveniently by restricting T to $\mathfrak{M}$, and T^* to a suitable closed subspace $\mathfrak{M}^*$ of $\mathfrak{H}'$, with the properties

$$T(\mathfrak{M}\cap\mathfrak{D})\subset\mathfrak{M}^*, \qquad T^*(\mathfrak{M}^*\cap\mathfrak{D}^*)\subset\mathfrak{M}. \tag{27}$$

This procedure is particularly advantageous when a degenerate eigenvalue of the H in question is converted into a nondegenerate one of $H_{\mathfrak{M}}$ by a suitable choice of $\mathfrak{M}$ so that application of theorem 1 becomes possible, or when the neighboring eigenvalues of $H_{\mathfrak{M}}$ are more widely separated than those of H, thus permitting us to take smaller α and larger β so as to make the estimate better. Moreover, though the smallest eigenvalue of H in our problem is equal to zero, the associated eigenfunctions being of the type $ax+by+c$, we can sometimes find $\mathfrak{M}$ such that the eigenvalue λ', originally intermediate, becomes the smallest eigenvalue of $H_{\mathfrak{M}}$ and hence its upper bounds can be obtained by

$$U_R=\frac{\|Tu\|^2}{\|u\|^2}\geqq\lambda', \qquad (u\in\mathfrak{M}\cap\mathfrak{D}), \tag{28}$$

the so-called Rayleigh principle. This seems more convenient than the estimation by the right inequality of (6), for it does not involve v, an element of $\mathfrak{D}^*$, for which a good choice is not easy because of the complication introduced by the boundary conditions. Therefore, we may prefer U_R to U as an upper bound for such an eigenvalue.

Nontrivial $\mathfrak{M}$, $\mathfrak{M}^*$ as mentioned above are often obtained by considering the symmetry properties of the operators H, T, and T^* reflecting those of C, as we shall illustrate in the succeeding section in the case of a square plate.

3. Vibration of a Square Plate

In this section the general results obtained so far are applied to the case of a square plate. Let C be the square with vertices (1,1), (−1, 1), (−1,−1), and (1,−1), which is the same as that treated by Ritz [2]. Bounds will be calculated for the *smallest positive* eigenvalue of $H=T^*T$ according to theorem 1 and the Remarks in section 2, i. e., lower bounds by means of (6) and upper bounds by means of (6) or (28).

3.1. We begin with a preliminary consideration. Let

$$\overline{J}[u]=(1-\mu)\int_D (u_{xx}^2+u_{yy}^2)dxdy. \tag{29}$$

Let the self-adjoint operator $\overline{H}$ in $\mathfrak{H}$ be the gradient operator of $\overline{J}[u]$. Explicitly, any element $\overline{w}$ in the domain of $\overline{H}$ is subjected to the boundary conditions

$$\left.\begin{aligned} &\frac{\partial^2\overline{w}}{\partial x^2}=\frac{\partial^3\overline{w}}{\partial x^3}=0, \qquad (x=\pm 1,-1<y<1)\\ &\frac{\partial^2\overline{w}}{\partial y^2}=\frac{\partial^3\overline{w}}{\partial y^3}=0, \qquad (-1<x<1, y=\pm 1), \end{aligned}\right\} \tag{30}$$

and we observe that

$$\overline{H}\overline{w}=(1-\mu)\left(\frac{\partial^4\overline{w}}{\partial x^4}+\frac{\partial^4\overline{w}}{\partial y^4}\right). \tag{31}$$

The eigenvalue problem $\overline{H}\,\overline{w}=\overline{\lambda}\overline{w}$ is reduced, by separation of variables to the eigenvalue problem

$$\left.\begin{aligned} &\frac{d^4u}{dx^4}=k^4u, \qquad (-<x<1),\\ &u''(\pm 1)=u'''(\pm 1)=0, \end{aligned}\right\} \tag{32}$$

and a similar one in the variable y. Equation (32) is nothing but the eigenvalue problem treated in the analysis of vibrations of a *free* bar of length 2, and is completely solved in textbooks [7,8]. If we denote the eigenvalues by k_n^4 $(n=0,1,2,\ \ldots)$ and note that 0 is the unique degenerate one with eigenfunctions $a+bx$, we have

$$\left.\begin{aligned} &k_0=k_1=0, \qquad 0<k_2<k_3<k_4<\ \ldots\ ,\\ &\text{where}\ ^{9}\\ &k_2=2.3650204, \qquad k_3=3.9266023,\\ &k_4=5.4978039, \qquad k_5=7.0685828, \end{aligned}\right\} \tag{33}$$

The normalized eigenfunction $u_n=u_n(x)$ associated with k_n^4 is given by

$$\left.\begin{aligned} &u_0=\frac{1}{\sqrt{2}}, \qquad u_1=\sqrt{\frac{3}{2}}x,\\ &u_n=\frac{\cosh k_n\cdot\cos k_nx+\cos k_n\cdot\cosh k_nx}{\sqrt{\cosh^2 k_n+\cos^2 k_n}}, \qquad \text{for even } n\geqq 2,\\ &u_n=\frac{\sinh k_n\cdot\sin k_nx+\sin k_n\cdot\sinh k_nx}{\sqrt{\sinh^2 k_n-\sin^2 k_n}}, \qquad \text{for odd } n\geqq 3. \end{aligned}\right\} \tag{34}$$

It should be noticed that u_n is an even or odd function, according as n is even or odd.

The eigenvalues and eigenfunctions of $\overline{H}$ are given by

$$\overline{\lambda}_{mn}=(1-\mu)(k_m^4+k_n^4), \qquad \overline{w}_{mn}=u_m(x)u_n(y), \qquad (m,n=0,1,2,\ \ldots). \tag{35}$$

We note that $\overline{w}_{mn}$ $(m,\ n=0,1,2\ldots)$ constitutes a complete orthonormal system of eigenfunctions of the self-adjoint operator $\overline{H}$.

3.2. Comparing two quadratic functionals $J[u]$ and $\overline{J}[u]$, or two operators H and $\overline{H}$, we can not only determine the constant β in theorem 1 in a rigorous fashion, but also the sym-

[9] k_n is obtained as a root of equation $\tan k=\tanh k$ or $\tan k=-\tanh k$, according as n is odd or even.

metry of the eigenfunction associated with the smallest positive eigenvalue. We note that

$$\overline{J}[u] \leqq J[u]. \tag{36}$$

From (36) it follows, by virtue of the properties of $\overline{H}$ stated above, that the spectrum of H consists only of discrete eigenvalues, and also that, if we number all eigenvalues of H and $\overline{H}$ in ascending order, counting any degenerate one repeatedly by its multiplicity, we have

$$\overline{\Lambda}_N \leqq \Lambda_N, \tag{37}$$

where $\overline{\Lambda}_N$ and Λ_N are the Nth eigenvalue of $\overline{H}$ and the Nth eigenvalue of H, respectively [7]. Thus the eigenvalues (35) of $\overline{H}$ are the lower bounds of the corresponding eigenvalues of H, and hence we can take β as

$$\beta^2 = \overline{\lambda}_{mn} = (1-\mu)(k_m^4 + k_n^4), \tag{38}$$

if the eigenvalue λ' of H in question is the rth eigenvalue from below and $\overline{\lambda}_{mn}$ is the $(r+1)$th eigenvalue of $\overline{H}$.

We turn to the study of the symmetry properties of H and $\overline{H}$, i. e., of closed subspaces specified by the symmetry properties of their elements, and to the reduction of each of these operators. For the square plate under consideration, the boundary conditions of H follow from (2) and the remark there and take the form

$$\left.\begin{aligned}
&\frac{\partial}{\partial x}\left[\frac{\partial^2 w}{\partial x^2}+(2-\mu)\frac{\partial^2 w}{\partial y^2}\right]=0, && (x=\pm 1,\ -1<y<1),\\
&\frac{\partial}{\partial y}\left[\frac{\partial^2 w}{\partial y^2}+(2-\mu)\frac{\partial^2 w}{\partial x^2}\right]=0, && (y=\pm 1,\ -1<x<1),\\
&\frac{\partial^2 w}{\partial x^2}+\mu\frac{\partial^2 w}{\partial y^2}=0, && (x=\pm 1,\ -1<y<1),\\
&\frac{\partial^2 w}{\partial y^2}+\mu\frac{\partial^2 w}{\partial x^2}=0, && (y=\pm 1,\ -1<x<1),\\
&\frac{\partial^2 w}{\partial x\,\partial y}=0, && (x=\pm 1,\ y=\pm 1).
\end{aligned}\right\} \tag{39}$$

In the deduction of the last condition of (39), use is made of the fact that, for instance,

$$\frac{\partial^2 w}{\partial n\,\partial y}=\frac{\partial^2 w}{\partial x\,\partial y} \quad \text{on the side } x=1, \qquad \frac{\partial^2 w}{\partial n\,\partial t}=-\frac{\partial^2 w}{\partial x\,\partial y} \quad \text{on the side } y=1,$$

and hence that the condition

$$\lim_{\substack{x=1\\ y\to 1}}\frac{\partial^2 w}{\partial n\,\partial t}=\lim_{\substack{x\to 1\\ y=1}}\frac{\partial^2 w}{\partial n\,\partial t} \qquad \text{means} \qquad \frac{\partial^2 w}{\partial x\,\partial y}=0 \quad \text{at the vertex } (1,\ 1).$$

Owing to the symmetry properties of (39) and those of the differential operator Δ^2, H is reduced by the following subspaces:

$\mathfrak{M}(o,o)$ = set of functions odd both in x and in y,

$\mathfrak{M}(o,e)$ = set of functions odd in x and even in y,

$\mathfrak{M}(e,o)$ = set of functions even in x and odd in y,

$\mathfrak{M}(e,e)$ = set of functions even both in x and in y,

which are mutually orthogonal and whose direct sum is the whole space $\mathfrak{H}$. We see immediately that $\overline{H}$ is also reduced by each of these subspaces, so that the inequality (37) still remains valid, if we regard H and $\overline{H}$ as operators in any of them. Let the eigenvalues of H in these subspaces be denoted as [10]

$$\begin{aligned} &\lambda_0<\lambda_1<\lambda_2<\cdots, && \text{in } \mathfrak{M}(o,o),\\ &\mu_0<\mu_1<\mu_2<\cdots, && \text{either in } \mathfrak{M}(o,e) \text{ or in } \mathfrak{M}(e,o),\\ &\nu_0<\nu_1<\nu_2<\cdots, && \text{in } \mathfrak{M}(e,e) \end{aligned}$$

the union of which is the total spectrum of H. On the other hand, the eigenfunction $\overline{w}_{mn}$ of $\overline{H}$ with the eigenvalue $\overline{\lambda}_{mn}$ belongs to $\mathfrak{M}(o,o)$, $\mathfrak{M}(o,e)$, $\mathfrak{M}(e,o)$, or $\mathfrak{M}(e,e)$, according as (m=odd, n=odd), (m=odd,n=even), (m=even, n=odd), or (m=even, n=even).

Because the zero point set $\mathfrak{N}$ of H (the eigenspace with the eigenvalue 0) consists of functions of the type $ax+by+c$, it follows that

$$\left.\begin{aligned} &\mathfrak{M}(o,o) \perp \mathfrak{N},\\ &\mathfrak{M}(o,e)\cap\mathfrak{N}=\{u;\ u=ax\},\\ &\mathfrak{M}(e,o)\cap\mathfrak{N}=\{u;\ u=by\},\\ &\mathfrak{M}(e,e)\cap\mathfrak{N}=\{u;\ u=c\}. \end{aligned}\right\} \tag{40}$$

and hence that

$$\lambda_0>0, \qquad \mu_0=\nu_0=0.$$

In consequence, the smallest positive eigenvalue of H is equal to $\min(\lambda_0,\mu_1,\nu_1)$. We can determine the order relations between λ_0, μ_1, and ν_1 as follows. Because (40) means that μ_0 is degenerate neither in $\mathfrak{M}(o,e)$ nor in $\mathfrak{M}(e,o)$, and ν_0 is not degenerate in $\mathfrak{M}(e,e)$, we note, according to (37), that $\overline{\lambda}_{12}(=\overline{\lambda}_{21})$ and $\overline{\lambda}_{22}$ are lower bounds of μ_1 and ν_1, respectively, and hence we have, by means of (33) and (35),

$$\left.\begin{aligned} &\mu_1\geqq\overline{\lambda}_{12}=\overline{\lambda}_{21}=(1-\mu)k_2^4=(1-\mu)\times 31.28\ \ldots,\\ &\nu_1\geqq\lambda_{22}=2(1-\mu)k_2^4=(1-\mu)\times 62.59.\ \ldots \end{aligned}\right\} \tag{41}$$

On the other hand, the substitution of the trial function $u=xy\in\mathfrak{M}(o,o)$ into (28) yields

$$\lambda_0\leqq(1-\mu)\times 18. \tag{42}$$

Combining (41) and (42), we conclude that the smallest positive eigenvalue of H is the smallest eigenvalue λ_0 in $\mathfrak{M}(o,o)$. Moreover, owing to (42) and the relations $\overline{\lambda}_{11}=0$, $\overline{\lambda}_{13}=\overline{\lambda}_{31}=(1-\mu)\times 237.72\ \ldots$, we obtain

$$\overline{\lambda}_{11}<\lambda_0<\overline{\lambda}_{13}=\overline{\lambda}_{31}, \tag{43}$$

which shows that $\overline{\lambda}_{11}$ is the unique eigenvalue of $\overline{H}$ less than λ_0, and hence λ_0 is not degenerate. Also we have, by means of (37), $\overline{\lambda}_{13}\leqq\lambda_1$, which enables us to take as β in theorem 1, with respect to $\lambda'=\lambda_0$, any number such that

$$\beta^2\leqq(1-\mu)\times 237.72\ \ldots. \tag{44}$$

Furthermore, we divide $\mathfrak{M}(o,o)$ into the following two mutually orthogonal subspaces $\mathfrak{M}$ and $\mathfrak{M}'$,

$$\begin{aligned} \mathfrak{M}&=\{u;\ u\in\mathfrak{M}(o,o), \qquad u(x,y)\equiv u(y,x)\},\\ \mathfrak{M}'&=\{u;\ u\in\mathfrak{M}(o,o), \qquad u(x,y)\equiv -u(y,x)\}, \end{aligned}$$

[10] Evidently, the spectra of $H\mathfrak{M}_{(e,o)}$ and those of $H\mathfrak{M}_{(e,o)}$ are identical, and any eigenfunction of one of them is converted into an eigenfunction of the other by permutation of x and y.

each of which is seen to reduce both of H and $\overline{H}$.

From (43) it follows that λ_0 is an eigenvalue of H not in $\mathfrak{M}'$ but in $\mathfrak{M}$, because the smallest eigenvalue of $\overline{H}$ in $\mathfrak{M}'$ is $\bar{\lambda}_{13}$ with eigenfunctions $\mathrm{Const}\cdot(\overline{w}_{13}-\overline{w}_{31})$, though this is at the same time an eigenvalue of $\overline{H}$ in $\mathfrak{M}$ with eigenfunctions $\mathrm{Const}\cdot(\overline{w}_{13}+\overline{w}_{31})$. In calculating bounds of λ_0, to which we confine ourselves hereafter, we may therefore restrict H and T to $\mathfrak{M}$.

3.3 We go on to the construction of the trial elements [11] u and v in theorem 1. Introducing six elements $u^{(1)}, \ldots, u^{(6)}$ of $\mathfrak{M}$, given by

$$\begin{aligned} u^{(1)}&=P_1(x)P_1(y), & u^{(2)}&=P_1(x)P_3(y)+P_3(x)P_1(y),\\ u^{(3)}&=P_3(x)P_3(y), & u^{(4)}&=P_1(x)P_5(y)+P_5(x)P_1(y),\\ u^{(5)}&=P_3(x)P_5(y)+P_5(x)P_3(y), & u^{(6)}&=P_5(x)P_5(y), \end{aligned}$$

where P_i represents Legendre's polynomial of degree i $(i=1,3,5)$, we put, in accordance with (26),

$$u=\alpha_1u^{(1)}+\alpha_2u^{(2)}+\ \ldots\ +\alpha_6u^{(6)} \tag{45}$$

with free parameters $\alpha_1,\alpha_2, \ldots, \alpha_6$ to be determined later. This u evidently belongs to $\mathfrak{M}\cap\mathfrak{T}$, because it is a polynomial and surely satisfies the regularity conditions of $\mathfrak{T}$.

The other element $v=\{v_1,v_2,v_3,v_4\}$ is constructed as follows. We can easily verify that the boundary conditions (24) of $\mathfrak{T}^*$ now reduce to the following forms:

$$\left.\begin{aligned} \mu\frac{\partial v_1}{\partial x}+(1-\mu)\frac{\partial v_2}{\partial x}+2(1-\mu)\frac{\partial v_4}{\partial y}&=0, && (x=\pm1,\ -1<y<1),\\ \mu\frac{\partial v_1}{\partial y}+(1-\mu)\frac{\partial v_3}{\partial y}+2(1-\mu)\frac{\partial v_4}{\partial x}&=0, && (-1<x<1,\ y=\pm1),\\ \mu v_1+(1-\mu)v_2&=0, && (x=\pm1,\ -1<y<1),\\ \mu v_1+(1-\mu)v_3&=0, && (-1<x<1,\ y=\pm1),\\ v_4&=0, && (x=\pm1,\ y=\pm1). \end{aligned}\right\} \tag{46}$$

In view of the symmetry of $\mathfrak{M}$, on the other hand, we can take as $\mathfrak{M}^*$ the subspace composed of elements v with the following properties of symmetry:

$$\left.\begin{aligned} &v_1,\ v_2,\ v_3 \text{ are odd both in } x \text{ and in } y,\\ &v_4 \text{ is even both in } x \text{ and in } y,\\ &v_1(x,y)\equiv v_1(y,x), \qquad v_2(x,y)\equiv v_3(y,x), \qquad v_4(x,y)\equiv v_4(y,x). \end{aligned}\right\} \tag{47}$$

Then the relations (27) obviously hold.

A general element v satisfying the conditions (47), and whose components are polynomials in x,y with the degrees shown below, is expressible as

$$\left.\begin{aligned} v&=\{v_1,v_2,v_3,v_4\},\\ v_1&=a_1xy+a_2(xy^3+x^3y)+a_3x^3y^3+a_4(xy^5+x^5y),\\ v_2&=b_1xy+b_2xy^3+b_2'x^3y+b_3x^3y^3+b_4xy^5+b_4'x^5y,\\ v_3&=b_1xy+b_2'xy^3+b_2x^3y+b_3x^3y^3+b_4'xy^5+b_4x^5y,\\ v_4&=c_1+c_2(x^2+y^2)+c_3x^2y^2+c_4(x^4+y^4). \end{aligned}\right\} \tag{48}$$

[11] If we are contented with a rough estimate of λ^0, we can construct the trial elements more easily (see [9]).

Moreover, for such a trial function v the boundary conditions (46) are equivalent to

$$\left.\begin{aligned} \sigma\frac{\partial v_1}{\partial x}+\frac{\partial v_2}{\partial y}+2\frac{\partial v_4}{\partial y}=0, &\qquad (x=1,\ -1<y<1),\\ \sigma v_1+v_2=0, &\qquad (x=1,\ -1<y<1),\\ v_4=0, &\qquad (x=y=1), \end{aligned}\right\} \tag{49}$$

where $\sigma=\mu/(1-\mu)$.

Substituting (48) into (49), putting $x=1$ and equating the coefficients of y, y^3, y^5 to zero or putting $x=y=1$, we obtain the conditions for v given by (48) to satisfy (49) and hence to belong to $\mathfrak{D}^*$. The results are the following six equalities:[12]

$$\left.\begin{aligned} &\sigma(a_1+3a_2+5a_4)+(b_1+3b_2'+5b_4')+(4c_2+4c_3)=0,\\ &\sigma(a_1+a_2+a_4)\quad+(b_1+b_2'+b_4')\qquad\qquad=0,\\ &\sigma(a_2+3a_3)\qquad+(b_2+3b_3)\qquad+8c_4\qquad=0,\\ &\sigma(a_2+a_3)\qquad+(b_2+b_3)\qquad\qquad=0,\\ &\sigma a_4\qquad\qquad+b_4\qquad\qquad\qquad=0,\\ &\qquad\qquad\qquad\qquad\qquad c_1+2c_2+c_3+2c_4=0. \end{aligned}\right\} \tag{50}$$

By inspection, we find the following 8 independent families, (1), (2), . . . , (8), of parameters satisfying the system (50) of 6 equations in 14 unknowns:

(1) $a_1=1,\quad b_1=-\sigma,$

(2) $a_2=1,\quad b_2=b_2'=-\sigma,$

(3) $b_1=-1,\ b_2'=1,\quad c_1=1,\ c_2=-1/2,$

(4) $a_3=1,\quad b_3=-\sigma$

(5) $c_1=c_3=1,\ c_2=-1,$

(6) $a_4=1,\quad b_4=b_4'=-\sigma,$

(7) $b_1=-1,\ b_4'=1,\quad c_1=1,\ c_3=-1,$

(8) $b_2=-2,\ b_3=2,\quad c_1=1,\ c_4=-1/2.$

The absent members of each family are equal to 0.

In this way, we have the following 8 elements $v^{(k)}=\{v_1^{(k)},\ v_2^{(k)},\ v_3^{(k)},\ v_4^{(k)}\}$ $(k=1,\ 2,\ \ldots,\ 8)$ contained in $\mathfrak{M}^*\cap\mathfrak{D}^*$.

$$\begin{aligned} v^{(1)}&=\{xy,\quad -\sigma xy,\quad -\sigma xy,\quad 0\},\\ v^{(2)}&=\{xy^3+x^3y,\quad -\sigma(xy^3+x^3y),\quad -\sigma(xy^3+x^3y),\quad 0\},\\ v^{(3)}&=\{0,\quad -xy+x^3y,\quad -xy+xy^3,\quad 1-(x^2+y^2)/2\},\\ v^{(4)}&=\{x^3y^3,\quad -\sigma x^3y^3,\quad -\sigma x^3y^3,\quad 0\},\\ v^{(5)}&=\{0,\quad 0,\quad 0,\quad (1-x^2)(1-y^2)\},\\ v^{(6)}&=\{xy^5+x^5y,\quad -\sigma(xy^5+x^5y),\quad -\sigma(xy^5+x^5y),\quad 0\},\\ v^{(7)}&=\{0,\quad -xy+x^5y,\quad -xy+xy^5,\quad 1-x^2y^2\},\\ v^{(8)}&=\{0,\quad 2(-xy^3+x^3y^3),\quad 2(-x^3y+x^3y^3),\quad 1-(x^4+y^4)/2\}. \end{aligned}$$

[12] The result of equating to zero the coefficients of y^5 in the first and second conditions of (49) coincides and gives the fifth condition of (50).

With these 8 elements as basis, we construct the trial function v in accordance with (26):

$$v=\beta_1 v^{(1)}+\beta_2 v^{(2)}+\ .\ .\ .\ +\beta_8 v^{(8)} \tag{51}$$

with free parameters $\beta_1,\beta_2,\ .\ .\ .\ ,\beta_8$.

Making use of the trial functions u and v given by (45) and (51) respectively, we get, after the necessary integrations,

$$\|Tu\|^2=\sum_{i,k=1}^{6} A_{ik}\alpha_i\alpha_k=(1-\mu)\sum A'_{ik}\alpha_i\alpha_k, \qquad (A_{ik}=A_{ki}),$$

$$\|u\|^2=\sum_{i,k=1}^{6} B_{ik}\alpha_i\alpha_k, \qquad (B_{ik}=B_{ki}),$$

$$T^*v\|^2=\sum_{i,k=1}^{8} C_{ik}\beta_i\beta_k=(1-\mu)\sum C'_{ik}\beta_i\beta_k, \qquad (C_{ik}=C_{ki}),$$

$$\|v\|^2=\sum_{i,k=1}^{8} D_{ik}\beta_i\beta_k=(1-\mu)\sum D'_{ik}\beta_i\beta_k, \qquad (D_{ik}=D_{ki}),$$

$$(Tu,u)=(u,T^*v)=\sum_{i=1}^{6}\sum_{k=1}^{8} E_{ik}\alpha_i\beta_k=(1-\mu)\sum\sum E'_{ik}\alpha_i\beta_k$$

with A'_{ik}, B_{ik}, C'_{ik}, D'_{ik}, E''_{ik} given by the tables.

A_{ik}

i \ k	1	2	3	4	5	6
1	8	16	8	16	16	8
2		$400\sigma+312$	96	$1120\sigma+672$	192	96
3			$\frac{600}{7}\sigma+\frac{2616}{7}$	$360\sigma+96$	$240\sigma+816$	288
4				$4648\sigma+3336$	$1008\sigma+336$	240
5					$\frac{22248}{11}\sigma+\frac{37296}{11}$	$\frac{1680}{11}\sigma+\frac{17520}{11}$
6						$840\sigma+2640$

B_{ik}

i	1	2	3	4	5	6	$B_{ik}=0 \quad (i\neq k)$
B_{ii}	$\frac{4}{9}$	$\frac{8}{21}$	$\frac{4}{49}$	$\frac{8}{33}$	$\frac{8}{77}$	$\frac{4}{121}$	

C'_{ik}

i	3	3	3	3	5	5	5	7	7	8	For other values of i and k, $C'_{ik}=0$.
k	3	5	7	8	5	7	8	7	8	8	
C'_{ik}	64	$\frac{178}{3}$	$\frac{256}{3}$	$\frac{348}{5}$	$\frac{256}{9}$	$\frac{512}{9}$	$\frac{256}{5}$	$\frac{8704}{63}$	$\frac{4096}{35}$	$\frac{17664}{175}$	

D'_{ik}

i \ k	1	2	3	4	5	6	7	8
1	$\frac{4}{9^\tau}$	$\frac{8}{15^\tau}$	$\frac{16}{45^\sigma}$	$\frac{4}{25^\tau}$	0	$\frac{8}{21^\tau}$	$\frac{32}{63^\sigma}$	$\frac{32}{75^\sigma}$
2		$\frac{368}{525^\tau}$	$\frac{64}{175^\sigma}$	$\frac{8}{35^\tau}$	0	$\frac{496}{945^\tau}$	$\frac{512}{945^\sigma}$	$\frac{256}{525^\sigma}$
3			$\frac{144}{35}$	$\frac{16}{175}$	$\frac{128}{45}$	$\frac{32}{135^\sigma}$	$\frac{992}{189}$	$\frac{2528}{525}$
4				$\frac{4}{49^\tau}$	0	$\frac{8}{45^\tau}$	$\frac{32}{225^\sigma}$	$\frac{32}{245^\sigma}$
5					$\frac{512}{225}$	0	$\frac{256}{75}$	$\frac{1024}{315}$
6						$\frac{656}{1617^\tau}$	$\frac{192}{539^\sigma}$	$\frac{64}{189^\sigma}$
7							$\frac{119744}{17325}$	$\frac{1088}{175}$
8								$\frac{63424}{11025}$

E'_{ik}

i	1	1	1	1	2	2	For other values of i and k, $E'_{ik}=0$.
k	3	5	7	8	7	8	
E'_{ik}	$\frac{16}{3}$	$\frac{32}{9}$	$\frac{64}{9}$	$\frac{32}{5}$	$\frac{64}{21}$	$\frac{64}{35}$	

Here σ and τ are constants given by $\sigma=\frac{\mu}{1-\mu}$, $\tau=\frac{1+\mu}{(1-\mu)^2}$.

In the numerical computation we take $\mu=0.225$, the value used by Ritz. Then the quantity $2\epsilon^2$ becomes an algebraic expression of the form

$$2\epsilon^2=\frac{x'Ax}{x'Bx}+\frac{y'Cy}{y'Dy}-2\frac{(x'Ey)^2}{(x'Bx)(y'Dy)}, \tag{52}$$

where x, y are the column vectors with components $\{\alpha_i\}$, $\{\beta_k\}$, respectively, x', y' are their transposed vectors, and A, B, C, D, E are matrices with numerical elements.

In order to minimize ϵ^2, we choose the following procedure. First we minimize the first term on the right-hand side of (52). This gives rise to an eigenvalue problem of order 6, for which we determine the lowest eigenvalue m (which is the minimum value in question) and the associated eigenvector $x=x_1$. Then we put $x=x_1$ into (52); this converts (52) into a fractional form of which the numerator and denominator are known quadratic forms in y. We minimize this expression; this is equivalent to solving another eigenvalue problem of order 8, and we determine the lowest eigenvalue m' and the associated eigenvector $y=y_1$. In the next step we should put $y=y_1$ into (52), converting (52) into a ratio of two quadratic forms in x, and determine its minimum m''. This procedure could be repeated indefinitely, and the sequence m', m'', . . . is certainly nonincreasing. It is not clear whether these values converge to the true minimum of $2\epsilon^2$. But this is not important, for actually we need not obtain this true minimum; it is sufficient for our purpose that a very small value of $2\epsilon^2$ is given by some set of x and y.

The actual computation was done by using SEAC, and it turned out that the value of m' was sufficiently small, so that further computation was not necessary. To avoid the uncontrollable error arising from the use of the machine, the components of x_1, y_1 thus obtained have been rounded off to five significant figures, and the value of $2\epsilon^2$ for these arguments has been calculated anew on a desk calculator. The final values are

$$\begin{aligned}
\alpha_1 &= \ \ 3.6100\ 000, & \beta_1 &= \ \ 2.0362\ 000,\\
\alpha_2 &= -0.2071\ 000, & \beta_2 &= -1.1853\ 000,\\
\alpha_3 &= -0.0357\ 000, & \beta_3 &= -1.6269\ 000,\\
\alpha_4 &= \ \ 0.0335\ 000, & \beta_4 &= \ \ 0.3121\ 000,\\
\alpha_5 &= -0.0012\ 000, & \beta_5 &= \ \ 0.5907\ 000,\\
\alpha_6 &= -0.0017\ 000, & \beta_6 &= \ \ 0.0112\ 000,\\
 & & \beta_7 &= \ \ 0.0176\ 000,\\
 & & \beta_8 &= \ \ 0.1233\ 000,
\end{aligned}$$

$$\epsilon^2 = \ \ 0.009172, \qquad \eta = \ \ 3.6266247.$$

We can take $\alpha=0$ and $\beta=13.5$ in (7) for U and L in conformity with (44). Thus we obtain

$$U=12.455433, \qquad L=12.430613,$$

where the rounding-off errors are within 5×10^{-5} by the most conservative estimates. Thus

$$12.4305<\lambda_0<12.4555.$$

For the upper bound we can also use U_R, given by (28). This gives

$$U_R=12.454620,$$

which is somewhat sharper than U. In this way we arrive at the final result:

$$12.4306<\lambda_0<12.4547. \tag{53}$$

If we adopt $\lambda_0=12.4427$, the average of upper and lower bounds, as the smallest positive eigenvalue of $H=T^*T$, the relative error is less than 1/1000.

The corresponding value of the fundamental frequency of a thin elastic square plate ($\mu=0.225$) with free edges is

$$\nu=\frac{\sqrt{\lambda_0}}{2\sqrt{3}\pi\sqrt{1-\mu^2}}\sqrt{\frac{E}{\rho}}\frac{h}{a^2}=0.3420\times\sqrt{\frac{E}{\rho}}\frac{h}{a^2},$$

with relative error less than 1/2000. Here $2a$ = edge length, $2h$ = thickness, ρ = density, and E = Young's modulus.

A remark is necessary regarding the relation between the result of Ritz [2] and that of this study. Ritz gives the estimate $\lambda_0 \leqq 12.43$, and this appeared exceedingly sharp in view of the results shown here (53). Ritz used products of eigenfunctions of free bars as trial functions $u^{(i)}$. This suggested that these trial functions might lead to a sharper upper bound than the one presented in this paper. Because the last figure in Ritz' result is unreliable, the same calculation was carried out for purposes of comparison by retaining more significant figures. The result obtained gives only $\lambda_0 < 12.488$, a less sharp estimate than the one herein. This seems to show that, as far as the fundamental frequency of a square plate is concerned, use of polynomial trial functions is preferable to products of eigenfunctions of free bars.

4. Concluding Remarks

4.1. This method is also applicable to a plate whose edge is not wholly free but subjected to conditions of a more general type. For instance, let us assume that C, the boundary of the plate under consideration, consists of three arcs, C_0, C_1, and C_2, and that the edge is free, supported, and clamped along C_0, C_1, and C_2, respectively. Among all angular points on C, we denote those on C_0 by $P_1, P_2, \ldots, P_s$ with $s=s_1, s_2, \ldots, s_s$. Then as in the case of the free plate discussed above, the vibration of this plate is characterized by the eigenvalue problem of a self-adjoint operator $\hat{H}$ in $\mathfrak{H}$. Again, $\hat{H}$ is the gradient operator of a quadratic functional $\hat{J}[u]$, which is the restriction of $J[u]$ to the class of functions u satisfying the boundary conditions

$$\left.\begin{aligned} u&=0 \qquad \text{on } C_1+C_2, \\ \frac{\partial u}{\partial n}&=0 \qquad \text{on } C_2. \end{aligned}\right\} \tag{54}$$

Thus, following a course parallel to that of section 2, we can reduce $\hat{H}$ to $\hat{T}^*\hat{T}$ and make theorem 1 applicable. The results of this decomposition are as follows. $\mathfrak{H}$ and $\mathfrak{H}'$ being the same as before, $\hat{T}u$ and $\hat{T}^*v$ are formally identical with Tu and T^*v, respectively, and now any u belonging to the domain of $\hat{T}$ is subjected to the boundary conditions (54) and any v belonging to the domain of $\hat{T}^*$ is subjected to the boundary conditions

$$\left.\begin{aligned} Q&=0 \qquad \text{on } C_0, +C_1, \\ P+\frac{d}{ds}R&=0 \qquad \text{on } C_0, \\ D_i&=0, \qquad (i=1,2,\ldots,n), \end{aligned}\right\} \tag{55}$$

where P, Q, R, D_i are those defined in section 2.

Applications of theorem 1 to the cases of such mixed boundary conditions will be treated elsewhere.

In addition, if both C_0 and C_1 are empty, i. e., the whole edge is clamped, another decomposition seemingly more convenient is possible. Namely, by means of (19) and the conditions $u=\partial u/\partial n=0$ on C, we have

$$\int_D \frac{\partial^2 u}{\partial x^2}\cdot\frac{\partial^2 u}{\partial y^2}dxdy=\int_D\left(\frac{\partial^2 u}{\partial x\partial y}\right)^2 dxdy=\int_D u\frac{\partial^4 u}{\partial x^2\partial y^2}dxdy,$$

and hence, in consideration of (10), we obtain

$$\hat{J}[u]=\int_D(\Delta u)^2 dxdy.$$

Thus, taking $\mathfrak{H}=\mathfrak{H}'=L^2(D;1)$ we can decompose $\hat{H}$ into the desired form by using T_c and T_c' such that

$$T_c u=\Delta u, \qquad \left(u=\frac{\partial u}{\partial n}=0 \quad \text{on } C\right),$$

$$T_c' v=\Delta v.$$

4.2. Before his derivation of theorem 1, one of the authors gave also the following theorem 2 [10], which stands in a close connection with the former.

THEOREM 2. *Let H be a self-adjoint operator of a Hilbert Space $\mathfrak{H}$, and let (α,β) be an open interval containing at most a nondegenerate eigenvalue of H but no other point of its spectrum. Let w be any vector of the domain $\mathfrak{D}_H$ of H with $\|w\|=1$, and set $\eta=(Hw,w)$, $\epsilon^2=\|(H-\eta)w\|^2=\|Hw\|^2-\eta^2$. If $\epsilon^2<(\eta-\alpha)\,(\beta-\eta)$, then there is certainly an eigenvalue λ' of H in (α,β) that satisfies the inequalities*

$$\eta-\frac{\epsilon^2}{\beta-\eta}\leqq\lambda'\leqq\eta+\frac{\epsilon^2}{\eta-\alpha}. \tag{56}$$

This theorem can be interpreted as follows. If we can construct a "trial function" w in accordance with the conditions stated above, we would obtain an estimate of the eigenvalue λ' in question by means of (56). Comparing theorem 1 with theorem 2, we note that, if a good choice of w is easy for the operator H under consideration, theorem 2 may be preferable inasmuch as it does not require the decomposition $H=T^*T$, and also it involves fewer quantities to be calculated. However, this is not the case so far as (Pr.) is concerned, for the difficulties in obtaining a suitable w seem greater than those in obtaining a suitable pair of u and v (essentially v) because of the increased complication of the boundary conditions of $\mathfrak{D}_H$. Furthermore, we have four components v_1, v_2, v_3, v_4 at our disposal in constructing the trial vector function v belonging to $\mathfrak{D}^*$, whereas we must make a single function w satisfy all boundary conditions in order that $w\in\mathfrak{D}_H$. For instance, let us consider the case of the square plate dealt with in section 3 and look for a polynomial trial function w contained in $\mathfrak{D}_H\cap\mathfrak{M}$. For any w belonging to $\mathfrak{M}$, the boundary conditions (39) of $\mathfrak{D}_H$ reduce to

$$\left.\begin{aligned}
\frac{\partial^3 w}{\partial x^3}+(2-\mu)\frac{\partial^3 w}{\partial x\partial y^2}&=0, \qquad (x=1,\ -1<y<1),\\
\frac{\partial^2 w}{\partial x^2}+\mu\frac{\partial^2 w}{\partial y^2}&=0, \qquad (x=1,\ -1<y<1),\\
\frac{\partial^2 w}{\partial x\partial y}&=0, \qquad (x=y=1).
\end{aligned}\right\} \tag{57}$$

On the other hand, a general form of a polynomial of degree $2N-2$, belonging to $\mathfrak{M}$ is given by

$$w=\sum_{r=2}^{N}\sum_{\substack{m+n=r\\ m,\,n=1\\ m\leqq n}}^{}A_{mn}(x^{2m-1}y^{2n-1}+x^{2n-1}y^{2m-1}). \tag{58}$$

Substituting (58) into (57), putting $x=1$ and equating the coefficients of all powers of y to zero, or putting $x=y=1$, we derive the conditions for w given by (58) to satisfy (57). This gives rise to a system of $2N-3$ equations in $N^2/4$ unknowns, or a system of $2N-4$ equations in $(N^2-1)/4$ unknowns, according as N is even or odd. The smallest value of N permitting nontrivial solutions is seen to be 7. Therefore, in order to obtain a function of the type (58) in $\mathfrak{D}_H\cap\mathfrak{M}$, we have to solve at least a system of 10 equations in 12 unknowns, leaving two homogeneous parameters, i. e., essentially only 1 free parameter in a 12-degree polynomial.

4.3. Weinstein and Aronszajn have developed an approximating method [11],[14] with a wide range of application, which also enables us to calculate upper and lower bounds of eigen-

[14] See [11] for a standard list of references concerning this method.

values of a certain kind of operators. Although the arguments used in establishing the convergence of their method are theoretically interesting, it appears that, from the viewpoint of practical applications, the essential parts of their method are the procedures leading from rough bounds to those that improve as sharply as possible. In this sense their method seems to have some similarity to the present one, and hence it will be worthwhile to reveal the mutual relations between these two methods and to compare their merits. However, we reserve this for some future occasion and remark here only that, with respect to lower bounds of eigenvalues in the case of the square plate treated in section 3, the eigenvalue problem of the operator $\overline{H}$ can play the role of the "auxiliary problem" in their method, of which the complete set of the exact eigenvalues and eigenvectors is required to be known.

5. References

[1] K. O. Friedrichs, Die Randwert und Eigenwert Probleme aus der Theorie der Elastischen Platten (Anwendung der Direkten Methoden der Variationsrechnung), Math. Ann. **98,** 206 to 247 (1927).

[2] W. Ritz, Theorie der Transversalschwingungen einer quadratischen Platte mit freien Rändern, Ann. Phys. **28,** 737 to 786 (1909).

[3] T. Kato, On some approximate methods concerning the operators T^*T, Math. Ann. **126,** 253 to 262 (1953).

[4] M. H. Stone, Linear transformations in Hilbert space (New York, 1932).

[5] F. J. Murray, Linear transformations between Hilbert spaces and the application of this theory to linear partial differential equations, Trans. Am. Math. Soc. **37,** 301 to 338 (1935).

[6] H. Fujita, Contribution to the theory of upper and lower bounds in boundary value problems, J. Phys. Soc. Japan **10,** 1 to 8 (1955).

[7] R. Courant and D. Hilbert, Methods of mathematical physics, I, chap. V and VI, 1st English ed. (Interscience Publishers, Inc., New York, N. Y., 1953).

[8] Lord Rayleigh, Theory of sound, I (Dover Publications, New York, N. Y., 1954).

[9] Y. Nakata and H. Fujita, On upper and lower bounds of the eigenvalues of a free plate, J. Phys. Soc. Japan **10,** 823 to 824 (1955).

[10] T. Kato, On the upper and lower bounds of eigenvalues, J. Phys. Soc. Japan **4,** 334 to 339 (1949).

[11] N. Aronszajn, Approximation methods for eigenvalues of completely continuous symmetric operators, Proceedings of the symposium on spectral theory and differential problems, 179 to 202 (Math. Dept. Oklahoma Agri. and Mech. College, 1955).

Washington, October 3, 1956.

Journal of Research of the National Bureau of Standards Vol. 59, No. 3, September 1957 Research Paper 2785

A Thermochemical Study of the Reaction of Calcium Hydroxide, Silica Gel, and Water

Edwin S. Newman

The heat of reaction of calcium hydroxide, silica gel, and water was measured by a heat-of-solution method. The reaction was carried out at 25° C in pastes having a water solid ratio of about 1.0. The heat of reaction, $-\Delta H$ at 25° C, for the reaction

$$Ca(OH)_2+SiO_2\cdot nH_2O=CaO\cdot SiO_2\cdot nH_2O$$

was found to be about 10.3 kilocalories. The heat of the reaction

$$CaO\cdot SiO_2\cdot nH_2O+mCa(OH)_2=(1+m)CaO\cdot SiO_2\cdot(n+m)H_2O$$

is about 1.6 kilocalories per mole of added $Ca(OH)_2$. About half of the total measured heat of reaction represents the heat of wetting of the reaction products. Differential thermal analyses and drying experiments indicated that $3CaO\cdot 2SiO_2\cdot 2H_2O$ was formed in some of the pastes.

1. Introduction

The reactions of lime with silica and water are of fundamental importance in the study of the hydration of portland cement, and are of particular interest in the study of the effect of pozzolans. The energy changes occurring dictate the direction and extent to which the reactions may proceed, and a knowledge of these changes will aid in elucidating the mechanism of the process.

Measurements of the heat of reaction of lime with silica and water fall into three general classes: (1) Determination of the heat of hydration of portland cement; (2) determination of the heat of hydration of the individual compounds occurring in cement; and (3) measurement of the heat of reaction between calcium hydroxide solutions and silica gel. Woods, Steinour, and Starke [1][1] developed the heat-of-solution method of determining the heat of hydration of portland cement, which has evolved into an acceptance test [2,3] for use when it is important to limit the heat evolved during the setting of concrete. Others [4,5,6] have measured the heat of hydration by direct methods, which are, however, limited to relatively short periods. The results of measurements falling in the first group are useful for control and have been extended to determining the contribution of the individual constituents of the cement to the heat of hydration. The direct measurements have been useful in explaining the important reactions that occur in the early stages of the setting of concrete.

The measurements of the heat of hydration of the individual compounds of portland cement have almost without exception been made by the heat-of-solution method. Lerch and Bogue [7], Brunauer, Hayes, and Hass [8], Brisi [9], Thorvaldson, Brown, and Peaker [10], Cirilli [11], and others have determined the heat of reaction of individual compounds with water. Many of these measurements were made with pastes of hydraulic material and water, approximating the proportions and consistency used in placing or testing portland cement. The heats of reaction obtained have been used to aid in the identification of the reaction products [8].

The third class of measurements, also made by the heat-of-solution method, have been made on the reaction products obtained [11, 12, 13] by the reaction between calcium hydroxide solution and silica gel performed in such a manner that a large quantity of solution came into contact with a small quantity of silica gel. These measurements also have been used to aid in identifying the reaction products obtained.

The present paper is the report of the results of heat-of-solution measurements made at intervals over an extended period on pastes of calcium hydroxide, water, and silica gel. The constituents were finely divided and in intimate contact with each other and with the small amount of water, so that local depletion of the calcium hydroxide in solution might be avoided. These measurements should agree with those made in class three above, and together with those of both class two and class three, should provide data for calculating the heats of formation of the reaction products.

2. Apparatus, Materials, and Procedure

2.1. Calorimetry

The heat-of-solution method of measuring the heat of a reaction was used in this work. The procedure consists in measuring the heats of solution of the reactants and the products of the reaction under investigation. A solvent in which all the materials will dissolve should be chosen, or proper corrections made for the heat effects of any insoluble substances. The final solution at the end of the heat-of-solution experiment made with the products must be identical in molar concentration and quantity with the final solution obtained at the end of the heat-of-solution experiment made with the reactants, or the heat effects of the reactions necessary to bring the two final solutions to identity must be obtained and used in the computations. Under these conditions, the heat of the reaction is the difference between the

[1] Figures in brackets indicate the literature references at the end of this paper.

sums of the heats of solution of the products and the sums of the heats of solution of equivalent amounts of the reactants in the same solvent.

In the present work, 1- to 2-g samples of hydrated paste were dissolved in a mixture of nitric and hydrofluoric acids. A total weight of 600.0 g of acid was used, of which 12.6 g (11.0 ml) was 48 percent HF, the remainder being HNO_3,26.03H_2O (2.000 *N* at 25° C) [14]. The composition of the calorimeter acid charge was therefore 0.302HF,1.10 HNO_3,29.11H_2O. Because some of the earlier work [9, 11, 12, 13] had been done with hydrochloric acid, some determinations were made using 600.0 g of HCl,26.61H_2O (2.000 *N* at 25° C) [14]. The heats of solution at 25° C were determined in an isothermal-jacket, platinum-lined calorimeter which has been described previously [15]. At the end of determinations in which HCl was used, the calorimeter acid was filtered and the undissolved silica recovered and weighed.

In determinations of the heat of solution using the nitric-hydrofluoric acid mixture, the quantity of sample dissolved was kept small enough to avoid the precipitation of CaF_2. In this manner the necessity of correcting for the heat effect of the precipitation was avoided. If precipitation occurs, about 9.1 kcal will be evolved for each mole of CaF_2 so formed [16], and the heat of solution obtained will be too high. The data of Brunauer, Kantro, and Weise [17] showed a heat effect of about 60 cal/g of CaO (3.4 kcal/mole) in excess of the normal value of the heat of solution of the CaO when the sample size was increased above about 0.37 g (in 420 g of mixed acids), where precipitation of CaF_2 was observed to begin. With calcium hydroxide in the present work with a larger calorimeter, the corresponding increase was about 20 cal/g of $Ca(OH)_2$ (1.5 kcal/mole) when the sample size was increased above about 1 g. It is evident that in both investigations only partial precipitation of CaF_2 occurred, as the full increase corresponding to 9.1 kcal/mole was not obtained. It has been observed that when the CaO is combined in a silicate much larger samples can be dissolved without precipitating CaF_2. With portland cement, for example, it is possible to dissolve completely 3-g samples in 425 g of mixed nitric-hydrofluoric acid [2] without precipitation of calcium fluoride, although there is approximately 1.5 g of CaO in the sample.

2.2. Differential Thermal Analysis

Differential-thermal-analysis curves were obtained with an apparatus that has been described previously [18]. The curves were recorded automatically, and the heating rate, controlled by a motor-driven variable transformer rotated at constant speed, was about 12.5 deg C/min.

2.3. Preparation of the Pastes

All materials were chemicals of analytical reagent quality. Single lots of calcium hydroxide and silicic acid were used in preparing all the pastes, in order to reduce possible variations in the results caused by differences in surface or other properties of the starting material.

The calcium hydroxide and the silica gel were heated over night at 1,200° C to obtain the losses on ignition. The residues were taken to be CaO and SiO_2, respectively. Seventy-gram mixtures of the unignited materials were prepared. weighing the components to the nearest 0.01 g. The weight of each material to be used was calculated from its ignition residue and the desired C/S ratio.[2] Fifteen mixtures were prepared over the range of molar C/S ratios from 0.3 to 3.3 in such a way as to bracket and to include the simple ratios 0.5, 1.0, 1.5, 2.0, and 3.0. The weighed materials were tumbled for 2 hr in bottles with a few wooden balls to insure uniformity of composition.

The individual mixtures were mixed with distilled water and stored in wax-sealed glass vials in the manner described in Federal Specification SS–C–158c [2]. A water-solids ratio of about 1.0 was used in order to obtain pastes with sufficient fluidity to fill the vials easily.

2.4. Testing the Hardened Pastes

One vial of each mixture was opened for testing at the ages of 1, 7, and 28 days, 16 weeks, and 1 and 2½ years. The samples were dried under vacuum for about 1 hr until enough water had been removed from the damp samples so that they could be crushed and passed through a No. 28 sieve without caking. The total residual water content of samples thus treated was about 50 percent. Crushing and sieving were done as expeditiously as possible to reduce reaction with CO_2 in the atmosphere. The samples were then placed in small rubber-stoppered Erlenmeyer flasks for ease in shaking. Portions were removed for heat-of-solution and loss-on-ignition measurements, CO_2 determinations, and chemical analysis. Only the first two measurements were made on every sample tested. The individual weighed portions of each paste were taken consecutively as quickly as possible, so that one loss-on-ignition value could be applied to all the samples of a single paste. The analytical procedures were started at once, and the heat-of-solution measurements were made thereafter, usually within 2 hr. The samples for the latter test were kept in weighing bottles until used, and no significant change of weight occurred in this period.

3. Results and Discussion

3.1. Heats of Solution of Calcium Hydroxide and Silica Gel

Twelve determinations of the heat of solution of $Ca(OH)_2$ in the HNO_3–HF mixture were made using samples of 0.8 to 1.0 g. No precipitation of CaF_2 was observed. Although the scatter was rather larger than desired, there appeared to be no correla-

[2] The usual notation of C=CaO, S=SiO_2, and H=H_2O will be used. The molar ratio CaO/SiO_2, for example, will be written as C/S.

tion with sample size over this short range. The individual values of the heats of solution were calculated to a molar basis on the assumption that the ignition residue was CaO. The average value, 31.70 ± 0.10 kcal/mole,[3] was somewhat higher than that given by Brunauer, Hayes, and Hass [8] but agreed with the value 31.7 calculated from data available in NBS Circular 500 [16]. The experimental value 31.70 kcal/mole was used for the heat of solution of calcium hydroxide in calculating the heat of reaction of calcium hydroxide and silica gel.

Eight determinations of the heat of solution of the silica gel were made using samples of 1.0 to 2.0 g. The average value 34.78 ± 0.13 kcal/mole was obtained and used in calculations. Roth and Chall [21] obtained 34.49 ± 0.02 kcal/mole at 50° C for silica gel containing about 66.7 percent of water. According to Mulert [22], the heat of solution of silica gel containing 10 percent of water is about 0.24 kcal/mole higher than that of gels containing large amounts of water. In calculations comparing heats of reaction obtained in this investigation with the results of others, correction has been made for this 0.24 kcal.

After removal of the weighed portions for the above mentioned tests, the remainder of the crushed sample was returned to the evacuation chamber until the following day when differential thermal analyses were made and, in some cases, X-ray patterns were obtained. At 1 and 2½ years the parts of the samples remaining after the usual first-day tests were evacuated through a dry-ice trap, according to the procedure of Copeland and Hayes [19], and the heat-of-solution measurements were repeated.

In general, standard analytical procedures were used [2]. The sample for the determination of loss on ignition was dried for 2 hr at 110° C, placed in a cold furnace, and heated to 1,200° C over night. In some of the tests when the standard analysis was not made, the residue from the loss-on-ignition test was fumed twice with HF and heated to 850° C, and the residue weighed as CaF_2 [20]. From the data thus obtained, the C/S ratio of the sample was calculated.

Some additional experiments were made to determine the effect of sample size on the heats of solution of calcium hydroxide and silica gel, and also to determine the effects of either material on the heat of solution of the other. It was found that, within the precision of the present work, neither predissolved $Ca(OH)_2$ nor predissolved silica gel had any significant effect on the heat of solution of the other. Variation of the size of the sample between 0.5 and 1.5 g also had no significant effect on the heat of solution of either substance. These observations were true only if calcium fluoride was not precipitated. With larger samples, if the silica gel was dissolved before the calcium hydroxide was added to the solution, no precipitation of CaF_2 occurred, and the normal value was obtained for the heat of solution of calcium hydroxide, even up to sample weights of 1.5 g. However, if the calcium hydroxide was added first, a high value for its heat of solution was obtained, although seemingly insignificant amounts of precipitated CaF_2 were visible. If the silica gel was then added to the same solution in the calorimeter, a low value was obtained for its heat of solution, and the calcium fluoride redissolved. In one experiment the sum of the high value obtained for the heat of solution of calcium hydroxide and the low value obtained for silica gel was equal, within 1.2 cal/g, to the sum of the normal value of the heat of solution of silica gel and the value obtained for the heat of solution of calcium hydroxide, when the presence of predissolved silica gel prevented the precipitation of calcium fluoride.

The heat of solution of the calcium hydroxide in HCl, $26.61H_2O$ (2.000 N at 25° C) was determined for use in calculations to be made using the heat of decomposition of the calcium hydroxide-silica gel pastes in that acid. The heat effect of adding the silica gel was also determined. The values obtained were 31.26 and 1.01 kcal/mole for the calcium hydroxide and silica gel, respectively. Tests showed that the presence of either substance previously added to the calorimeter solution did not alter significantly the heat effect obtained for the other material.

3.2. Heats of Solution of the Pastes

The analyses and heats of solution of the pastes are given in table 1. The heats of solution were calculated to kilocalories per mole of silica in the paste. For this purpose, the percentage of silica in the paste, s, was calculated from the original molar C/S ratio and the percentage residue on ignition, R, by the equation $s = 1.071R/(C/S + 1.071)$, in which 1.071 is the ratio of the molecular weights of SiO_2 and CaO, 60.06 and 56.08, respectively.

The C/S ratios calculated from the analyses in table 1 were usually somewhat less than the proportions weighed in making the pastes. However, these calculated ratios are affected by any analytical errors and do not allow for MgO, Fe_2O_3, Al_2O_3, or other nonvolatile impurities in the original materials. Because the proportions of the original mixes and the molar heats of solution of the calcium hydroxide and silica gel were calculated on the basis of the ignited weights of the starting materials, the original C/S ratios were used in all computations.

3.3. Heats of Reaction

Based on 1 mole of silica, the equation representing the formation of a hydrated calcium silicate by the reaction of calcium hydroxide and silica gel in a paste may be written

$$(C/S)Ca(OH)_2 + SiO_2 \cdot pH_2O + qH_2O \rightarrow$$
$$x(aCaO \cdot bSiO_2 \cdot nH_2O) + (C/S - ax)Ca(OH)_2$$
$$+ (1 - bx)SiO_2 \cdot pH_2O + (q - nx + pbx + ax)H_2O \quad (1)$$

The heat of the reaction to form the hydrated calcium silicate may be found from the difference in

[3] The standard deviation of the average is given here and elsewhere in this paper. Heats unless otherwise indicated refer to $-\Delta H$ at 25° C.

TABLE 1. *Analyses and heats of solution of calcium hydroxide—silica gel pastes*

Molar ratio CaO/SiO_2	Age	Analytical results					Heat of solution $-\Delta H$ at 25° C		Fraction of sample insoluble in HCl
		CaO	SiO_2	CO_2	Loss on ignition	Molar ratio CaO/SiO_2 observed	HCl, 26.61 H_2O	0.274 HF, HNO_3, 26.36 H_2O	
1	2	3	4	5	6	7	8	9	10
	Days	%	%	%	%		*cal/g*	*cal/g*	%
	1	------	------	----	50.51	------	------	259.2	------
	7	------	------	----	50.47	------	------	256.9	------
	28	------	------	----	15.57	------	57.6	------	60.57
	28	------	------	----	47.31	------	------	275.7	------
	112	[2](11.53)	(39.21)	----	49.26	0.315	34.23	265.8	38.56
	365	12.49	41.37	----	45.24	.323	36.08	286.9	42.00
0.300	[1]365P	19.76	69.91	1.03	9.48	.303	------	514.9	------
	837	10.48	38.28	0.28	51.03	.293	------	256.9	------
	837P	------	------	----	10.67	------	------	503.7	------
	1	------	------	----	51.46	------	------	251.7	------
	7	------	------	----	50.55	------	------	254.9	------
	28	------	------	----	51.67	------	------	250.5	------
.400	112	(13.31)	(36.55)	----	50.14	.390	43.25	257.8	33.67
	365	14.42	37.33	----	48.24	.414	45.30	266.8	35.18
	365P	24.78	64.14	1.34	9.72	.414	------	510.0	------
	916	13.94	37.71	0.64	47.79	.396	71.39	269.7	35.66
	916P	------	------	----	11.85	------	------	490.1	------
	1	------	------	----	51.76	------	------	245.5	------
	7	------	------	----	53.41	------	------	233.9	------
	28	------	------	----	21.03	------	92.7	------	49.51
	28	------	------	----	53.28	------	------	237.8	------
.500	112	(16.16)	(34.72)	----	49.12	.498	54.29	258.7	30.23
	365	14.73	31.19	----	53.96	.506	48.69	234.5	27.57
	365P	28.20	59.60	1.06	10.51	.507	------	499.6	------
	914	12.83	27.44	0.42	59.79	.501	42.74	205.7	24.40
	914P	------	------	----	11.76	------	------	486.6	------
	1	------	------	----	52.45	------	------	244.0	------
	7	------	------	----	51.22	------	------	249.6	------
	28	------	------	----	51.50	------	------	242.8	------
.700	112	(20.35)	(31.88)	----	47.82	.685	71.37	260.1	22.31
	365	21.37	32.49	----	45.66	.704	73.32	266.4	23.50
	365P	35.55	54.30	1.30	9.75	.701	------	499.4	------
	848	19.13	29.71	0.74	50.83	.690	66.32	245.0	19.45
	848P	------	------	----	10.68	------	------	489.5	------
	1	------	------	----	52.55	------	------	246.6	------
	7	------	------	----	53.50	------	------	228.5	------
	28	------	------	----	23.56	------	138.5	------	17.02
	28	------	------	----	53.26	------	------	230.6	------
.900	112	(22.85)	(27.80)	----	49.35	.880	78.62	248.1	6.08
	365	23.06	27.33	----	49.20	.904	78.39	246.5	4.76
	365P	40.97	49.38	1.62	8.83	.889	------	494.0	------
	841	25.23	30.81	0.97	43.62	.877	87.52	276.1	5.85
	841P	------	------	----	10.24	------	------	485.1	------
	1	------	------	----	52.42	------	------	246.8	------
	7	------	------	----	53.31	------	------	230.7	------
	28	------	------	----	53.93	------	------	229.1	------
1.000	112	(23.80)	(26.31)	----	49.89	.969	84.34	245.1	5.19
	365	25.92	28.27	----	45.47	.982	90.26	267.3	4.61
	365P	42.84	46.56	1.62	8.93	.985	------	495.9	------
	916	23.11	25.46	0.90	50.81	.972	105.7	237.8	2.59
	916P	------	------	----	10.74	------	------	475.1	------
	1	------	------	----	50.30	------	------	257.5	------
	7	------	------	----	51.07	------	------	248.5	------
	28	------	------	----	49.45	------	------	248.3	------
1.200	112	(27.06)	(26.49)	----	46.45	1.094	98.98	261.6	4.55
	365	28.47	27.23	----	43.82	1.120	102.5	275.1	4.34
	365P	45.34	43.93	1.85	9.59	1.105	------	488.6	------
	848	25.54	24.76	1.01	49.28	1.105	91.49	247.9	2.53
	848P	------	------	----	11.25	------	------	480.1	------
	1	------	------	----	52.04	------	------	252.2	------
	7	------	------	----	51.16	------	------	248.8	------
	28	------	------	----	49.60	------	------	252.5	------
	112	(28.30)	(20.71)	----	50.99	1.464	116.2	243.9	3.55
1.500	365	33.13	23.69	----	42.48	1.498	131.7	285.0	3.90
	365P	50.65	36.77	2.07	11.54	1.475	------	480.3	------
	570	28.24	20.53	----	50.90	1.473	------	242.6	------
	570P	------	------	1.94	13.00	------	------	------	------
	846	------	------	1.38	44.46	------	------	273.8	------
	846P	------	------	----	12.84	------	------	466.8	------

Molar ratio CaO/SiO_2	Age	Analytical results					Heat of solution $-\Delta H$ at 25° C		Fraction of sample insoluble in HCl
		CaO	SiO_2	CO_2	Loss on ignition	Molar ratio CaO/SiO_2 observed	HCl, 26.61 H_2O	0.274 HF, HNO_3, 26.36 H_2O	
1	2	3	4	5	6	7	8	9	10
	Days	%	%	%	%		*cal/g*	*cal/g*	%
	1	------	------	----	50.41	------	------	261.3	------
	7	------	------	----	51.46	------	------	245.0	------
	28	------	------	----	53.92	------	------	233.0	------
1.600	112	(28.39)	(19.97)	----	51.64	1.523	116.4	242.8	3.61
	365	34.95	23.93	----	40.30	1.564	143.5	295.0	3.90
	365P	51.48	35.16	1.78	12.42	1.568	------	475.4	------
	917	27.61	18.98	0.97	52.98	1.558	112.1	232.3	2.43
	917P	------	------	----	13.06	------	------	466.0	------
	1	------	------	----	48.60	------	------	271.2	------
	7	------	------	----	54.47	------	------	239.7	------
	28	------	------	----	24.33	------	222.1	------	9.59
	28	------	------	----	56.73	------	------	222.1	------
2.000	112	(31.49)	(17.86)	----	50.65	1.888	136.4	250.2	3.08
	365	31.62	17.59	----	50.29	1.925	136.1	248.1	1.96
	365P	54.61	30.31	2.05	14.27	1.930	------	467.1	------
	849	30.96	17.13	1.25	51.51	1.936	133.7	241.2	1.90
	849P	------	------	----	14.55	------	------	457.9	------
	1	------	------	----	51.73	------	------	255.7	------
	7	------	------	----	52.37	------	------	246.4	------
	28	------	------	----	52.47	------	------	244.0	------
2.300	112	------	------	----	51.30	------	137.3	246.2	2.65
	365	35.02	17.07	----	47.06	2.197	157.5	267.0	2.66
	365P	56.29	27.41	2.09	15.36	2.199	------	461.3	------
	917	30.13	14.63	0.88	54.82	2.206	136.9	227.3	2.34
	917P	------	------	----	16.30	------	------	451.7	------
	1	------	------	----	48.02	------	------	275.1	------
	7	------	------	----	53.80	------	------	240.7	------
	28	------	------	----	52.55	------	------	245.0	------
	112	------	------	----	49.47	------	159.0	259.7	2.60
2.500	365	39.07	17.21	----	42.78	2.431	178.3	290.6	1.85
	365P	57.81	25.16	2.05	16.26	2.461	------	457.6	------
	849	33.30	14.79	1.31	51.29	2.411	151.9	246.8	1.55
	849P	------	------	----	17.42	------	------	449.8	------
	1	------	------	----	51.42	------	------	262.3	------
	7	------	------	----	51.33	------	------	252.9	------
	28	------	------	----	51.25	------	------	251.1	------
2.900	112	(35.38)	(14.14)	----	50.48	2.680	167.1	255.4	2.15
	365	36.08	13.70	----	49.74	2.821	165.4	255.2	1.39
	365P	59.10	22.37	3.08	17.66	2.830	------	443.6	------
	917	35.79	13.70	----	49.96	2.798	164.5	257.5	0.86
	917P	------	------	----	17.86	------	------	439.8	------
	1	------	------	----	48.81	------	------	273.9	------
	7	------	------	----	48.57	------	------	267.9	------
	28	------	------	----	53.50	------	------	242.2	------
3.000	112	(35.88)	(13.67)	----	50.45	2.811	169.5	256.2	2.54
	365	48.06	17.89	----	33.37	2.877	224.3	340.2	2.39
	365P	59.44	21.94	3.16	17.75	2.902	------	446.1	------
	918	40.29	15.02	1.27	44.36	2.873	229.9	285.7	1.76
	918P	------	------	----	17.63	------	------	446.9	------
	1	------	------	----	47.94	------	------	279.8	------
	7	------	------	----	50.11	------	------	260.5	------
	28	------	------	----	23.76	------	278.5	------	6.09
	28	------	------	----	51.47	------	------	253.4	------
3.333	112	(38.70)	(13.23)	----	48.07	3.133	185.5	268.8	2.53
	365	44.28	14.89	----	39.84	3.185	211.0	310.2	2.33
	365P	60.42	21.02	2.42	17.75	3.078	------	452.2	------
	846	------	------	1.37	49.26	------	179.3	261.7	0.97
	846P	60.51	20.37	----	18.37	3.181	------	442.4	------

[1] "P" indicates that sample was kept at water vapor pressure of about ½ micron (ice at dry ice temperature) until loss fell below 0.5 mg/g/day.
[2] Figures in parentheses were obtained by fuming the ignition-loss sample with HF and weighing the CaF_2 formed, as described in the text.

the sums of the heats of solution of the products and the reactants in the usual manner. If heats of dilution are neglected, the uncombined calcium hydroxide, silica gel, and water will contribute nothing to this difference, because their molar heats of solution will be the same after the reaction as before. Equation (1) can then be rewritten

$$ax\mathrm{Ca(OH)_2}+bx\mathrm{SiO_2}\cdot p\mathrm{H_2O}+(nx-ax-pbx)\mathrm{H_2O}\rightarrow x(a\mathrm{CaO}\cdot b\mathrm{SiO_2}\cdot n\mathrm{H_2O})+\Delta H \qquad (2)$$

where ΔH is the observed difference between the heat of solution of the paste containing the hydrated calcium silicate and the sum of the heats of solution of the reactants from which the paste was formed. If ΔH is calculated per mole of silica in the whole paste, its value increases with the amount of silica entering the reaction (i. e., bx) until a final constant value is reached when all of the silica has been combined ($bx=1$). This calculation does not depend on a knowledge of the composition of the hydrated calcium silicates formed. If the final values of ΔH are plotted against the C/S ratios of a series of pastes, the curve will consist of a series of straight lines intersecting at the compositions of the hydrated calcium silicates formed. The slope of each line will be proportional to the heat of the reaction involved.

In the foregoing discussion a number of corrections have been neglected. These are: The heat effect of dissolving silica gel and calcium hydroxide separately rather than simultaneously, the effect of sample size on the value obtained for the heat of solution (excluding the effect of precipitated CaF_2), and the heat effect of diluting the calorimeter acid with the water formed in the hydration reaction or present in the paste. Experiments have already been described that showed the first two of these effects to be negligible in the present work. The heat of solution of the water contained in the paste is approximately equal to the partial molar heat content of water in HNO_3, $26{\cdot}03H_2O$ and in HF, $100H_2O$, 0.002 and 0.0004 kcal/mole of H_2O, respectively [16]. These quantities are also negligible.

The heat-of-reaction technique was used by Cirilli [12] to determine the composition of the hydrated calcium silicate produced by the reaction between calcium hydroxide solution and silica gel. He determined the heat of decomposition of the reaction product in hydrochloric acid in calories per gram of CaO. The heat of solution calculated from these measurements remained constant up to C/S=1 and then increased with further increase in C/S. It was hoped that the procedure used in the present investigation would, by reason of the longer times of reaction and larger C/S ratios involved, give on the curve of ΔH versus C/S ratio a more definite change of slope indicating the formation and composition of a compound containing more CaO than monocalcium silicate hydrate, such as the $3CaO{\cdot}2SiO_2{\cdot}nH_2O$ reported by Cirilli and others. Unfortunately this hope was not realized.

In figure 1 are shown the heats of reaction of $Ca(OH)_2$, silica gel, and water (reaction 2) for each of the pastes of table 1, plotted as a function of the time. The major portion of the heat of reaction was released in 1 to 7 days. At C/S ratios larger than 0.5, the reaction proceeded further slowly. This behavior suggests that at any C/S ratio the monocalcium silicate hydrate reported by Cirilli was formed promptly, and that a more basic product was formed subsequently in pastes with C/S ratios

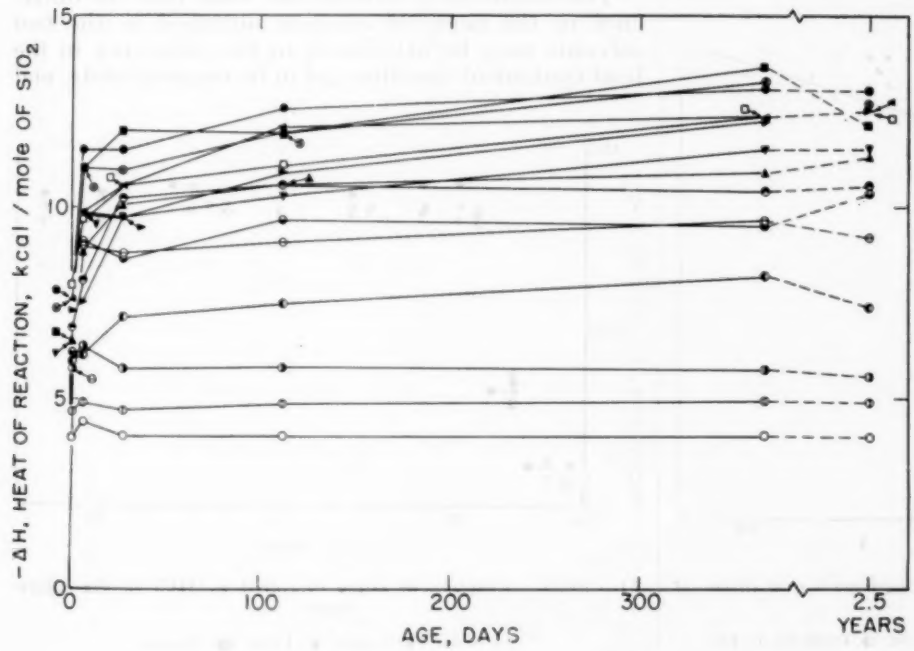

FIGURE 1.—*Heat of reaction of calcium hydroxide and silica gel as a function of time of contact.*

C/S	C/S	C/S
○0.3	◒1.0	◀2.3
◔0.4	◓1.2	□2.5
◑0.5	▲1.5	■2.9
◐0.7	▼1.6	⊗3.0
⊖0.9	▶2.0	●3.3

larger than 1. In figure 2 are shown the heats of reaction of the pastes at 1 year plotted against the C/S ratio. The two straight lines A and B shown in the figure, represent the least-squares equations calculated from the present data for C/S ratios, for A, of 0.3 to 1.0 inclusive, and, for B, of 1.0 to 3.33 inclusive. The average value of the intersections of these two lines with C/S=1 is 10.3 kcal/mole of silica. This value is taken as the heat of reaction of calcium hydroxide and silica gel to form the monocalcium silicate hydrate. The corresponding value calculated from Cirilli's data [11,12,13] is 10.96 kcal/mole. The slope of the line between C/S=1 and C/S=3.33 is 1.58. The value of 1.6 kcal/mole of added $Ca(OH)_2$ is therefore taken as the heat of reaction of calcium hydroxide and 1 mole of monocalcium silicate at 1 year to form material of C/S ratios higher than one. This heat of reaction is so small that it easily might be heat of adsorption of calcium hydroxide on the monocalcium silicate hydrate. The precision of the data is not adequate to show definitely a change of slope indicating a change in the way the lime is combined, such as that reported by Cirilli at C/S=1.5.

The data taken at 2½ years are similar to the 1 year results. The heat of reaction and the slope of the line B were found to be 10.5 and 1.06 kcal/mole, respectively. The slightly increased amounts of CO_2 found in the samples at the later age may in part account for the differences in the heat effects. No correction has been made for the small CO_2 content of any of the samples. It is more likely, however, that surface or other changes in the pastes are responsible for the differences.

Brunauer, Hayes, and Hass [8] determined the heat of hydration of C_3S and C_2S to be 22.0 and 4.1 kcal/mole, respectively. From their results the heats of reaction of $Ca(OH)_2$, water, and silica gel to form the hydrated calcium silicates produced by the hydration of C_3S and C_2S have been calculated to be 11.96 and 12.13 kcal/mole, respectively. These values are plotted in figure 2. Considering the uncertainties involved, the agreement is good.

The heats of reaction calculated from Cirilli's data are also plotted in figure 2. The agreement is excellent until the C/S ratio becomes larger than 1.0. Cirilli's results are based on the assumption that the silica gel contributed nothing to the heat of solution in HCl, being precipitated at the end of the heat-of-solution experiment in its original form. In the present work this assumption could not be made, because the heats of reaction as measured with nitric-hydrofluoric acid mixtures were not the same as those determined using hydrochloric acid. A considerable amount of the silica in the paste remained dissolved in the HCl at the end of each determination, and its heat of solution was included in the measured value. In figure 3 is shown the fraction of the silica dissolved in the HCl, plotted as a function of the C/S ratio of the paste. If the soluble silica were taken as an indication of the reaction between calcium hydroxide, silica gel, and water, as was done by Shaw and MacIntire [23], it would appear that the reaction was not ended, even after the lapse of 2½ years and in the presence of excess $Ca(OH)_2$. The measurement of the fraction of soluble silica does seem to represent some property of the paste, as it generally increases with increased age of the paste, and it would appear reasonable to correct the measured heat of reaction accordingly. However, if a correction is made, using the silica insoluble in HCl to represent unreacted silica, large (at low C/S) and inconsistent values are obtained for the heat of reaction. The values shown in figures 1 and 2, therefore, have not been corrected.

Thermochemical calculations show that the difference in the heats of reaction obtained in the two solvents may be attributed to the difference in the heat content of the silica gel in its original state, and

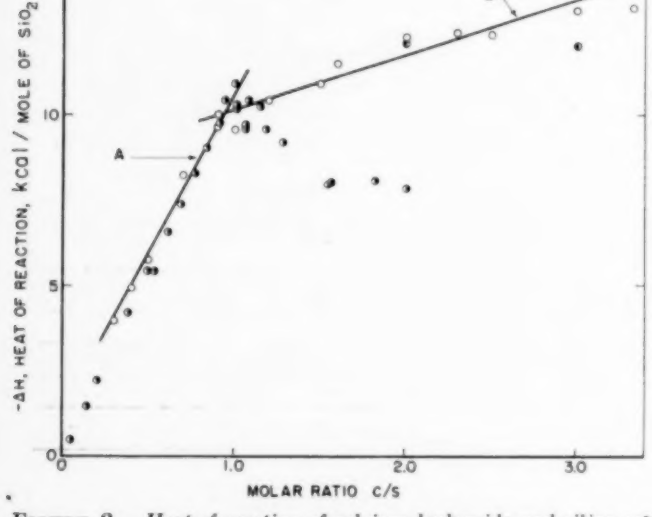

FIGURE 2.—*Heat of reaction of calcium hydroxide and silica gel at 1 year.*

○, Newman; ◐, Brunauer, Hayes, and Hass [8]; ◑, Cirilli [11, 12, 13].

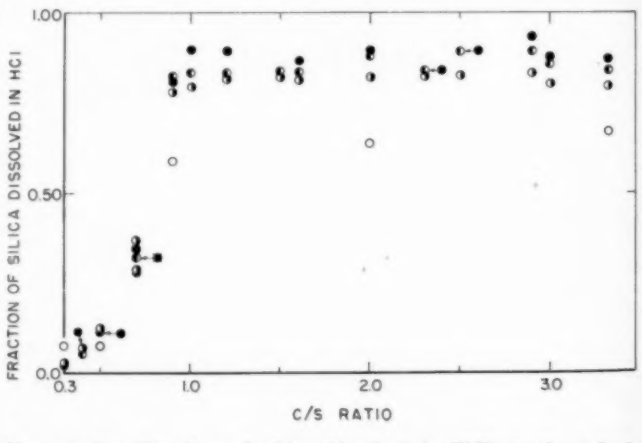

FIGURE 3.—*Fraction of silica dissolved in* HCl *in the calorimeter.*

○, 28-day; ◑, 16-week; ◐, 1-year; ●, 2½-year.

as a component of the hydrochloric acid solutions resulting when the hydrated pastes were dissolved. The differences, after dividing by the fractions of the silica dissolved in the hydrochloric acid solutions, were scattered about an average value (excluding those determined at C/S ratios of less than 0.7) of $\Delta H = -4.8 \pm 0.25$ kcal/mole of dissolved silica. This value may be considered as a measure of the heat of gelation of silica gel from the low-molecular-weight form occurring in hydrochloric acid solution. Tourky [24] has given $\Delta H = -8.9$ kcal/mole as the heat of gelation from alkaline solution, and Greenberg [25] has estimated a value of -2.7 kcal/mole for the heat of polymerization of silica gel.

3.4. Heat of Adsorption of Water

It has been concluded [8] that under the conditions of drying used in this work all of the water adsorbed on the hydrated calcium silicate in the paste would be removed. The difference in the heats of solution of the pastes before and after drying should, therefore, be equal to the heat of adsorption of the water. These heats of adsorption are shown in figure 4 as a function of the C/S ratio. The values found both at 1 year and 2½ years are given; the latter are generally the smaller. The heats of adsorption of water on the reactants were calculated from similar heats of solution determined before and after drying the calcium hydroxide and silica gel. The line representing the reactants is shown in figure 4, calculated from the equation $H_{SiO_2} + (C/S)H_{CaO} = H_{reactants}$, where H_{SiO_2} is the heat of adsorption of water on the dried silica gel (of composition $SiO_2, 0.21H_2O$) and H_{CaO} is the heat of adsorption of water on the dried $Ca(OH)_2$. The data indicate that the heat of adsorption is considerably larger for the pastes than for the reactants, and that it becomes slightly larger as the C/S ratio increases. Older samples show less heat of adsorption of water. These phenomena may be caused by differences in surface area of the materials. Brunauer et al. [8] have calculated the heat of adsorption of water on hydrated di- and tricalcium silicate from their data combined with that of Verbeck and Foster [26] and found values corresponding to 4.8 kcal/mole of SiO_2. Their values, about 2 kcal/mole smaller than those found in the present work, are plotted in figure 4. Five values calculated from Cirilli's data are also shown.

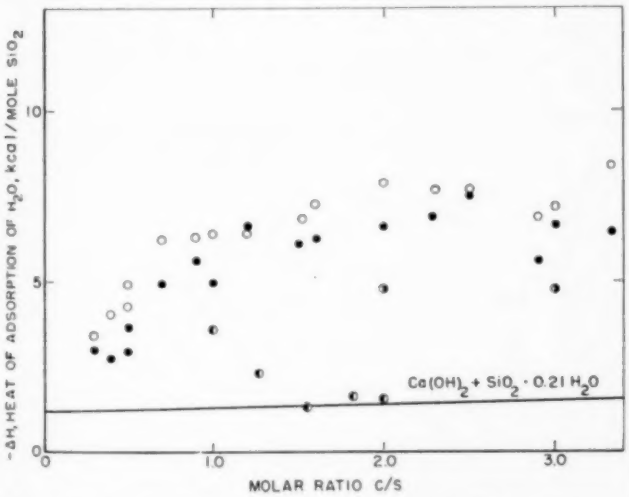

FIGURE 4.—*Heat of adsorption of water on hydrated pastes.*

○, 1-year, Newman; ●, 2½-year, Newman; ◑, Brunauer, Hayes, and Hass [8]; ◐, Cirilli [11, 12, 13].

3.5. Differential Thermal Analysis

Differential thermal analyses (DTA) were obtained for each sample at each age of test. Partially dried samples were tested. Figures 5, 6, and 7 show some of the curves of particular interest. Curves obtained at 16 weeks are shown in figures 5 and 6. Figure 7

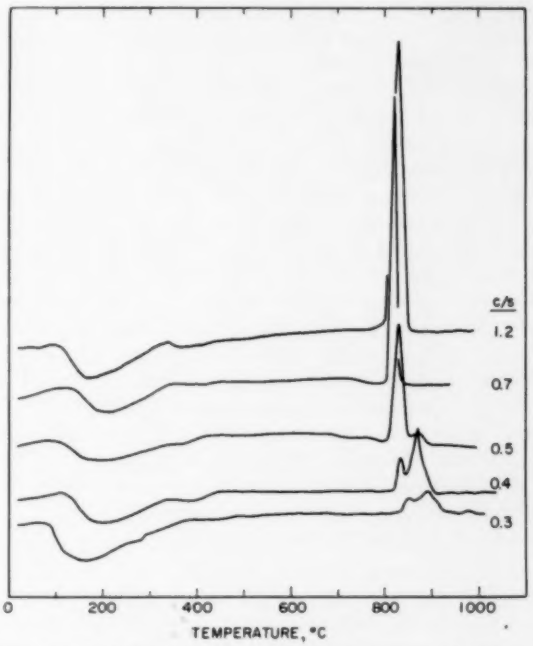

FIGURE 5.—*Differential-thermal-analysis curves of pastes at 16 weeks.*

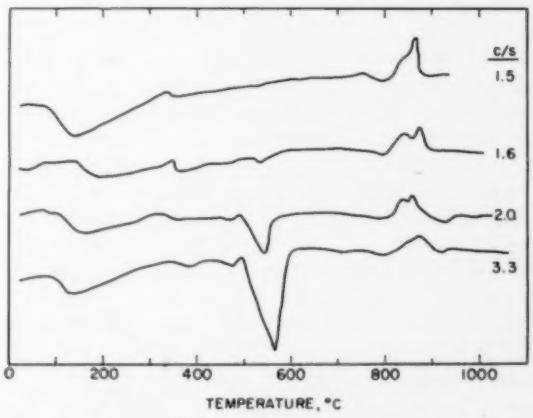

FIGURE 6.—*Differential-thermal-analysis curves of pastes at 16 weeks.*

shows the curves obtained at six ages of test for the sample with a C/S ratio of 1.5. All the features observed for any of the samples are shown on one or another of these curves. The curves all show a broad endotherm in the range 80° to 350° C, which is attributed in part to the loss of adsorbed and free water and which resembles that found for silica gel. Two other endotherms found in the range 350° to 500° C were assumed to be associated with the loss of chemically bound water from the hydrated calcium silicates formed in the pastes.

The presence of calcium hydroxide is clearly shown in the curves in figure 6, representing samples with C/S ratios of 1.6 or more at the age of 16 weeks. The endotherm representing its decomposition in the DTA apparatus occurs between 480° and 600° C with individual peak temperatures of 525° to 570° C in the various samples. The increased amount of calcium hydroxide with increased C/S ratio is clearly indicated by the relative sizes of the endotherms. The continued reaction of $Ca(OH)_2$ with silica gel, or with hydrated calcium silicate already formed with a C/S ratio less than 1.5, is clearly shown by the curves of figure 7, where the curves for a sample of that ratio are plotted for the different ages tested. The large amount of $Ca(OH)_2$ present at 1 day is reduced by continued reaction, as indicated by the reduced size of the endotherm with increased age, until at 16 weeks no $Ca(OH)_2$ was found by DTA. Curves not presented showed no $Ca(OH)_2$ at 1 day for samples having C/S ratios of 0.9 or less. DTA curves of all samples with C/S ratios greater than 1.5 showed the presence of $Ca(OH)_2$ at all ages tested. It is concluded from this part of the DTA curves that the calcium hydroxide reacts very rapidly with the silica gel up to a C/S ratio of about 1, and that little further reaction occurs, within the time limit of these tests, after a silicate with the C/S ratio of 1.5 has been formed.

Two exotherms representing reactions between CaO and SiO_2 in the DTA apparatus were found, one at about 830° C and one at about 900° C. The exact temperatures at which they are located on the DTA curves are dependent on many variables, including the degree of packing and the size of the samples, the placing of the thermocouples, and the fraction of the sample entering the reactions, so for convenience the exotherms will be identified merely by their relative positions at the higher or lower temperature. (The approximately linear time-temperature curves of the samples were violently distorted when these exotherms occurred, but the exotherms are plotted as though each time-temperature curve had followed the straight line connecting its branches above and below the exotherms. This method of plotting is approximately equivalent to plotting the differential temperature against the temperature of the inert body over this portion of the DTA curve.)

These two exotherms indicate that changes occurred in the pastes after the $Ca(OH)_2$ had disappeared. For example, from the curves in figure 7, the exotherm at the higher temperature was the smaller at 1 day but grew, somewhat at the expense of the other, as the age of the sample increased. The lower endotherms, however, never completely disappeared from the curve for the sample with a C/S ratio of 1.5. Similar behavior occurred at higher ratios, although the intensity of the upper exotherm was less than at 1.5. At lower C/S ratios except for the sample with a ratio of 1.2, there was practically no change of the two exotherms with age of the pastes. There was, however, a change with change in composition. As the C/S ratio increased from 0.3 to 0.7 the lower exotherm increased at the expense of the upper until the latter disappeared. At ratios of 0.7 to 1.0 only the lower exotherm was found, but at higher ratios both were again present. Up to 4 weeks the sample with a C/S ratio of 1.2 behaved like that with the 1.5 ratio, but at later ages only the lower exotherm was present.

The behavior of the exotherms indicates a change in the nature of the reacted paste between C/S ratios of 1.2 and 1.5. It must be emphasized that the exotherms represent reactions occurring in the furnace after the hydrated compounds have been destroyed, and they can not at present be related directly to the nature of the paste itself. X-ray patterns were made on samples obtained by interrupting DTA's at temperatures below, between, and above the two exotherms, but the reactions causing the exotherms were not identified. Lines of CaO, of β and γC_2S, and α and β CS were found in all the patterns. Kalousek [27] found similar exotherms at somewhat different temperatures for mixtures of CaO and SiO_2 that had undergone hydrothermal treatment, and also for a product of the composition

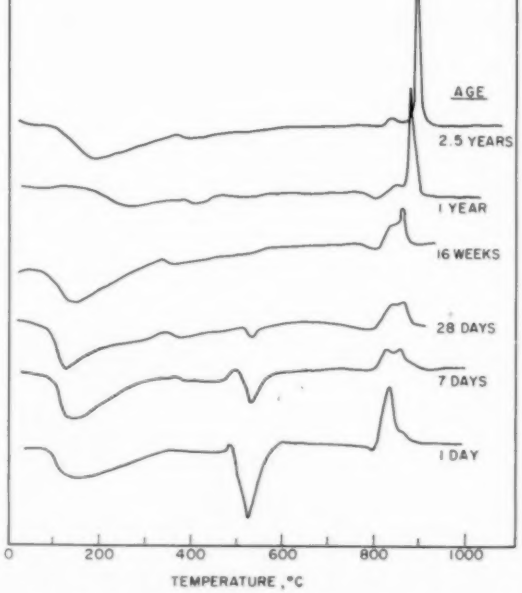

FIGURE 7.—*Differential-thermal-analysis curves of pastes with C/S ratio of 1.5.*

$C_3S_4H_n$ prepared at room temperature. Differences in apparatus and techniques could easily account for differences in his observed temperatures and those found here.

3.6. Nonevaporable Water

The nonevaporable water remaining in the dried pastes must be held in 1 of 3 ways. A portion is chemically bound in $Ca(OH)_2$ in samples containing that material in excess either free or adsorbed. A portion is retained by the silica gel remaining in samples having a proportion of unreacted silica. The remainder of the water is retained in the calcium silicate, and a study of the data in table 1 should indicate the amount of water so held in these pastes.

Bernal [28] and Taylor [29] have given formulas corresponding to $3CaO{\cdot}2SiO_2{\cdot}3H_2O$ and $3CaO{\cdot}2SiO_2{\cdot}2H_2O$, respectively, for the composition of one of the hydrated calcium silicates formed at room temperatures. Accordingly, computations were made from the data in table 1 to see to which, if either, of these compositions the hydrated silicate formed in the pastes corresponded. The amounts of SiO_2 and CaO in the dried samples were calculated from the original C/S ratios and the losses on ignition. The water in each paste was taken as the difference between the ignition loss and the CO_2 content. The total CaO was reduced by the amount assumed combined with the CO_2 to form $CaCO_3$. It had been found that vacuum drying at room temperature would not reduce the water content of the silica gel below an H/S ratio of 0.21, and it was assumed that this amount of water was retained by any unreacted silica in the pastes. It was assumed that in pastes of C/S ratios less than 1.00 the constituents would be SiO_2, $0.21H_2O$ and CSH_n, and that in pastes of C/S ratios larger than 1.5 the constituents would be $Ca(OH)_2$ and $C_{1.5}SH_n$. The values of n were calculated on these assumptions from the CaO, SiO_2, and H_2O contents of the dried pastes. For the two samples with C/S ratios between 1.0 and 1.5, the values of n were calculated on the assumption that C_mSH_n was formed, where m is the corrected C/S ratio of the paste.

The results of these calculations are shown in figure 8, where the values of n are plotted against the corrected C/S ratios. The value of n is less than the C/S ratio at all values of C/S greater than 0.7, and is approximately 1 at C/S ratios greater than 1.5. The hydrated silicate formed in many of these pastes, therefore, appears to correspond in composition to Taylor's formula, $3CaO{\cdot}2SiO_2{\cdot}2H_2O$.

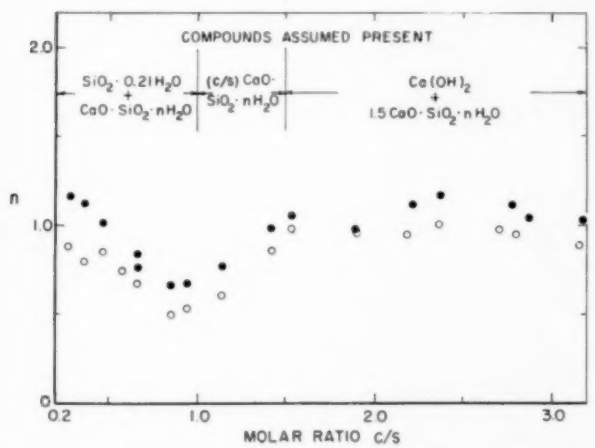

FIGURE 8.—*Nonevaporable water content of hydrated pastes of calcium hydroxide and silica gel.*

○, 1-year; ●, 1½-year.

4. Summary

The heat of reaction of calcium hydroxide in pastes with silica gel and water was measured by a heat-of-solution method. It was found that the heat of the reaction

$$Ca(OH)_2 + SiO_2 \cdot nH_2O = CaO \cdot SiO_2 \cdot nH_2O$$

is about 10.3 kcal, of which about 5 kcal is the heat of wetting of the reaction product. The heat of the reaction

$$CaO \cdot SiO_2 \cdot nH_2O + mCa(OH)_2 = (1+m)CaO \cdot SiO_2 \cdot (n+m)H_2O$$

is about 1.6 kcal per mole of added $Ca(OH)_2$.

Calcium hydroxide reacts with silica gel and water in pastes at room temperature to form hydrated calcium silicate with a C/S ratio as high as 1.5. Above that ratio the $Ca(OH)_2$ is less firmly bound so that its presence is revealed by differential thermal analysis, although the heat of reaction per mole of silica continues to increase. Continued changes in the paste with time and with C/S ratio are indicated by changes in the behavior of the heated pastes in the DTA furnace at temperatures above 800°C.

Drying experiments indicated that the nonevaporable water remaining in the pastes was less than that equivalent to the CaO on a 1:1 molar basis. Above a C/S ratio of 1.5 the compositions of the dried pastes corresponded to the formula $[3CaO{\cdot}2SiO_2{\cdot}2H_2O]\,[Ca(OH)_2]_x$.

5. References

[1] H. Woods, H. H. Steinour, and H. R. Starke, Ind. Eng. Chem. **24,** 1207 (1932).
[2] Federal Specification for cements, hydraulic, SS–C–158c.
[3] ASTM Designation C186–55.
[4] R. W. Carlson, Proc. Am. Soc. Testing Materials **34,** 322 (1934).
[5] R. W. Carlson and L. R. Forbrich, Ind. Eng. Chem., Anal. Ed. **10,** 382 (1938).
[6] W. Lerch, Proc. Am. Soc. Testing Materials **46,** 1252 (1946).
[7] W. Lerch and R. H. Bogue, BS J. Research **12,** 645 (1934) RP684.
[8] S. Brunauer, J. C. Hayes, and W. E. Hass, J. Phys. Chem. **58,** 279 (1954).
[9] C. Brisi, Ricerca sci. **24,** 1436 (1954).
[10] T. Thorvaldson, W. G. Brown, and C. R. Peaker, J. Am. Chem. Soc. **52,** 3927 (1930).
[11] V. Cirilli, Ricerca sci. **10,** 459 (1939).
[12] V. Cirilli, Ann. chim. appl. **28,** 151 (1938).
[13] V. Cirilli, Ann. chim. appl. **28,** 239 (1938).

[14] International Critical Tables, National Research Council **3,** 58 (McGraw-Hill Book Co., Inc., New York, N. Y., 1933).
[15] E. S. Newman and L. S. Wells, J. Research NBS **20,** 825 (1938) RP1107.
[16] F. D. Rossini, D. D. Wagman, W. H. Evans, S. Levine, and I. Jaffe, Selected values of chemical thermodynamic properties, NBS Circ. 500 (U. S. Government Printing Office, Washington 25, D. C., 1952).
[17] S. Brunauer, D. L. Kantro, and C. H. Weise, J. Phys. Chem. **60,** 771 (1956).
[18] E. S. Newman and L. S. Wells, J. Research NBS **36,** 137 (1946) RP1696.
[19] L. E. Copeland and J. C. Hayes, ASTM Bul. 194, p. 70 (Dec. 1953).
[20] W. F. Hillebrand, G. E. F. Lundell, H. A. Bright, and J. I. Hoffman, Applied inorganic analysis, 2d ed. (J. Wiley & Sons, Inc., New York, N. Y., 1953).
[21] W. A. Roth and P. Chall, Z. Elektrochem. **34,** 185 (1928).
[22] O. Mulert, Z. anorg. Chem. **75,** 198 (1912).
[23] W. M. Shaw and W. H. MacIntire, Soil Sci. **29,** 429 (1930).
[24] A. Tourky, Chemistry & Industry **1942,** 254.
[25] S. A. Greenberg (private communication).
[26] G. J. Verbeck and C. W. Foster, Proc. Am. Soc. Testing Materials **50,** 1235 (1950).
[27] G. L. Kalousek, Proc. Third International Symposium, Chemistry of Cement, London, 1952, p. 299 (Cement and Concrete Assoc., 52 Grosvenor Gardens, London, SW1, 1954).
[28] J. D. Bernal, ibid, p. 233.
[29] H. F. W. Taylor, J. Chem. Soc. **1953,** 163.

WASHINGTON, February 15, 1957.

Journal of Research of the National Bureau of Standards Vol.59, No. 3, September 1957 Research Paper 2786

On Some Expansions for Bessel Integral Functions

F. Oberhettinger[1]

Investigations by van der Pol and Humbert concerning the Bessel integral function of order zero are extended to Bessel functions of other kinds and to functions related to Bessel functions.

The Bessel integral function of order zero,

$$Ji_0(x)=-\int_x^\infty t^{-1}J_0(t)dt, \tag{1}$$

was introduced by van der Pol [8].[2] Equivalent [3, 4, 6] with (1) is

$$Ji_0(x)=\frac{1}{\pi}\int_0^\pi Ci(x\sin t)dt. \tag{2}$$

Various properties of this function have been investigated by Humbert [4]. A number of definite integrals, especially of the Fourier or Laplace transform type, can be reduced to (1). For this reason tables of $Ji_0(x)$ have been published previously [5]. The numerical computation of $Ji_0(x)$ requires the transformation of the integral in (1) into an expression involving a series in either ascending powers (for not too large x) or descending powers (for large x) of the variable x. One of these expansions [4, 6] is

$$Ji_0(x)=\gamma+\log\frac{x}{2}+\sum_{n=1}^\infty\frac{(-1)^n(x/2)^{2n}}{2n(n!)^2}, \tag{3}$$

where one can write

$$\sum_{n=1}^\infty\frac{(-1)^n(x/2)^{2n}}{2n(n!)^2}=\int_0^x t^{-1}[J_0(t)-1]dt.$$

An asymptotic expansion of $Ji_0(x)$ for large x [5, 7] is listed in (6). The preparation of a set of numerical tables by the Computation Laboratory made it necessary to derive expansions of types (3) and (6) for functions defined similarly to (1) but with $J_0(t)$ replaced by another kind of Bessel or related function. The established results are listed below. (A list of notations and auxiliary formulas is given at the end of this paper.)

$$\frac{\pi}{2}Yi_0(x)=-\frac{\pi}{2}\int_x^\infty t^{-1}Y_0(t)dt=\frac{1}{2}\left(\log\frac{x}{2}\right)^2+\gamma\log\frac{x}{2}$$
$$+\frac{\gamma^2}{2}-\frac{\pi^2}{12}-\sum_{n=1}^\infty\frac{(-1)^n(x/2)^{2n}}{2n(n!)^2}\left[\psi(n+1)+\frac{1}{2n}-\log\frac{x}{2}\right], \tag{4}$$

$$Ki_0(x)=-\int_x^\infty t^{-1}K_0(t)dt=-\frac{1}{2}\left(\log\frac{x}{2}\right)^2-\gamma\log\frac{x}{2}-\frac{\gamma^2}{2}-\frac{\pi^2}{24}+\sum_{n=1}^\infty\frac{(x/2)^{2n}}{2n(n!)^2}\left[\psi(n+1)+\frac{1}{2n}-\log\frac{x}{2}\right]. \tag{5}$$

Both these expressions correspond to (3) and are suitable for not too large x.

For large x we have the asymptotic expansions of the following functions:

$$\int_x^\infty t^{-1}\begin{Bmatrix}J_0(t)\\Y_0(t)\end{Bmatrix}dt\sim\begin{Bmatrix}J_0(x)\\Y_0(x)\end{Bmatrix}\left[\frac{2}{x^2}-\frac{2^2\cdot4}{x^4}+\frac{2^2\cdot4^2\cdot6}{x^6}-\cdots\right]-\begin{Bmatrix}J_1(x)\\Y_1(x)\end{Bmatrix}\left[\frac{1}{x}-\frac{2^2}{x^3}+\frac{2^2\cdot4^2}{x^5}-\frac{2^2\cdot4^2\cdot6^2}{x^7}+\cdots\right], \tag{6}$$

[1] Guest worker, National Bureau of Standards, from The American University.

[2] Figures in brackets indicate the literature references at the end of this paper.

$$\int_x^\infty t^{-1}K_0(t)dt \sim -K_0(x)\left[\frac{2}{x^2}+\frac{2^2\cdot 4}{x^4}+\frac{2^2\cdot 4^2\cdot 6}{x^6}+\cdots\right]+K_1(x)\left[\frac{1}{x}+\frac{2^2}{x^3}+\frac{2^2\cdot 4^2}{x^5}+\frac{2^2\cdot 4^2\cdot 6^2}{x^7}+\cdots\right], \tag{7}$$

$$\int_x^\infty t^{-1}[\boldsymbol{H}_0(t)-Y_0(t)]dt \sim \frac{2}{\pi x}\sum_{n=0}^{\infty}(-1)^n\left[\frac{(2n)!}{n!}\right]^2\frac{(2x)^{-2n}}{2n+1}, \tag{8}$$

$$\int_0^x [\boldsymbol{H}_0(t)-Y_0(t)]\,dt-\frac{2}{\pi}\log(2x)-\frac{2}{\pi}\gamma \sim -\frac{2}{\pi}\sum_{n=1}^{\infty}(-1)^n\frac{(2n)!(2n-1)!}{(n!)^2}(2x)^{-2n}, \tag{9}$$

$$\int_0^x [I_0(t)-\boldsymbol{L}_0(t)]\,dt-\frac{2}{\pi}\log(2x)-\frac{2}{\pi}\gamma \sim -\frac{2}{\pi}\sum_{n=1}^{\infty}\frac{(2n)!(2n-1)!}{(n!)^2}(2x)^{-2n}. \tag{10}$$

Furthermore, we derive the identity

$$\int_x^\infty t^{-2}\boldsymbol{H}_1(t)dt=(2x)^{-1}\boldsymbol{H}_1(x)+\frac{1}{2}\int_x^\infty t^{-1}\boldsymbol{H}_0(t)dt. \tag{11}$$

Note that with (6) we know the asymptotic expansion of $\int_x^\infty t^{-1}\boldsymbol{H}_0(t)dt$ for large x by virtue of (8). With this and the known asymptotic expansion of $\boldsymbol{H}_1(x)$ (see (21)), the asymptotic expansion of (11) is likewise known.

a. *Proof of* (4) *and* (5). We write

$$\int_x^\infty t^{-1}J_\nu(t)dt=\int_0^\infty t^{-1}J_\nu(t)dt-\int_0^x t^{-1}J_\nu(t)dt,$$

and since (using term-by-term integration)

$$\int_0^x t^{-1}J_\nu(t)dt=\sum_{m=0}^{\infty}\frac{(-1^m(x/2)^{\nu+2m}}{m!\Gamma(\nu+m+1)(\nu+2m)},$$

we obtain by (23)

$$\int_x^\infty t^{-1}J_\nu(t)dt=\frac{1}{\nu}\left[1-\frac{(x/2)^\nu}{\Gamma(1+\nu)}\right]-\sum_{m=1}^{\infty}\frac{(-1)^m(x/2)^{\nu+2m}}{m!\Gamma(\nu+m+1)(\nu+2m)}.$$

This defines an integral function of ν. If we now let ν tend to zero, using (13) we obtain the expansion (3). In order to prove (4), we differentiate the preceeding formula with respect to ν. If we again let ν tend to zero, using (12) and (13) we obtain (4). Finally, the relation

$$K_0(t)=\frac{1}{2}i\pi[J_0(it)+iY_0(it)],$$

together with (3) and (4), yields (5).

b. *Proof of* (6) *and* (7). We replace the Lommel functions in (24) by their asymptotic expansion (22), and the results in (6) follow immediately. Again, the relation

$$K_0(t)=\frac{1}{2}i\pi[J_0(it)+iY_0(it)],$$

together with (6), yields (7). (Note that the asymptotic expansion of

$$\int_x^\infty t^u\begin{Bmatrix}J_\nu(t)\\Y_\nu(t)\\K_\nu(t)\end{Bmatrix}dt$$

can be obtained in the same way.)

c. *Proof of* (8). From (21) we have, for $v=0$ and large t,

$$t^{-1}[\boldsymbol{H}_0(t)-Y_0(t)]\sim\frac{2}{\pi}\sum_{n=0}^{\infty}(-1)^n 2^{-2n}\left[\frac{(2n)!}{n!}\right]^2 t^{-2n-2}.$$

Integrating term by term, we obtain (8).

d. *Proof of* (9). We use (19) and obtain, interchanging the order of integration,

$$\int_0^x[\boldsymbol{H}_0(t)-Y_0(t)]dt=\frac{2}{\pi}\int_0^{\infty}v^{-1}(1+v^2)^{-1/2}(1-e^{-xv})dv.$$

Because it is necessary to represent the l. h. s. function of x as an integral of the Laplace transform type in order to apply Watson's lemma [1] for the determination of its asymptotic expansion, we form, using (14),

$$\int_0^x[\boldsymbol{H}_0(t)-Y_0(t)]dt-\frac{2}{\pi}\log x=\frac{2}{\pi}\int_0^{\infty}v^{-1}[(1+v^2)^{-1/2}-e^{-v}]dv+\frac{2}{\pi}\int_0^{\infty}e^{-xv}v^{-1}[1-(1+v^2)^{-1/2}]dv.$$

The first integral on the r. h. s. is a constant equal to $\gamma+\log 2$. The second integral is of the Laplace transform type and can easily be developed asymptotically for large x. We obtain first

$$\begin{aligned}\int_0^{\infty}v^{-1}[(1+v^2)^{-1/2}-e^{-v}]dv&=\lim_{\delta\to 0}\left[\int_{\delta}^{\infty}v^{-1}(1+v^2)^{-1/2}dv-\int_{\delta}^{\infty}v^{-1}e^{-v}dv\right]\\&=\lim_{\delta\to 0}\left\{Ei(-\delta)-\log\left[\frac{1+(1+v^2)^{1/2}}{v}\right]_{\delta}\right\}\\&=\gamma+\log 2,\qquad\text{by (15).}\end{aligned}$$

The asymptotic expansion of the second integral for large x is as follows. We expand

$$v^{-1}[1-(1+v^2)^{-1/2}]=-\sum_{n=1}^{\infty}\frac{(-1)^n(2n)!2^{-2n}v^{2n-1}}{(n!)^2}.$$

The application of Watson's lemma [1] gives (9).

e. *Proof of* (10). We use (20) to obtain

$$\int_0^x[I_0(t)\boldsymbol{L}_0(t)]dt=\frac{2}{\pi}\int_0^1 v^{-1}(1-v^2)^{-1/2}(1-e^{-vx})dv,$$

and proceed precisely as before, arriving at the intermediate result

$$\int_0^x[I_0(t)-\boldsymbol{L}_0(t)]dt-\frac{2}{\pi}\log(2x)-\frac{2}{\pi}\gamma=\frac{2}{\pi}\left\{-Ei(-x)+\int_0^1 v^{-1}e^{-vx}[1-(1-v^2)^{-1/2}]dv\right\}.$$

We expand

$$v^{-1}[1-(1-v^2)^{-1/2}]=-\sum_{n=1}^{\infty}\frac{2^{-2n}(2n)!v^{2n-1}}{(n!)^2}.$$

The application of Watson's lemma [1] gives (10). (Note that the term $-Ei(-x)$ is purely formal and may be omitted, because its asymptotic expansion consists of the product of an exponential function with negative exponent and a series in descending powers of x.)

f. *Proof of* (11). By means of (18) we obtain

$$\int_x^{\infty}t^{-2}\boldsymbol{H}_1(t)dt=-\frac{2}{\pi}\int_0^1(1-v^2)^{1/2}\,\mathrm{si}\,(vx)dv.$$

By partial integration,

$$\int_x^\infty t^{-2}\boldsymbol{H}_1(t)dt=-\frac{1}{2}\,\mathrm{si}\,(x)+\frac{1}{2}\,x^{-1}\boldsymbol{H}_1(x)+\frac{1}{\pi}\int_0^1 v^{-1}\sin^{-1}v\,\sin\,(vx)dv,$$

but

$$\int_0^1 v^{-1}\sin^{-1}v\,\sin\,(vx)dv=\frac{1}{2}\,\pi\,\mathrm{si}\,(x)+\frac{1}{2}\,\pi\int_x^\infty t^{-1}\boldsymbol{H}_0(t)dt,$$

and (11) follows at once.

Notations:

$J_\nu(t)$ = Bessel function of the first kind.
$Y_\nu(t)$ = Bessel function of the second kind.
$I_\nu(t)$ = modified Bessel function of the first kind.
$K_\nu(t)$ = modified Bessel function of the second kind.
$\boldsymbol{H}_\nu(t)$ = Struve's function.
$\boldsymbol{L}_\nu(t)=-ie^{-i\nu\pi/2}\boldsymbol{H}_\nu(it)$.

All these functions are Bessel or related functions of the order ν.

$\Gamma(z)$ = Gamma function.
$\psi(z)=\Gamma'(z)/\Gamma(z)$.
$\gamma=-\psi(1)=0.577215\ \ldots\ldots$ (Euler's constant).
$S_{\mu,\nu}(z)$ = Lommel's function.

$$\left[\frac{\partial J_\nu(z)}{\partial\nu}\right]_{\nu=0}=\frac{\pi}{2}Y_0(z)\qquad[9,\text{ p. }61,62]\tag{12}$$

$$\frac{1}{\Gamma(1+z)}=1+\gamma z+\left(\gamma^2-\frac{\pi^2}{6}\right)\frac{z^2}{2}+O(z^3)\tag{13}$$

(Taylor expansion of $1/\Gamma(1+z)$ near $z=0$).

Integral representations:

$$\log x=\int_0^\infty v^{-1}(e^{-v}-e^{-xv})dv\qquad[2,\text{ p. }17]\tag{14}$$

$$\mathrm{Ei}(-\delta)=-\int_\delta^\infty v^{-1}e^{-v}dv\tag{15}$$

$$\mathrm{Ci}(\delta)=-\int_\delta^\infty v^{-1}\cos v\,dv\tag{16}$$

$$\mathrm{si}(\delta)=-\int_\delta^\infty v^{-1}\sin v\,dv.\tag{17}$$

The last three functions are the exponential integral, the cosine integral, and the sine integral, respectively.

$$\Gamma\left(\nu+\frac{1}{2}\right)\boldsymbol{H}_\nu(t)=2\pi^{-1/2}\left(\frac{1}{2}t\right)^\nu\int_0^1(1-v^2)^{\nu-(1/2)}\sin(vt)dv,\qquad\mathrm{Re}\,\nu>-\frac{1}{2}\qquad[9,\text{ p. }328]\tag{18}$$

$$\boldsymbol{H}_0(t)-Y_0(t)=\frac{2}{\pi}\int_0^\infty e^{-tv}(1+v^2)^{-1/2}dv\qquad[9,\text{ p. }331]\tag{19}$$

$$I_0(t)-\boldsymbol{L}_0(t)=\frac{2}{\pi}\int_0^1 e^{-tv}(1-v^2)^{-1/2}dv.\qquad[9,\text{ p. }338]\tag{20}$$

Asymptotic expansions for large z:

$$\boldsymbol{H}_\nu(z)-Y_\nu(z)\sim\pi^{-3/2}\cos(\pi\nu)\left(\frac{1}{2}z\right)^{\nu-1}\sum_{n=0}^{\infty}\frac{(-1)^n\Gamma(\frac{1}{2}-\nu+n)(2n)!}{n!z^{2n}} \qquad \text{[9, p. 333]} \qquad (21)$$

$$S_{\mu,\nu}(z)\sim z^{\mu-1}\left\{1-\frac{(\mu-1)^2-\nu^2}{z^2}+\frac{[(\mu-1)^2-\nu^2][\mu-3)^2-\nu^2]}{z^4}-\cdots\right\}. \qquad \text{[9, p. 351]} \qquad (22)$$

Integral formulas:

$$\int_0^\infty t^{\mu-1}J_\nu(t)dt=2^{\mu-1}\Gamma\left(\frac{1}{2}+\frac{1}{2}\mu\right)/\Gamma\left(1+\frac{1}{2}\nu-\frac{1}{2}\mu\right), \qquad -\operatorname{Re}\nu<\operatorname{Re}\mu<\frac{3}{2} \qquad \text{[9, p. 391]} \quad (23)$$

$$\int_z^\infty t^{-1}\begin{Bmatrix}J_0(t)\\Y_0(t)\end{Bmatrix}dt=2x\begin{Bmatrix}J_0(x)\\Y_0(x)\end{Bmatrix}S_{-2,1}(x)-x\begin{Bmatrix}J_1(x)\\Y_1(x)\end{Bmatrix}S_{-1,0}(x). \qquad \text{[9, p. 350]} \qquad (24)$$

[1] E. T. Copson, Theory of a complex variable, p. 218 (Oxford Univ. Press, London, 1946).

[2] A. Erdelyi, Higher transcendental functions, vol. 1, Bateman Manuscript Project, Calif. Inst. Technol. (McGraw-Hill Book Co., Inc., New York, N. Y., 1953).

[3] P. Humbert, Sur les fonctions de Bessel integrales, Compt. rend. **195**, 854–855 (1932).

[4] P. Humbert, Bessel integral functions, Proc. Edinburgh Math. Soc. **3**, 276–285 (1933).

[5] A. N. Lowan, G. Blanch, and M. Abramowitz, Table of $Ji_0(\mathrm{x})=\int_x^\infty J_0(t)/t\,dt$ and related functions, J. Math. Physics **22**, 51–57 (1943).

[6] G. Petiau, La theorie des fonctions de Bessel, p. 251–258 (Centre National de la Recherche Scientifique, Paris, 1955).

[7] V. G. Smith, An asymptotic expansion of $Ji_0(x)=-\int_x^\infty J_0(t)/t\,dt$, J. Math. Physics **22**, 58–59 (1943).

[8] B. van der Pol, On the operational solution of linear differential equations and an investigation of the properties of their solutions, Phil. Mag. **8**, 861–898 (1929).

[9] G. N. Watson, Bessel functions (Cambridge Univ. Press, England, 1944).

WASHINGTON, February 27, 1957.

Journal of Research of the National Bureau of Standards Vol. 59, No. 3, September 1957 Research Paper 2787

Table of the First Moment of Ranked Extremes

Julius Lieblein* and Herbert E. Salzer**

Let a sample in n independent random values from the extreme-value distribution, with c.d.f. $\Phi(y)=\exp(-e^{-y})$, be arranged in decreasing order and denoted by $y_1, y_2, \ldots, y_m, \ldots, y_n$. The table gives the expected values for all these order statistics for sample size not exceeding 25. For the larger samples, up to $n=100$, the expected values are given only for the first 26 largest values.

1. Explanation and Use of Table

Table 1, prepared at the suggestion of Bradford F. Kimball, gives the expected values, $E(y_m)$, of order statistics from the type I distribution of "reduced" largest values, $\text{Prob}\{Y\leq y\}=\Phi(y)=\exp(-e^{-y})$. This distribution was discussed in considerable detail in a series of lectures by E. J. Gumbel [1].[1] The entries were computed from the formula given by B. F. Kimball [2],

$$E(y_m)=C+\sum_{t=0}^{m-1}(-1)^t\binom{n}{t}\Delta^t \ln(n-t), \qquad m=1,2,\ldots,n, \quad (1)$$

where

$$y_1\geq y_2\geq \ldots \geq y_m\geq \ldots \geq y_{n-1}\geq y_n$$

denotes the order statistics, that is, the observations in a sample of n arranged in *decreasing* order of magnitude. The quantity $C=0.57721566\ldots$ is Euler's constant. The values $E(y_m)$ are tabulated herein for

$$m=1(1)\min(n,26)$$

$$n=1(1)10(5)60(10)100.$$

The table of the first moment of ranked extremes is one of the many tables furnishing pertinent information concerning the extreme-value distribution of type I. At one time Kimball [2] advocated use of such values in plotting extreme-value data on a special-scale extreme-value plotting paper. Because in this method the *largest* sample values are important, computations have not been carried beyond the 26th largest value ($m=26$) for sample sizes $n>26$. Subsequent investigation [3] indicated other criteria that should be given consideration, such as the shortest confidence interval of fixed probability, which applies to the plotting position.

However, there arise other situations in which it is important to know where these mean values $E(y_m)$ are located, and with the great increase in application of the extreme-value distribution this table should be a valuable asset.

A recent important use relates to the determination of best linear unbiased estimators for the parameters u, β of the distribution of largest values [2] in general form

$$\text{Prob}\{X\leq x\}=F(x)=\exp(-e^{-y}), \qquad y=(x-u)/\beta,$$

or in general, for estimators of a given linear combination such as $u+a\beta$ with a known. The condition of unbiasedness involves a knowledge of the means, $E(y_m)$, of the order statistics in samples from the reduced distribution $\Phi(y)$. These are provided by the present table. The second condition, "best" i. e., minimum variance subject to the first condition, involves in addition the variances and covariances of the order statistics $\sigma^2(y_m)$, $\sigma(y_m y_p)$.

This problem has been treated by Lieblein [4], and numerical results up to $n=6$ appear in a paper by Lieblein and Zelen [5].

2. Interpolation Chart [3] for $E(y_m)$

In order to furnish values of $E(y_m)$ for samples of sizes not included in the table an interpolation chart designed by B. F. Kimball is appended (fig. 1).

The curves in the chart connect points having the same ranking. Thus, the lowest curve is for the expected values of the largest in a sample of size n; the second lowest curve relates to the second largest, etc. Each curve has two branches that meet at a vertex situated at the expected value of the median for an odd sample size. These vertices are connected by a nearly vertical line, and it is interesting to note how rapidly they approach the population median $-\ln(-\ln 0.50)=0.3665\ldots$ as sample size n increases.

*Present address, David Taylor Model Basin, Washington, D. C.
**Present address, Convair-Astronautics, San Diego, Calif.

[1] Figures in brackets indicate the literature references at the end of this paper.

[2] The scale parameter β is the same as the parameter $1/a$ used in reference [1].

[3] This section has been contributed by B. F. Kimball.

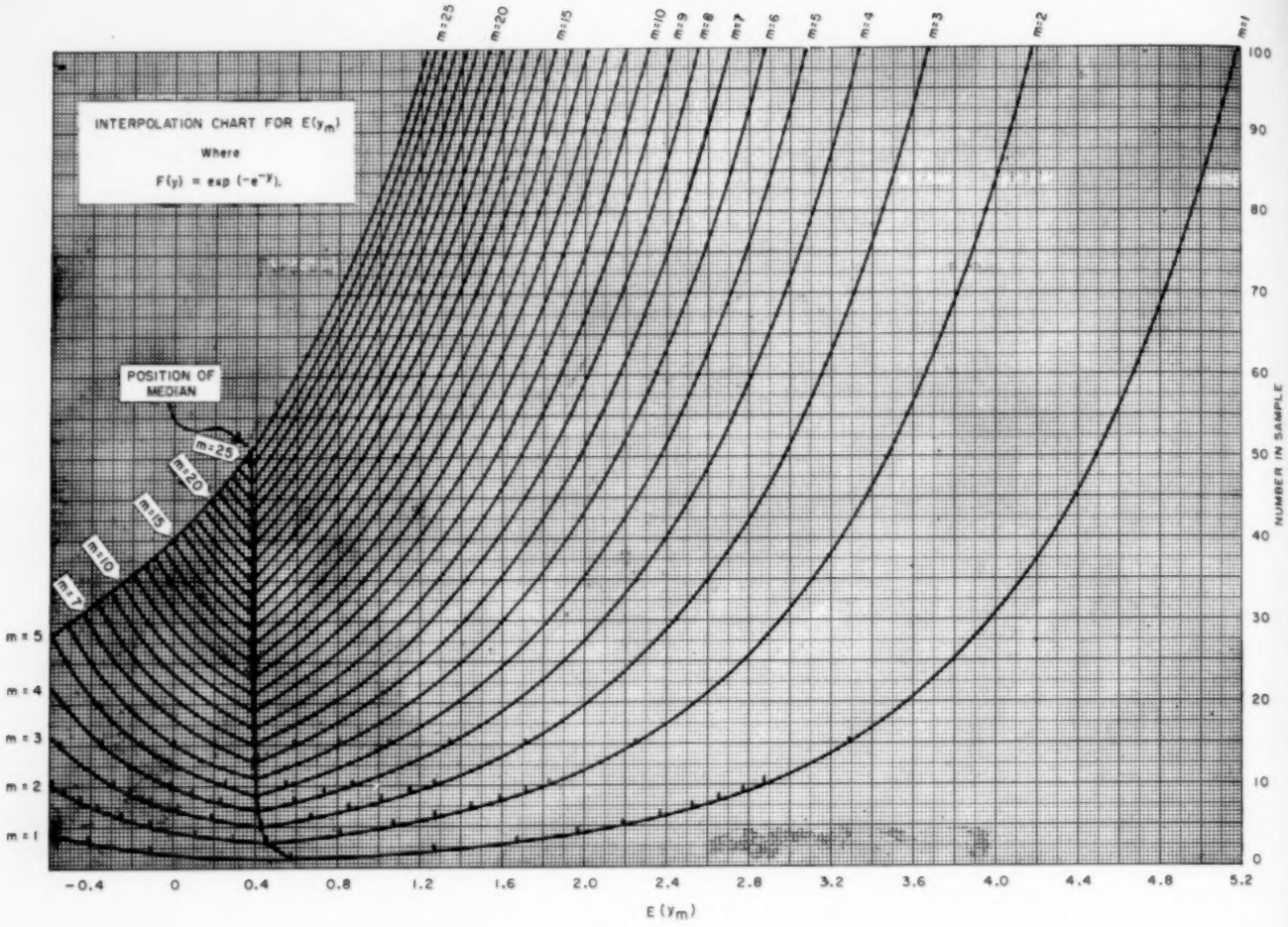

FIGURE 1.

The curves for m=constant rising to the left do not necessarily terminate in the positions shown in this figure. However, values in the range beyond the curves as shown are rarely needed. In other words, the line joining these apparent end-points might better have been omitted.

For samples of n not in the table, the interpolation chart may be used mainly for finding the expected values for the ranks in the upper half of the sample. For example, let $n=75$. Then the intersections of the horizontal line $n=75$ with the curves $m=1$, $m=2, \ldots,$ are read from the horizontal scale at the bottom as follows:

$n=75$

m	$E(y_m)$
1	4.90
2	3.88
3	3.38
4	3.04
.	.
.	.
.	.
26	0.88

3. Method of Computation

Logarithms of N from 1 to 120 to 48 decimal places from J. Wolfram's table [6] were punched on cards. The successive differences of the logarithms were then obtained with the aid of the IBM CPC-I. Sufficient differences were taken to attest to the accuracy of the functions and the individual differences. Values of the binomial coefficients were obtained from Peters and Stein's table [7], and the computation of $E(y_m)$ from eq (1) was then performed using desk calculators. The following partial check was then applied for $n \leq 25$:

$$\frac{1}{n}\sum_{m=1}^{n} E(y_m)=C.$$

For $n>25$ a differencing check was applied. The results are believed to be correct to within 2 units in the last significant figure.

TABLE 1

$$E(y_m) = C + \sum_{t=0}^{m-1} (-1)^t \binom{n}{t} \Delta^t \ln (n-t)!, \text{ where } C = \text{Euler's constant} = 0.57721566\ .$$

Rank from top m	$n=1$	$n=2$	$n=3$	Rank from top m
1	0. 57721 566	+1. 2703 628	1. 6758 280	1
2		−0. 1159 315	+0. 4594 326	2
3			−0. 4036 136	3
m	$n=4$	$n=5$	$n=6$	m
1	1. 9635 100	2. 1866 536	2. 3689 751	1
2	0. 8127 817	1. 0709 358	1. 2750 458	2
3	+. 1090 835	+0. 4255 506	0. 6627 159	3
4	−. 5735 126	−. 1068 945	+. 1883 853	4
5		−. 6901 671	−. 2545 345	5
6			−. 7772 937	6
m	$n=7$	$n=8$	$n=9$	m
1	2. 5231 258	2. 6566 572	2. 7744 402	1
2	1. 4440 711	1. 5884 061	1. 7143 929	2
3	0. 8524 826	1. 0110 660	1. 1474 521	3
4	. 4096 935	0. 5881 770	0. 7382 939	4
5	+. 0224 042	+. 2312 101	. 4005 308	5
6	−. 3653 099	−. 1028 793	+. 0957 534	6
7	−. 8459 576	−. 4527 868	−. 2021 957	7
8		−. 9021 249	−. 5243 843	8
9			−. 9493 425	9
m	$n=10$	$n=15$	$n=20$	m
1	2. 8798 008	3. 2852 659	3. 5729 479	1
2	1. 8261 956	2. 2503 728	2. 5470 821	2
3	1. 2671 822	1. 7132 872	2. 0200 359	3
4	0. 8690 818	1. 3493 534	1. 6583 531	4
5	. 5436 122	1. 0478 353	1. 3785 557	5
6	+. 2574 495	0. 8018 873	1. 1471 396	6
7	−. 0120 439	. 5851 754	0. 9472 338	7
8	−. 2836 893	. 3872 821	. 7690 671	8
9	−. 5845 581	. 2010 161	. 6063 833	9
10	−. 9898 741	+. 0206 140	. 4548 347	10
11		−. 1594 579	. 3111 607	11
12		−. 3458 052	. 1727 124	12
13		−. 5485 327	+. 0371 321	13
14		−. 7883 747	−. 0979 135	14
15		−1. 1326 841	−. 2350 333	15
16			−. 3775 607	16
17			−. 5304 220	17
18			−. 7022 321	18
19			−. 9119 529	19
20			−1. 2232 104	20
m	$n=25$	$n=30$	$n=35$	m
1	3. 7960 915	3. 9784 130	4. 1325 637	1
2	2. 7755 416	2. 9613 665	3. 1179 999	2
3	2. 2542 557	2. 4438 174	2. 6030 713	3
4	1. 8988 407	2. 0923 991	2. 2544 241	4
5	1. 6258 959	1. 8237 416	1. 9887 029	5
6	1. 4020 114	1. 6044 708	1. 7725 500	6
7	1. 2104 327	1. 4178 745	1. 5892 723	7
8	1. 0415 346	1. 2543 779	1. 4293 167	8
9	0. 8892 472	1. 1079 713	1. 2866 988	9
10	. 7494 644	0. 9746 216	1. 1574 147	10
11	. 6192 453	. 8514 772	1. 0386 471	11
12	. 4963 746	. 7364 333	0. 9283 319	12
13	. 3791 010	. 6278 773	. 8249 044	13
14	. 2659 691	. 5245 305	. 7271 437	14
15	. 1557 008	. 4253 445	. 6340 712	15
16	+. 0471 025	. 3294 297	. 5448 828	16
17	−. 0616 213	. 2360 031	. 4589 015	17
18	−. 1699 655	. 1443 471	. 3755 427	18
19	−. 2812 545	+. 0537 740	. 2942 883	19
20	−. 3968 504	−. 0364 087	. 2146 659	20
21	−. 5195 330	− 1269 375	. 1362 310	21
22	−. 6536 981	−. 2186 413	+. 0585 513	22
23	−. 8073 485	−. 3125 115	−. 0188 098	23
24	−. 9984 861	−. 4098 117	−. 0963 110	24
25	−1. 2882 598	−. 5122 664	−. 1744 547	25
26		−. 6224 196	−. 2538 157	26
m	$n=40$	$n=45$	$n=50$	m
1	4. 2660 954	4. 3838 782	4. 4892 387	1
2	3. 2533 828	3. 3725 996	3. 4791 033	2
3	2. 7403 936	2. 8611 039	2. 9687 929	3
4	2. 3937 809	2. 5160 483	2. 6249 676	4
5	2. 1301 969	2. 2540 897	2. 3642 868	5

Rank from top m	$n=40$	$n=45$	$n=50$	Rank from top m
6	1. 9162 926	2. 0418 841	2. 1534 099	6
7	1. 7353 848	1. 8627 537	1. 9756 620	7
8	1. 5779 311	1. 7071 623	1. 8215 109	8
9	1. 4379 596	1. 5691 446	1. 6849 953	9
10	1. 3114 804	1. 4447 183	1. 5621 370	10
11	1. 1956 921	1. 3310 904	1. 4501 482	11
12	1. 0885 487	1. 2262 243	1. 3469 974	12
13	0. 9885 067	1. 1285 871	1. 2511 576	13
14	. 8943 693	1. 0369 939	1. 1614 507	14
15	. 8051 863	0. 9505 080	1. 0769 470	15
16	. 7201 865	. 8683 738	0. 9968 991	16
17	. 6387 319	. 7899 709	. 9206 958	17
18	. 5602 845	. 7147 813	. 8478 294	18
19	. 4843 816	. 6423 661	. 7778 727	19
20	. 4106 182	. 5723 476	. 7104 609	20
21	. 3386 325	. 5043 959	. 6452 792	21
22	. 2680 942	. 4382 186	. 5820 524	22
23	. 1986 951	. 3735 525	. 5205 370	23
24	. 1301 405	. 3101 567	. 4605 148	24
25	+. 0621 408	. 2478 069	. 4017 883	25
26	−. 0055 967	. 1862 904	. 3441 759	26
m	$n=55$	$n=60$	$n=70$	m
1	4. 5845 489	4. 6715 602	4. 8257 109	1
2	3. 5753 462	3. 6631 331	3. 8184 993	2
3	3. 0659 996	3. 1545 855	3. 3111 996	3
4	2. 7231 708	2. 8125 802	2. 9704 763	4
5	2. 4635 211	2. 5537 800	2. 7129 934	5
6	2. 2537 117	2. 3448 473	2. 5054 151	6
7	2. 0770 701	2. 1691 110	2. 3310 720	7
8	1. 9240 664	2. 0170 428	2. 1804 376	8
9	1. 7887 415	1. 8826 854	2. 0475 566	9
10	1. 6671 204	1. 7620 653	1. 9284 576	10
11	1. 5564 180	1. 6523 995	1. 8203 598	11
12	1. 4546 060	1. 5516 619	1. 7212 394	12
13	1. 3601 612	1. 4583 314	1. 6295 780	13
14	1. 2719 091	1. 3712 359	1. 5442 063	14
15	1. 1889 245	1. 2894 532	1. 4642 047	15
16	1. 1104 647	1. 2122 431	1. 3888 367	16
17	1. 0359 236	1. 1390 029	1. 3175 026	17
18	0. 9647 993	1. 0692 342	1. 2497 078	18
19	. 8966 708	1. 0025 197	1. 1850 392	19
20	. 8311 807	0. 9385 062	1. 1231 476	20
21	. 7680 221	. 8768 913	1. 0637 356	21
22	. 7069 285	. 8174 137	1. 0065 469	22
23	. 6476 664	. 7598 456	0. 9513 592	23
24	. 5900 293	. 7039 865	. 8979 781	24
25	. 5338 321	. 6496 584	. 8462 324	25
26	. 4789 079	. 5967 022	. 7959 700	26
m	$n=80$	$n=90$	$n=100$	m
1	4. 9592 423	5. 0770 253	5. 1823 859	1
2	3. 9529 397	4. 0714 283	4. 1773 523	2
3	3. 4465 700	3. 5657 784	3. 6722 760	3
4	3. 1067 984	3. 2267 412	3. 3338 229	4
5	2. 8502 897	2. 9709 823	3. 0786 589	5
6	2. 6437 091	2. 7651 672	2. 8734 497	6
7	2. 4703 881	2. 5926 280	2. 7015 279	7
8	2. 3208 011	2. 4438 397	2. 5533 687	8
9	2. 1889 938	2. 3128 486	2. 4230 189	9
10	2. 0709 961	2. 1956 850	2. 3065 092	10
11	1. 9640 281	2. 0895 700	2. 2010 610	11
12	1. 8660 674	1. 9924 818	2. 1046 529	12
13	1. 7755 969	1. 9029 038	2. 0157 689	13
14	1. 6914 486	1. 8196 690	1. 9332 423	14
15	1. 6127 044	1. 7418 600	1. 8561 563	15
16	1. 5386 292	1. 6687 427	1. 7837 772	16
17	1. 4686 252	1. 5997 200	1. 7155 086	17
18	1. 4021 995	1. 5343 001	1. 6508 589	18
19	1. 3389 408	1. 4720 725	1. 5894 186	19
20	1. 2785 021	1. 4126 915	1. 5308 422	20
21	1. 2205 878	1. 3558 625	1. 4748 362	21
22	1. 1649 442	1. 3013 329	1. 4211 483	22
23	1. 1113 514	1. 2488 842	1. 3695 608	23
24	1. 0596 175	1. 1983 258	1. 3198 839	24
25	1. 0095 742	1. 1494 908	1. 2719 514	25
26	0. 9610 726	1. 1022 318	1. 2256 168	26

The calculations were done in the Computation Laboratory of the National Bureau of Standards. Computations were performed under the supervision of Herbert E. Salzer. The final checking was carried out under the direction of Irene Stegun.

4. References

[1] Statistical theory of extreme values and some practical applications, NBS Appl. Math. Series 33 (1954). See especially lecture 3, p. 19–21, and, for a summary of the characteristics of the distribution, table 3.1 on p. 24–25. For a companion volume of tables see Probability tables for the analysis of extreme-value data, NBS Appl. Math. Series 22 (1953).

[2] B. F. Kimball, Assignment of frequencies to a completely ordered set of sample data, Trans. Am. Geophysical Union **27,** 843–846 (1946). See also discussion of this article in **28,** 951–953 (1947).

[3] B. F. Kimball, An aid to judging precision and bias of graphical fit to data plotted on normal or extreme-value plotting paper, (submitted for publication).

[4] J. Lieblein, On the exact evaluation of the variances and covariances of order statistics in samples from the extreme-value distribution, Ann. Math. Stat. **24,** 282–287 (1953).

[5] J. Lieblein and M. Zelen, Statistical investigation of the fatigue life of deep-groove ball bearings, J. Research NBS **57,** 273–316 (1956) RP2719.

[6] J. Wolfram, Tabula logarithmorum naturalium, p. 641–684 of G. von Vega, Thesaurus logarithmorum completus, Leipzig, 1794 (reprints published by Stechert Hafner, Inc., New York, N. Y., 1923).

[7] J. Peters and J. Stein, Part of appendix to Peters' Zehnstellige Logarithmentafel, Band I (Berlin, 1922).

WASHINGTON, February 26, 1957.

Journal of Research of the National Bureau of Standards Vol. 59, No. 3, September 1957 Research Paper 2788

An Approximate Expression for Gamma-Ray Degradation Spectra

U. Fano and Ann T. Nelms

The equation for gamma-ray degradation spectra is reduced to a form suitable for a simple approximation. The approximation is valid in a wavelength range between two Compton wavelengths larger than the wavelength of the source and the region where photoelectric absorption becomes very intense; this range is wide for low Z materials. Input data are provided for application to various materials and source energies. The results of sample calculations are shown and compared with those obtained by standard numerical calculation.

In the course of gamma-ray penetration, the spectrum of multiply scattered, degraded, secondaries approaches a shape that depends only on the properties of the medium.[1] This limiting spectrum is that which arises when a gamma-ray source is distributed uniformly throughout a medium and the only relevant factor is the accumulation at each point of secondaries of various energies. When degradation spectra were first calculated numerically,[2] M. H. Johnson pointed out, in a private discussion, that the main features of the degradation spectrum at low energies are determined by very simple arguments. A formalism of degradation theory, starting from this remark and from the corresponding neutron theory,[3] was developed later.[4] But this theory was not applied in actual gamma-ray calculations, because these were being carried out routinely by direct numerical computation.[5] Lately, the extension of calculations to degraded photon energies ≈ 20 kev has made it desirable to try to evaluate the simple approximate analytical formulas and compare the results with those obtained by numerical integration of the basic equations. These low photon energies are of interest, e. g., in LiH. This paper contains a description of the procedure, beginning with the qualitative analysis, together with a discussion of the results of the comparison.

If successive steps of degradation by Compton scattering, characterized by wavelength shifts $\xi=\lambda-\lambda'$, have approximately equal statistical distribution (see footnote 4) with a mean $\langle\xi\rangle$, the probability for each photon to attain a wavelength between λ and $\lambda+\Delta\lambda$ at the end of one of the steps of degradation is $\Delta\lambda/\langle\xi\rangle$.[6] If the photon does "land" in this interval, it will "spend" there a mean free path $1/\mu_{\text{scatt}}(\lambda)$, where μ_{scatt} is the probability of scattering per unit pathlength and coincides with the total $\mu(\lambda)$ when absorption is disregarded. For a source strength of S photons per unit volume and unit time, we thus expect at each point a flux of photons in the assigned wavelength range

$$I(\lambda)\Delta\lambda=S[1/\mu(\lambda)](\Delta\lambda/\langle\xi\rangle) \tag{1}$$

per unit area and per unit time. This approximate spectral distribution is expressed in the scale of wavelengths because it is in this scale that the statistical distribution of successive steps of degradation is more nearly a constant.

Equation (1) is subject to three main limitations: (a) It does not hold at photon energies $\gtrsim 500$ kev, where the distribution of degradation steps varies rapidly from step to step; (b) it represents the spectrum for a "steady state" of degration, which does not hold for photons that have been scattered only a very few times because their spectral distribution depends on the source wavelength ("transient" effect) (see footnote 4); (c) it does not take into account outright photon absorption, by photoelectric effect. The effect of absorption can easily be included in (1) as a progressive decay of intensity as λ increases, provided the probability of absorption at each step is small.

Equation (1) is contained as a special case in the solution of degradation problems by successive approximations (see footnote 4). In this solution the degradation spectrum is resolved into steady state and transient components. A numerical calculation of the first few terms of this solution for the X-ray degradation would be possible, but it was found more convenient to proceed as in the analogous electron degradation problem.[7] One starts from an integral form of the degradation equation, namely

$$\int_{\lambda_0}^{\lambda} d\lambda' I(\lambda')\left[\mu_{\text{abs}}(\lambda')+\int_{\lambda}^{\lambda'+2} k(\lambda',\lambda'')d\lambda''\right]=S \tag{2}$$

which represents a sort of "balance sheet" of photons in the entire wavelength range from λ_0 to λ. The source injects S photons per unit volume and unit time at λ_0. Of these, $\int_{\lambda_0}^{\lambda} d\lambda' I(\lambda')\mu_{\text{abs}}(\lambda')$ are lost through outright absorption, and the remainder by Compton scattering with final wavelength $\lambda''>\lambda$,

[1] See, e. g., U. Fano, Nucleonics **11**, Nos. 8 and 9, 55 (1953).
[2] P. R. Karr and J. C. Lamkin, Phys. Rev. **76**, 1843 (1949).
[3] See, e. g., R. Marshak, Rev. Mod. Phys. **19**, 185 (1947), and in particular, G. Placzek, Phys. Rev. **69**, 423 (1946).
[4] U. Fano, Phys. Rev. **92**, 328 (1953).
[5] Calculations of penetration by the moment method, as given by H. Goldstein and J. E. Wilkins, Jr., NYO Report 3075 (1954), include, under the name of "zero-th moment", the spectrum discussed here.
[6] This problem is similar to the determination of the probability that a pedestrian will step on a line drawn across a sidewalk. The probability equals the length of the pedestrian's foot divided by his mean step length.
[7] L. V. Spencer and U. Fano, Phys. Rev. **93**, 1172 (1954).

where $k(\lambda',\lambda'')d\lambda''$ is the probability per unit path-length that a photon of wavelength λ' be scattered to a final wavelength between λ'' and $\lambda''+d\lambda''$. Note that the wavelengths are expressed in Compton units of $h/mc=2.4\times10^{-10}$ cm.

Equation (2) should now be transformed so that it displays an approximate solution similar to (1) and so that the necessary corrections can be easily estimated and then calculated either by successive approximation or by numerical solution of the new equation. To minimize the difficulties (a) and (b) indicated above, we restrict our discussion to wavelengths $\lambda>\lambda_0+2$; thus no photon from the source can reach λ in a single Compton scattering, because $k(\lambda',\lambda'')=0$ for $\lambda''>\lambda'+2$. As a first step we transform the Compton scattering term in (2), by setting $\lambda''=\lambda'+\xi$ and $\lambda'=\lambda-\eta$, and find

$$\int_{\lambda_0}^{\lambda}d\lambda' I(\lambda')\int_{\lambda}^{\lambda'+2}k(\lambda',\lambda'')d\lambda''$$
$$=\int_0^2 d\eta I(\lambda-\eta)\int_{\eta}^{2}k(\lambda-\eta,\lambda-\eta+\xi)d\xi$$
$$=\int_0^2 d\xi\int_0^{\xi}d\eta I(\lambda-\eta)k(\lambda-\eta,\lambda-\eta+\xi). \quad (3)$$

Because the procedure that is being developed is expected to apply when I and k vary slowly with η, it is convenient to represent (3) in a form suited to expansion in powers of η. This is done by an operator symbol based on the power expansion formula

$$f(\lambda-\eta)=f(\lambda)-\eta\frac{\partial}{\partial\lambda}f(\lambda)+\frac{1}{2}\eta^2\frac{\partial^2}{\partial\lambda^2}f(\lambda)$$
$$+\ldots=e^{-\eta\frac{\partial}{\partial\lambda}}f(\lambda). \quad (4)$$

The integrand on the right of (3) can therefore be indicated in the form

$$I(\lambda-\eta)k(\lambda-\eta,\lambda-\eta+\xi)=e^{-\eta\frac{\partial}{\partial\lambda}}I(\lambda)k(\lambda,\lambda+\xi). \quad (5)$$

We consider in particular the value ot (3) for η set equal to zero in the exponent of (5). This value is

$$I(\lambda)\int_0^2 d\xi\,\xi k(\lambda,\lambda+\xi)=I(\lambda)M_1(\lambda). \quad (6)$$

The function $M_1(\lambda)$ defined here is the first moment of tbe wavelength shift and may be expressed as $\mu_{\text{scatt}}\langle\xi\rangle$, which coincides with the denominator of (1). We add the right side of (6) to the expression (3) and subtract its left side from (3), utilize (5) and combine the result with the degradation equation (2), which becomes

$$I(\lambda)M_1(\lambda)+\int_{\lambda_0}^{\lambda}d\lambda' I(\lambda')\mu_{\text{abs}}(\lambda')$$
$$+\int_0^2 d\xi\int_0^{\xi}d\eta\left(e^{-\eta\frac{\partial}{\partial\lambda}}-1\right)I(\lambda)k(\lambda,\lambda+\xi)=S. \quad (7)$$

The solution (1) is thereby obtained if the integrals in this equation can be disregarded by assuming $\mu_{\text{abs}}\approx0$, and $\eta\partial/\partial\lambda\approx0$ in the exponent.

Consider now the absorption, represented by the first integral in (7), taking into account that IM_1 should be effectively constant in the absence of absorption. The absorption term is then written

$$\int_{\lambda_0}^{\lambda}d\lambda'\mu_{\text{abs}}(\lambda')I(\lambda')=\int_{\lambda_0}^{\lambda}d\lambda'\beta(\lambda')[I(\lambda')M_1(\lambda')], \quad (8)$$

showing that IM_1 is effectively reduced, as λ increases, by a fraction

$$\beta(\lambda)\Delta\lambda=\frac{\mu_{\text{abs}}(\lambda)}{M_1(\lambda)}\Delta\lambda=\frac{\mu_{\text{abs}}(\lambda)}{\mu_{\text{scatt}}(\lambda)}\frac{\Delta\lambda}{\langle\xi\rangle} \quad (9)$$

in every small interval $\Delta\lambda$. Notice that this fraction has the dimensions of a pure number. This absorption effect, taken by itself, would cause IM_1 to decay, as λ increases, according to $\exp\left[-\int_{\lambda_0}^{\lambda}\beta(\lambda')d\lambda'\right]$. Accordingly we replace the spectral distribution $I(\lambda)$ with a new unknown $w(\lambda)\approx1$ defined by the expression

$$I(\lambda)=\frac{S}{M_1(\lambda)}e^{-\int_{\lambda_0}^{\lambda}\beta(\lambda')d\lambda'}w(\lambda). \quad (10)$$

When this expression for $I(\lambda)$ is substituted in (7), the source strength S drops out as a common factor. In the first term we use the identity

$$e^{-\int_{\lambda_0}^{\lambda'}\beta(\lambda')d\lambda'}=1-\int_{\lambda_0}^{\lambda}d\lambda'\beta(\lambda')e^{-\int_{\lambda_0}^{\lambda'}\beta(\lambda'')d\lambda''}, \quad (11)$$

so that the second term from this expression may be combined with the absorption term in (7). In the second integral of (7) the term $\exp\left[-\int_{\lambda_0}^{\lambda}\beta(\lambda')d\lambda'\right]$ may be factored out utilizing the operator formula

$$e^{-\eta\frac{\partial}{\partial\lambda}}e^{-\int_{\lambda_0}^{\lambda}\beta(\lambda')d\lambda'}=e^{-\int_{\lambda_0}^{\lambda}\beta(\lambda')d\lambda'}e^{-\eta\left[\frac{\partial}{\partial\lambda}-\beta(\lambda)\right]}; \quad (12)$$

after factoring, (11) is applied again. Equation (7) becomes now

$$w(\lambda)+\int_{\lambda_0}^{\lambda}d\lambda'\beta(\lambda')e^{-\int_{\lambda_0}^{\lambda'}\beta(\lambda'')d\lambda''}\left\{w(\lambda')-\int_0^{\xi}d\xi\int_0^{\xi}d\eta\right.$$
$$\left.e^{-\eta\left[\frac{\partial}{\partial\lambda}-\beta(\lambda)\right]}\frac{k(\lambda,\lambda+\xi)}{M_1(\lambda)}w(\lambda)\right\}+\int_0^2 d\xi\int_{\xi}^{\xi}d\eta$$
$$\left(e^{-\eta\left[\frac{\partial}{\partial\lambda}-\beta(\lambda)\right]}-1\right)\frac{k(\lambda,\lambda+\xi)}{M_1(\lambda)}w(\lambda)=1. \quad (13)$$

This equation is fully equivalent to the initial eq (2), for $\lambda>\lambda_0+2$. Its zero-order approximation solution is $w(\lambda)=1$, obtained by disregarding all the

integrals. To obtain a better approximation, the integrals may be evaluated by whatever procedure appears expedient. We proceed here by expanding into powers of the operator $\partial/\partial\lambda$ and of the rate of absorption β, to first order only. The integral over λ' yields no contribution to first order, because of the factor $\beta(\lambda')$ and because the factor contained in the curly brackets vanishes in zero-th order. Where the zero order approximation $\{\ \}=0$ is poor, for $\lambda<\lambda_0+2$, $\beta(\lambda')$ is very small for most materials. The second integral is evaluated to first order by writing

$$\int_0^\xi d\eta \left(e^{-\eta\left[\frac{\partial}{\partial\lambda}-\beta(\lambda)\right]}-1\right)\approx-\int_0^\xi d\eta\ \eta\left[\frac{\partial}{\partial\lambda}-\beta(\lambda)\right]$$
$$=-\frac{1}{2}\xi^2\left[\frac{\partial}{\partial\lambda}-\beta(\lambda)\right] \tag{14}$$

and $w(\lambda)\approx 1$. Integration over ξ yields the first order estimate of the second integral

$$-\left[\frac{\partial}{\partial\lambda}-\beta(\lambda)\right]\frac{1}{2}\frac{M_2(\lambda)}{M_1(\lambda)} \tag{15}$$

where $M_2(\lambda)=\int_0^2 d\xi\ \xi^2 k(\lambda,\lambda+\xi)$ indicates the second moment of the wavelength shift ξ. Thus we find

$$w(\lambda)=1+\frac{\partial}{\partial\lambda}\frac{1}{2}\frac{M_2(\lambda)}{M_1(\lambda)}-\beta(\lambda)\frac{1}{2}\frac{M_2(\lambda)}{M_1(\lambda)}+\cdots \tag{16}$$

and

$$I(\lambda)=\frac{S}{M_1(\lambda)}\,e^{-\int_{\lambda_0}^{\lambda}\beta(\lambda')\,d\lambda'}\left[1+\frac{\partial}{\partial\lambda}\frac{1}{2}\frac{M_2(\lambda)}{M_1(\lambda)}\right.$$
$$\left.-\beta(\lambda)\frac{1}{2}\frac{M_2(\lambda)}{M_1(\lambda)}+\cdots\right]. \tag{17}$$

The function $(1/2)M_2/M_1$ was determined analytically using the Klein-Nishina formula for Compton scattering. A graphical differentiation was used to obtain $(\partial/\partial\lambda)(1/2)M_2/M_1$. These data, which are the same for all materials, are given in figure 1. The absorption exponent $\int_0^\lambda d\lambda'\beta(\lambda')$, where only photoelectric absorption is included in the tabulations of $\beta(\lambda')$, is given for a few materials in figure 2. The computation of $\beta(\lambda')$ utilized total attenuation coefficients from G. Grodstein [8] and the total Compton cross section from the Klein-Nishina formula. The integration was carried out numerically. Figure 3 gives values of $M_1^{-1}(\lambda)$. The solid curve is a dimensionless plot of the quantity $[(\mu_{\text{Compton}}/\mu_{\text{Thompson}})\langle\xi\rangle]^{-1}$, which is independent of atomic number. For a particular material, the nomograph on the left permits the conversion to units of g/cm². If the source yields S photons $g^{-1}sec^{-1}$, $S/M_1(\lambda)$ is in units $cm^{-2}sec^{-1}(h/mc)^{-1}$.

With the data from figures 1 to 3 the zero-th order expression may be calculated, and the importance of the first order correction may be evaluated

[8] G. W. Grodstein, NBS Circular 583 (1957).

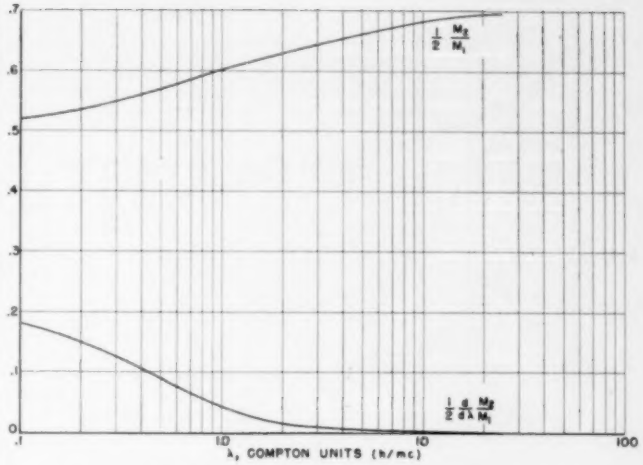

FIGURE 1. *Graph of corrective parameters in eq 17.*

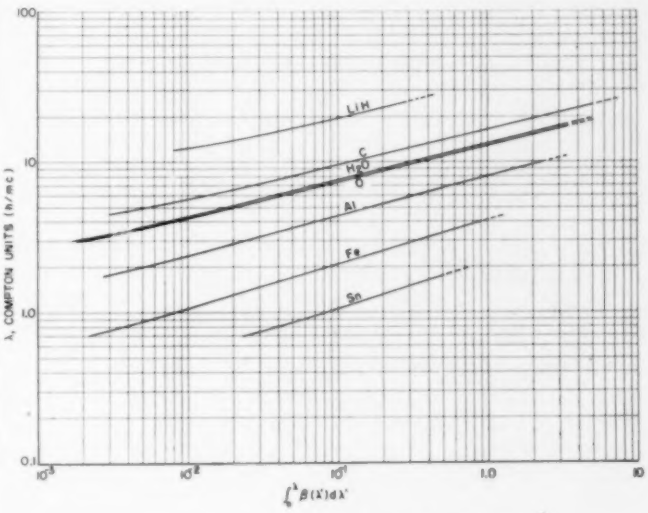

FIGURE 2. *The absorption exponent* $\int_0^\lambda \beta(\lambda')d\lambda'$ *for several materials.*

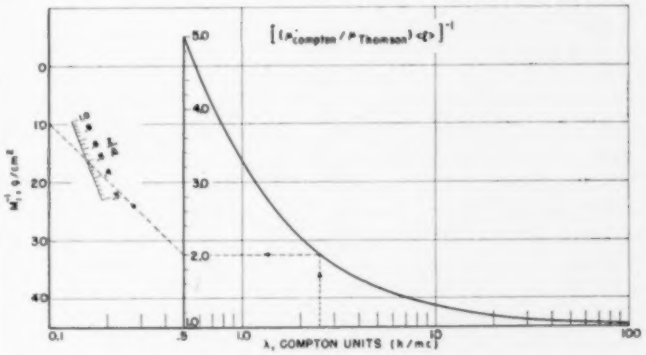

FIGURE 3. *Spectral distribution of photon track length.*

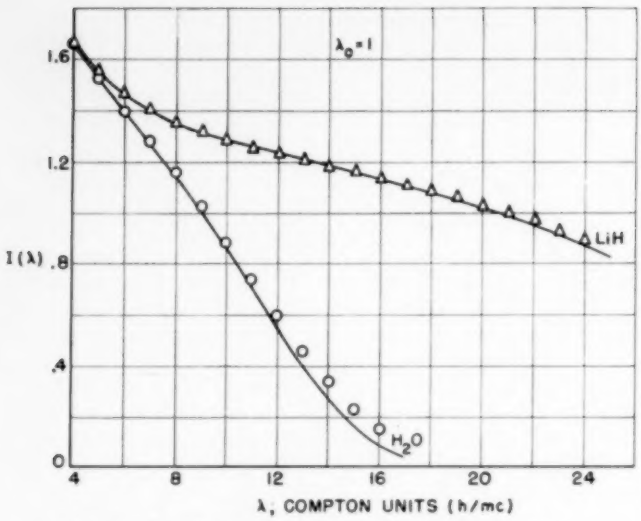

FIGURE 4. *Degradation spectra for* LiH *and* H_2O.
——, Approximation, eq (17); ○,△, exact numerical integration.

readily. This has been done for two cases, namely gamma rays with initial wavelength $\lambda_0=1$ in LiH and H_2O, the source strength S being unity. The results are the curves in figure 4. The points in the figure show the results of direct numerical integration. The agreement is well within the expected accuracy of the approximation. The departures at increasing wavelength reflect the increasing strength of photoabsorption, which leads eventually to a breakdown of the validity of the assumption that the absorption changes little over a wavelength range $\langle\xi\rangle\approx 1$.

Of general interest is the absorption "cut-off" of the spectra. This point, which may be characterized by a parameter λ_Z satisfying the relation $\int_0^{\lambda_Z}\beta(\lambda')$

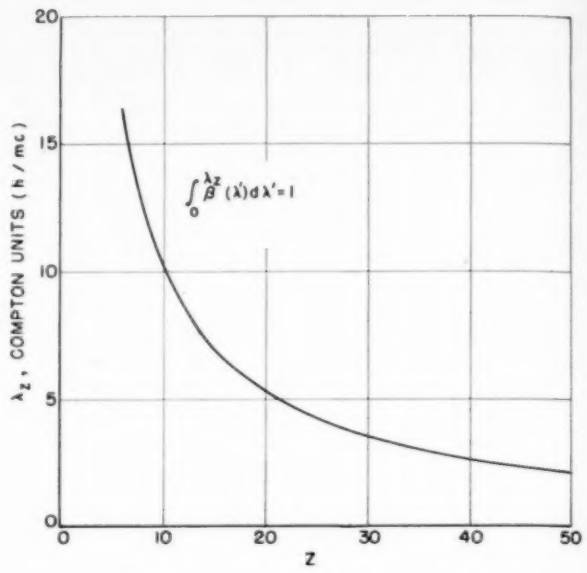

FIGURE 5. *Absorption "cut-off" of the spectral distribution.*

$d\lambda'=1$. It is the wavelength or energy at which the absorption reduces sharply the spectral distribution. Figure 5 gives a curve of λ_Z versus the atomic number Z. Again, the values for $\beta(\lambda')$ take into account only photoelectric absorption.

The authors thank L. V. Spencer and M. Berger for many helpful discussions, and J. C. Lamkin, who contributed the results of the direct numerical integration.

WASHINGTON, March 12, 1957.

Journal of Research of the National Bureau of Standards Vol. 59, No. 3, September 1957 Research Paper 2789

Some Infrared Bands of Deuterium Sulfide [1]

Harry C. Allen, Jr., Earle K. Plyler, and L. R. Blaine

Two regions of the D_2S spectrum have been observed, 5 and 3.6 μ. An analysis of the absorption in the 3.6 μ region attributes it to two overlapping bands with excited states $(v_1,v_2,v_3)=(1,1,0)$ and $(0,1,1)$. The band center of the (0,1,1) band is found to be some 50 cm^{-1} lower than the previously accepted value while the (1,1,0) band center is found some 60 cm^{-1} higher than the previous determination. The absorption near 5 μ seems to arise from the (0,0,1) band centered near 1906 cm^{-1}. Overlapping atmospheric absorption makes a detailed analysis impossible at this time. This band center is almost 100 cm^{-1} lower than previously reported. The excited state constants for the two bands near 3.6 μ are

(1,1,0) $\nu_0=2742.77$ $A^*=5.478$ $B^*=4.512$ $C^*=2.395$

(0,1,1) $\nu_0=2754.44$ $A^*=5.531$ $B^*=4.521$ $C^*=2.405$.

1. Introduction

Although the spectrum of hydrogen sulfide is now fairly well understood, very little work has been done on the totally deuterated compound. The spectrum of D_2S was investigated with low resolution by Bailey, Thompson, and Hale [1] [2] and with somewhat higher resolution by Nielsen and Nielsen [2]. In general these two groups agreed as to the regions of absorption, the only real discrepancy arising in the region near 3.6 μ. Although Nielsen and Nielsen resolved the rotational structure in several regions they did not present a rotational analysis of any of their data. The vibrational assignments of the two groups were completely different. With this considerable confusion existing it was thought advisable to reinvestigate the spectrum of D_2S.

One D_2S band has been successfully analyzed [3] previously, and in the present work the analysis of the rotational structure in the region of 2750 cm^{-1} is reported. The fundamental region near 1900 cm^{-1} was also investigated although the atmospheric absorption in this region makes a complete rotational analysis quite impossible at this time.

2. Experimental Procedure

The intensity of absorption of D_2S is weak, thus it was necessary to use several centimeters pressure of the gas and a path length of 10 m to observe the absorption in the 3.6 μ region. The absorption at 5 μ could be observed satisfactorily with a 1 m cell and several centimeters pressure of the gas.

The spectra were recorded with the grating instruments of the Radiometry Section, using a 7,500 lines/in. grating with a ruled surface of about 6 by 8 in. and a cooled PbTe cell as a detector. The resolution was about 0.2 cm^{-1} The wavelengths of the lines were measured by employing a Fabry-Perot interferometer as previously described [4].

3. Analysis

Figure 1 is a reproduction of a recorder trace of the absorption near 2750 cm^{-1}. The absorption shows a well-defined P-, Q-, R-branch type of structure. The appearance of a collected Q-branch indicates that the change in electric moment is along the least inertial axis, hence A-type selection rules must be invoked [5].

Assignments of the strong lines in the P- and R-branches of the band could be made by using the previously determined ground state [3] of D_2S. From these assignments estimates were made of the excited state inertial parameters from which a trial spectrum was calculated using published tables of the reduced energy [6], $E(K)$.

Relative intensities of the transitions were calculated by combining the Boltzman factor and appropriate nuclear spin statistics with the published values of the line strength [5]. Line strength values were used for $K=0.5$. These were found to be close enough for our purposes. This trial spectrum was compared with the observed spectrum and adjustments were made to improve the agreement by means of the partial derivatives of the energy with respect to the various inertial constants [3]. The final adjustment of the parameters was obtained by carrying out a least squares treatment [3] in which some 90 assignments were used. The agreement between the observed absorption and calculated transitions for these 90 assignments was excellent. The average deviation between the observed and calculated values was 0.07 cm^{-1}.

After assigning the strong transitions of the A-type band, it was found that there was a sizable number of strong absorption peaks still unaccounted for. Closer examination revealed that these peaks arose from a second transition obeying the selection rules for a B-type band. Proceeding in the same manner as for the A-type band it was possible to assign unambiguously about 70 transitions to these absorption peaks with an average deviation of 0.06 cm^{-1}. Strong transitions of these two bands account for almost all the absorption in this region.

[1] The work reported herein was supported by the U. S. Atomic Energy Commission.

[2] Figures in brackets indicate the literature references at the end of this paper.

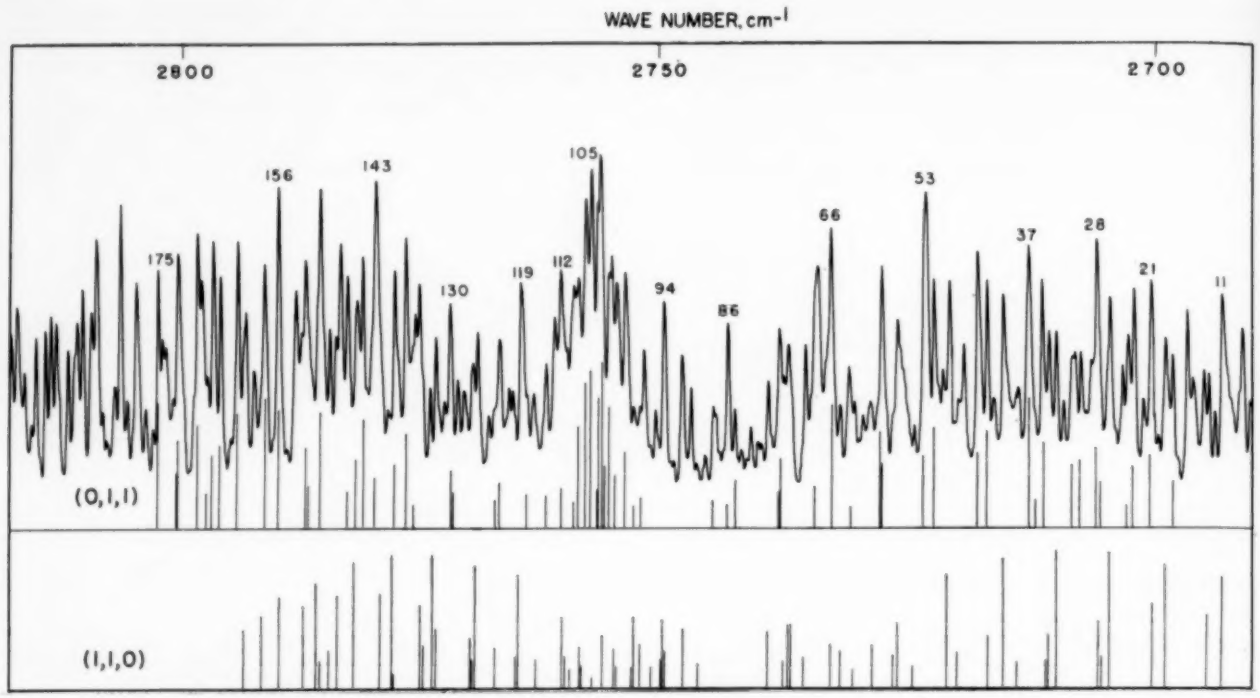

FIGURE 1. *Comparison of observed and calculated spectrum of* D_2S *near 3.6 μ.*
The numbers on the peaks correspond to the numbers in column 1 of table 1.

The remaining peaks are due to a piling up of weaker transitions or to absorption by HDS which was present to a few percent in the sample. Because the moments of inertia in D_2S are relatively large, the resulting line spacing in the vibrational rotational bands is quite close, resulting in severe overlapping of the absorptions due to neighboring transitions both in the same band and in two closely lying bands. This situation leads to some difficulty in making an analysis for it cuts down the number of assignments that can be made, thus introducing more uncertainty into the determination of the inertial constants than one would like. The strongest transitions in the P- and R-branches of both bands arise from levels that are strongly dependent on C^*. These levels could be readily identified and assigned, hence the value of C^* for each band should be very good. The strong Q-branch transitions of the A-type band arise from levels strongly dependent on A^*. Although the calculated Q-branch reproduces the observed absorption in remarkable detail, indicating a good value for A^*, this may be somewhat fortuitous because many transitions of the B-type band are calculated to fall in this same region. The transitions determining B^* most directly in both bands as well as A^* in the B-type band are spread throughout the band and in general are weaker transitions. As a result these inertial constants are probably somewhat more uncertain than the others although the general excellence of the fit for the transitions in the two bands that could be unambiguously assigned indicates that the constants determined should be fairly reliable.

Figure 1 compares the observed absorption with the two calculated bands whereas table 1 compares the observed and calculated frequencies of some of the stronger transitions.

The excited state constants leading to the fit shown are

A-type $\nu_0=2754.44\ \text{cm}^{-1}$ $A^*=5.531$ $B^*=4.521$ $C^*=2.403$

B-type $\nu_0=2742.77\ \text{cm}^{-1}$ $A^*=5.478$ $B^*=4.512$ $C^*=2.395$.

The previously determined ground [3] state was found to be adequate for both bands.

The absorption in the 5 μ region is too complicated by atmospheric absorption to enable a quantitative analysis. However, the D_2S absorption seems to have a Q-branch located near 1906 cm^{-1} indicating an A-type band. The main transitions of the P- and R-branches that are free from contamination by water vapor absorption indicate that the center of the band is $1906 \pm 1\ \text{cm}^{-1}$.

4. Vibrational Assignment

The A-type band at 2754.44 cm^{-1} must have v_3 odd. The most likely transition with v_3 odd that could occur in this frequency region is the transition with the upper state $(v_1,v_2,v_3)=(0,1,1)$. The B-type band must have v_3 even and hence the most likely assignment on the basis of frequency is for the excited state to be (1,1,0).

TABLE 1. *Comparison of observed and calculated spectra* [a]

Line	Observed	Transition	Calculated 0,1,1	Calculated 1,1,0	Intensity calculated
	cm^{-1}		cm^{-1}	cm^{-1}	
1	2687.79	$9_{-9}-10_{-10}$		2687.71	5.0
		$9_{-9}-10_{-9}$		2687.71	2.5
2	2688.57				
3	2689.14	$8_{-8}-9_{-8}$		2689.20	3.9
		$8_{-7}-9_{-7}$			
4	2689.84				
5	2690.32				
6	2690.54				
7	2691.40				
8	2691.74				
9	2692.50				
10	2693.13				
11	2693.38	$8_{-8}-9_{-8}$		2693.38	5.5
		$8_{-7}-9_{-9}$		2693.38	2.7
12	2694.12				
13	2694.78	$7_{-4}-8_{-6}$		2694.83	4.1
		$7_{-3}-8_{-5}$		2694.83	2.0
14	2695.22				
15	2696.10				
16	2696.33				
17	2696.83				
18	2698.29	$8_{-3}-9_{-4}$	2698.22		3.0
		$7_{-6}-8_{-8}$		2698.96	5.8
19	2698.95	$7_{-7}-8_{-7}$		2698.96	2.9
20	2699.78				
21	2700.44	$9_{-9}-10_{-10}$	2700.39		4.6
		$9_{-8}-10_{-9}$	2700.39		
22	2701.22				
23	2702.12	$8_{-5}-9_{-6}$	2702.13		3.9
		$8_{-6}-9_{-7}$	2702.13		
24	2702.74	6_0-7_1	2702.64		1.5
25	2703.33				
26	2704.45	$6_{-6}-7_{-6}$		2704.45	6.1
		$6_{-5}-7_{-7}$		2704.45	3.0
27	2704.80	6_0-7_0	2704.76		2.9
28	2705.78	$8_{-7}-9_{-8}$	2705.87		5.3
		$8_{-8}-9_{-9}$	2705.87		
29	2706.42				
30	2707.38	$7_{-5}-8_{-6}$	2707.38		4.4
		$7_{-4}-8_{-8}$	2707.38		
31	2707.96	$6_{-2}-7_{-2}$	2708.16		1.8
32	2708.26	$6_{-1}-7_{-2}$	2708.37		3.6
		5_0-6_2	2708.42		3.1
33	2703.13				
34	2709.84	$5_{-4}-6_{-6}$		2709.84	6.1
		$5_{-3}-6_{-6}$		2709.84	3.1
35	2710.54	4_2-5_2		2710.40	3.9
36	2711.22	$7_{-7}-8_{-8}$	2711.29		5.4
		$7_{-6}-8_{-7}$	2711.29		
37	2712.56	$6_{-3}-7_{-4}$	2712.53		4.7
		$6_{-4}-7_{-5}$	2712.54		
		$5_{-1}-6_{-2}$	2712.65		3.0
38	2713.53	5_0-6_1	2713.59		1.8
39	2713.70				
40	2714.10				
41	2714.75	$3_{-1}-4_{-1}$		2714.90	1.6
		$4_{-4}-5_{-4}$		2715.14	5.8
42	2715.08	$4_{-3}-5_{-3}$		2715.15	2.9
43	2715.98	4_0-5_{-1}	2716.16		1.9
44	2716.63	$6_{-6}-7_{-7}$	2716.62		6.2
		$6_{-5}-7_{-6}$	2716.62		
45	2717.40				
46	2717.58	$5_{-3}-6_{-4}$	2718.61		4.8
		$5_{-2}-6_{-3}$	2718.66		
47	2718.94				
48	2719.12	2_0-3_0		2719.07	2.6
		4_1-5_0	2719.26		3.4
49	2719.50				
50	2720.36	$3_{-3}-4_{-3}$		2720.33	2.6
		$3_{-2}-4_{-4}$		2720.38	5.1
51	2721.06				
52	2721.86	$5_{-5}-6_{-6}$	2721.88		6.3
		$5_{-4}-6_{-5}$	2721.88		
53	2722.70	$4_{-1}-5_{-2}$	2722.77		3.0
		3_1-4_0	2722.94		3.9
54	2723.92	1_1-2_1		2723.93	1.3
55	2725.52	$2_{-2}-3_{-2}$		2725.30	4.0
		$2_{-1}-3_{-3}$		2725.61	2.0
56	2725.82	3_2-4_1	2725.61		1.2
		$5_{-3}-5_{-1}$		2725.96	1.1
57	2726.79				
58	2727.11	$4_{-3}-5_{-4}$	2727.07		6.0
		$4_{-4}-5_{-5}$	2727.07		
59	2727.54	$6_{-2}-6_0$		2727.55	2.7
60	2728.28				
61	2728.45	5_0-5_0		2728.62	1.0
62	2729.01				
63	2729.84	$1_{-1}-2_{-1}$		2729.94	1.4
64	2730.28	2_2-3_1	2730.52		1.5
65	2731.24	1_0-2_{-2}		2731.19	2.3
		2_0-3_{-1}	2732.16		2.2
66	2732.14	$3_{-3}-4_{-4}$	2732.16		5.4
		$3_{-2}-4_{-3}$	2732.22		2.7
		$4_{-2}-1_0$		2732.00	2.7
67	2732.44				
68	2732.68				
69	2733.41				
70	2733.68	2_1-3_0	2733.86		1.8
71	2734.14				
72	2734.72	0_0-1_0		2734.85	1.9
73	2735.13				
74	2736.16	4_0-4_2		2736.20	4.6
75	2736.42	3_1-3_1		2736.34	1.7
		$2_{2}-2_0$		2736.44	2.1
76	2736.88	$3_{-1}-3_1$		2736.72	1.9
77	2737.30	$2_{-1}-3_{-2}$	2737.33		4.3
78	2738.15				
79	2738.52	2_0-2_2		2738.48	3.7
80	2739.33				
81	2739.52	$2_{-2}-2_0$		2739.72	1.5
82	2740.24				
83	2740.76				
84	2741.31	$3_{-3}-3_0$	2741.33		1.1
85	2741.92	$1_{-1}-2_{-2}$	2741.91		3.1
86	2742.57	1_0-2_{-1}	2742.64		1.4
87	2743.94				
88	2744.19	$4_{-1}-4_0$	2744.35		1.8
89	2745.06				
90	2745.82	1_1-1_{-1}		2745.83	1.5
91	2746.44				
92	2747.33	2_2-2_0		2747.42	3.5
93	2748.34				
94	2749.18	3_1-3_{-1}		2749.05	1.9
		2_0-2_{-2}		2749.23	2.2
95	2750.14				
96	2751.31				
97	2751.72	4_1-4_2	2751.59		3.3
		4_1-4_2		2751.72	2.8
98	2752.38	1_0-1_{-1}	2752.32		1.3
99	2753.24	2_1-2_2	2753.27		4.9
		5_2-5_2	2753.38		2.0
100	2754.10	$2_{-2}-1_0$		2754.16	2.5
101	2754.56				
102	2754.84	4_2-4_1	2755.08		7.9
		3_2-3_2	2755.73		6.7
		$4_{-}-4_2$	2755.74		3.9
103	2755.72	5_1-5_2	2755.80		4.0
		6_0-6_2		2755.86	
104	2756.04	5_2-5_1	2756.06		8.0
		2_2-2_0	2756.09		2.4
105	2756.71	1_1-1_0	2756.55		2.9
		6_0-6_2	2756.63		3.6
106	2757.28	7_6-7_7	2757.31		3.0
		7_7-7_6	2757.38		6.0
107	2758.03				
108	2758.54	6_0-5_2		2758.50	2.6
		4_2-4_1	2758.56		1.7
109	2758.86	$5_{-1}-5_{-3}$		2759.03	1.2
110	2759.35	6_0-6_1		2759.31	1.2
111	2759.75	$3_{-2}-2_{-2}$		2759.71	4.4
112	2759.95	3_1-3_0	2759.69		2.6
		$3_{-2}-2_{-1}$		2759.78	2.2
113	2760.56				
114	2761.48	$1_{-1}-0_0$	2761.37		2.0
115	2761.80	2_1-1_1		2761.62	1.4
116	2762.60				
117	2762.90				
118	2763.46	5_1-5_0	2763.63		2.1
119	2764.04	$4_{-4}-3_{-2}$		2764.07	5.7
		$4_{-3}-3_{-3}$		2764.13	2.9
120	2764.90				
121	2765.36				
122	2766.34	$2_{-1}-1_0$	2766.19		2.9
123	2766.92	$2_{-2}-1_{-2}$	2766.90		1.7
124	2767.38				
125	2768.64	$5_{-5}-4_{-3}$		2768.56	3.3
		$5_{-4}-4_{-4}$		2768.60	6.6
		$4_{-2}-3_0$		2768.75	3.5
126	2769.14				
127	2769.96				
128	2770.64				
129	2771.38	$3_{-2}-2_{-1}$	2771.27		2.3
130	2771.52	$3_{-1}-2_{-2}$	2771.59		4.7
131	2772.12				
132	2772.96	3_2-2_2		2772.91	3.7
		$6_{-5}-5_{-3}$		2772.93	3.6
		$6_{-6}-5_{-4}$		2772.93	7.2
133	2773.55				
134	2774.32	$5_{-2}-4_{-2}$		2774.38	4.6
135	2774.69				
136	2775.12				
137	2775.49	3_0-2_1	2775.44		1.5
138	2776.06	$4_{-3}-3_{-2}$	2776.01		6.0
		$4_{-4}-3_{-3}$	2776.06		
139	2776.93				
140	2777.24	$7_{-7}-6_{-5}$		2777.20	3.6
		$7_{-6}-6_6$		2777.20	7.3
		$5_{-1}-4_1$		2777.25	1.0
		$3_{-1}-2_0$		2777.32	

TABLE 1. *Comparison of observed and calculated spectra* [a]—Continued

Line	Observed	Transition	Calculated		Intensity calculated	Line	Observed	Transition	Calculated		Intensity calculated
			0,1,1	1,1,0					0,1,1	1,1,0	
	cm^{-1}		cm^{-1}	cm^{-1}			cm^{-1}		cm^{-1}	cm^{-1}	
141	2777.93	4_1-3_1		2778.07		157	2790.75	5_0-4_1	2790.85		2.0
142	2778.73	$6_{-3}-5_{-2}$		2778.68	2.6	158	2791.08	$6_{-2}-5_{-2}$	2791.29		5.7
		$6_{-1}-5_{-2}$		2778.60	5.1	159	2792.11				
143	2779.22	3_1-2_2	2779.10		3.2	160	2793.06	$8_{-4}-7_{-2}$		2793.13	2.3
144	2779.61					161	2793.26	$8_{-3}-7_{-3}$		2793.22	1.9
145	2780.65	$5_{-5}-4_{-4}$	2780.61		6.9	162	2793.90	$8_{-8}-7_{-7}$	2793.86		7.2
		$5_{-4}-4_{-3}$	2780.61					$8_{-7}-7_{-6}$	2793.86		
		$4_{-4}-3_0$	2781.13		4.4	163	2794.68				
146	2781.29	$8_{-6}-7_{-6}$		2781.35	7.0	164	2795.66	$7_{-5}-6_{-4}$	2795.66		5.6
		$8_{-7}-7_{-7}$		2781.35	3.5			$7_{-4}-6_{-3}$	2795.66		
147	2782.26	$4_{-2}-3_{-1}$	2782.06		2.3	165	2796.46	$6_{-1}-5_0$	2796.34		4.6
148	2782.97	$7_{-5}-6_{-3}$		2783.01	.6	166	2797.12	$6_{-2}-5_{-1}$	2797.27		2.3
		$7_{-4}-6_{-4}$		2783.03	5.3	167	2797.68				
149	2783.50	$6_{-2}-5_0$		2783.54	2.5	168	2798.10	$9_{-9}-8_{-8}$	2798.12		6.2
150	2784.18					169	2798.44	$9_{-8}-8_{-7}$	2798.12		
151	2785.12	$6_{-5}-5_{-4}$	2785.10		7.4	170	2799.64				
		$6_{-6}-5_{-5}$	2785.10								
		$6_{-1}-5_{-1}$		2785.11	1.8			$8_{-5}-7_{-4}$	2800.04		
152	2786.33	$5_{-2}-4_{-1}$	2786.21		1.8	171	2800.18	$8_{-6}-7_{-6}$	2800.04		5.5
153	2786.69	$5_{-1}-4_{-2}$	2786.50		3.6			6_1-5_2	2800.08		3.5
154	2787.20	$8_{-8}-7_{-8}$		2787.30	2.6	172	2800.73				
		$8_{-6}-7_{-4}$		2787.30	5.1	173	2801.44				
155	2787.77					174	2801.78				
156	2789.54	$7_{-7}-6_{-6}$	2789.53		7.4	175	2802.28	$10_{-9}-9_{-8}$	2802.29		6.0
		$7_{-6}-6_{-5}$	2789.53					$10_{-10}-9_{-9}$	2802.29		

[a] Because so many absorption peaks are composites of several transitions, only those for which definite assignments could be made are included in the table. Line numbers correspond to numbering of peaks in figure 1.

The band center of the (0,1,1) band is some 40 cm^{-1} lower than the Bailey, Thompson, and Hale value whereas it is some 70 cm^{-1} higher than the center of the absorption observed by Nielsen and Nielsen.

The *A*-type band at 1906 cm^{-2} is in the region where one would normally expect the stretching fundamentals. The band type demands that this absorption be assigned to the (0,0,1) band. Such an assignment places the band center of ν_3 nearly 100 cm^{-1} lower than that reported by Nielsen and Nielsen.

5. Discussion

With the help of these new band centers it is possible to make some estimates of the (0,1,0) band center. The difference between the (0,1,1) and (0,0,1) frequencies is ~848 cm^{-1}. This difference is the band center of the (0,1,0) band minus X_{23}, the interaction between ν_2 and ν_3. This interaction can be estimated from the corresponding interaction in H_2S as about 10 cm^{-1} leading to a value of 858 cm^{-1} as the frequency of (0,1,0). Using the (1,1,0) frequency, and as ν_1 the Raman [7] line at 1892 cm^{-1} one finds 851 cm^{-1} which includes X_{12}.

This frequency can also be estimated from the spectrum of crystalline [8] H_2S and D_2S which leads to a value of 855 cm^{-1}.

The existing data in this region by Nielsen and Nielsen runs out at 853 cm^{-1}, so this absorption seems to represent only the *R*-branch of the bending fundamental. Attempts to analyze their data as an *R*-branch were unsuccessful. Their data show no regular series that can be identified with the main strong *R*-branch series. However, the three pieces of evidence offered above strongly argue for a ν_2 band center close to 855 cm^{-1} fully 80 cm^{-1} lower than the value previously suggested [2].

These findings argue strongly for more work on the D_2S spectrum, which will be undertaken shortly at the Bureau.

In conclusion the authors thank R. E. Florin for preparing the D_2S and Carroll Dannemiller for doing the least squares calculations on SEAC.

6. References

[1] C. R. Bailey, J. W. Thompson, and J. B. Hale, J. Chem. Phys. **4,** 625 (1936).
[2] A. H. Nielsen and H. H. Nielsen, J. Chem. Phys. **5,** 277 (1937).
[3] H. C. Allen, Jr., R. E. Naylor, and E. K. Plyler, J. Research NBS **53,** 321 (1954) RP2549.
[4] E. K. Plyler, L. R. Blaine, and E. D. Tidwell, J. Research NBS **55,** 279 (1955) RP2630.
[5] P. C. Cross, R. M. Hainer, and G. W. King, J. Chem. Phys. **12,** 240 (1944).
[6] G. W. King, R. M. Hainer, and P. C. Cross, J. Chem. Phys. **11,** 27 (1943).
[7] G. M. Murphy and J. E. Vance, J. Chem. Phys. **6,** 426 (1938).
[8] J. B. Lohman, F. P. Redding, and D. F. Hornig, J. Chem. Phys. **19,** 252 (1951).

WASHINGTON, March 1, 1957

Journal of Research of the National Bureau of Standards Vol. 59, No. 3, September 1957 Research Paper 2790

Some Effects of Low Temperatures and Notch Depth on the Mechanical Behavior of an Annealed Commercially Pure Titanium[1]

Glenn W. Geil and Nesbit L. Carwile

Unnotched and notched specimens (60° notch angle, 0.05-inch root radius and various notch depths) of an annealed commercially pure titanium were slowly strained to fracture in tension at +150° or +100° to −196° C, to reveal the combined effects of temperature and notch geometry on the tensile behavior of the metal. Impact tests were made on Charpy V-notch specimens at +300° to −196° C for a determination of the impact notch-toughness of the titanium. True stress-true strain relations were determined for the titanium in tension and a study was made of the effects of test temperature, stress system, and interstitial content on the mechanism of deformation and work-hardening characteristics of the metal.

1. Introduction

Several investigators [1 to 5][2] have published results of their studies to determine the mechanisms involved in the tensile deformation of unnotched specimens of titanium and some of its alloys. The data obtained on single crystals [4,5] and on coarse-grained polycrystalline specimens [1,2,3] indicate that the tensile properties and the mechanisms involved in the tensile deformation of alpha titanium are quite temperature sensitive and complex. A large proportion of the deformation in tests at −196° C was by twinning [1,2]; the amount of twinning, in general, decreased with increase in temperature. Single and duplex slip on the prismatic planes also occurred in the deformation at −196° C [1,4]. With increase in temperature to +25° C, slip was observed on prismatic planes and also on pyramidal planes [1,4] and the basal plane [2]. The amount of slip on pyramidal planes increased considerably as the temperature was raised to +500° and +800° or +815° C [1,3].

Very few data are available on the combined effect of notches and low temperatures on the tensile behavior of titanium and its alloys; most of the published data were obtained on titanium alloys either in tests at different temperatures on specimens with a constant notch geometry [6,7,8], or in tests at room temperature on specimens of selected notch depths [9]. Results obtained at the Bureau in tension tests at different temperatures on a heat of annealed commercially pure titanium [10] contained some data on notched specimens of selected notch depths. However, the quantity of titanium available for these tests was relatively small, and only an exploratory investigation of the effect of low temperatures on the properties of notched specimens was possible.

An additional heat of commercially pure titanium was procured for use in the present study of the combined effects of low temperatures and notch geometry on the tensile behavior, as a part of a comprehensive program at the Bureau to evaluate the fundamental factors affecting the deformation of metals. The present paper summarizes the data obtained at low temperatures in Charpy V-notched impact and in tension on both unnotched and notched specimens of selected notch depths of this heat of titanium.

2. Material and Test Procedures

2.1. Material

All test specimens were prepared from bars processed from a single heat of commercially pure titanium (ASTM Designation B265–52T, grade 2). The bars were supplied in the form of 1-in. rounds in the hot-rolled and annealed condition; the bars were fine grained (fig. 1). The impurities (numerical values are in percent by weight) determined[3] in the titanium were as follows: Oxygen, 0.21; nitrogen, 0.04; hydrogen, 0.012; carbon, 0.04; silicon, 0.02; iron, *W;* chromium, *W;* tin, *W;* aluminum, *VW;* magnesium, *VW;* manganese, *VW;* nickel, *VW;* copper, *T;* tungsten, not determined.

2.2. Specimens

The forms and dimensions of the tensile specimens are shown in figure 2. The reduced section (D=0.40 in.) of the unnotched specimens was slightly tapered. The notched specimens were machined with a constant root radius of 0.05 in. and a constant minimum diameter, d, of 0.35 in., thereby minimizing the size effect. The notch depth[4] was varied by changing the diameter, D, of the cylindrical portion of the specimen adjacent to the notch.

ASTM standard (E23–47T) Charpy V-notch specimens were prepared from one bar of the titanium.

[1] This investigation was partially supported by the Materials Laboratory, Directorate of Research, Wright Air Development Center, USAF.

[2] Figures in brackets indicate the literature references at the end of this paper.

[3] Chemical analysis determinations for nitrogen, carbon, and silicon were made by the Analytical Chemistry Section of NBS. Determinations for oxygen and hydrogen were made by D. I. Walter at the Naval Research Laboratory by a modified vacuum fusion method [11]. The spectrographic-analysis determinations designated by letters were made by the Spectrochemistry Section of NBS. In general, *W* denotes weak (0.01 to 0.1%), *VW* denotes very weak (0.001 to 0.01%), and *T* denotes trace (0.0001 to 0.001%). The spectrographic method used was not sensitive for determination of tungsten.

[4] Notch depth is expressed as the percent of cross-sectional area removed in machining the notch in the specimen and it is equal to 100 $(D^2-d^2)/D^2$.

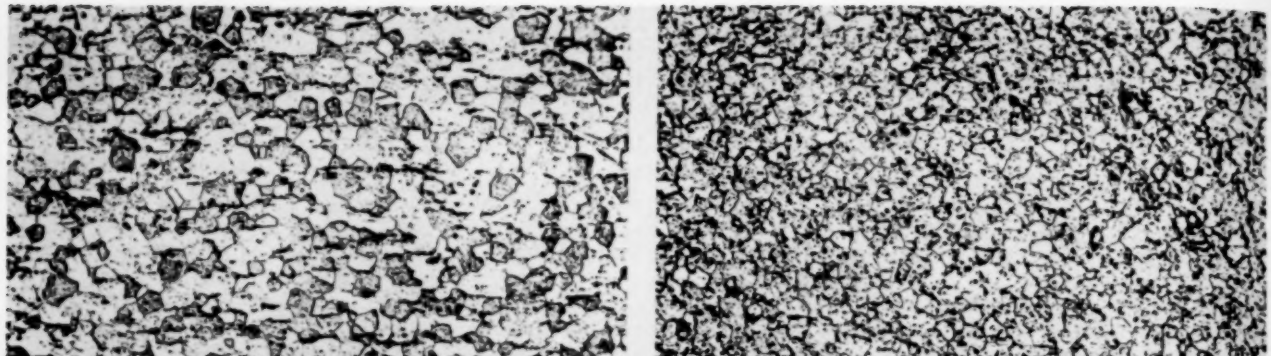

FIGURE 1. *Microstructure of the annealed commercially pure titanium.*

X 100. Left, longitudinal section; right, transverse section. Etchant: 1 part HF, 10 parts HCl, 10 parts HNO_3 and 80 parts water.

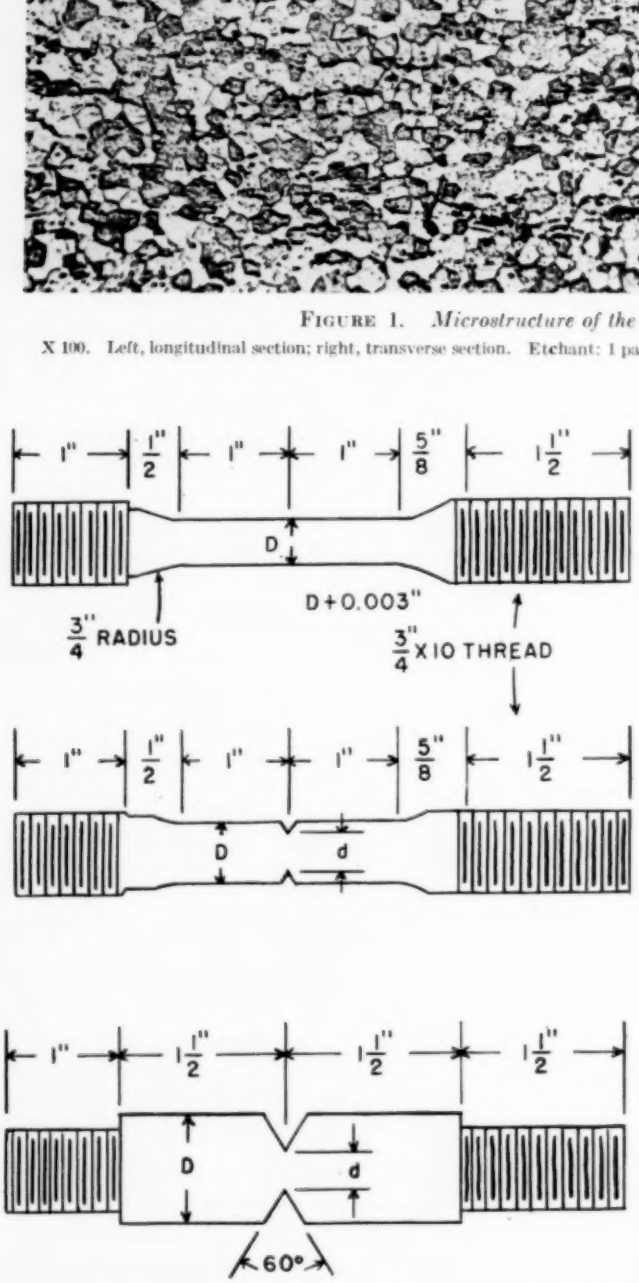

FIGURE 2. *Dimensions and forms of notched and unnotched tensile specimens.*

2.3. Test Procedures

The Charpy V-notch tests were made at temperatures ranging from +300° to −196° C in a machine of 224.1 ft-lb capacity and a striking velocity of 16.85 ft/sec. The specimens, except those tested at room temperature (about +25° C), were immersed in a bath at the selected temperature for a minimum period of 30 min, and then quickly transferred to the impact machine and broken. The total time elapsing between the removal from the bath and the breaking of the specimens ranged from 3 to 4 sec and there was no significant change in the temperature of the specimens during this period.

A detailed description of the tensile test equipment and the method of maintaining the selected temperature is given in previous publications [12, 13, 14]. The tensile tests were made at temperatures ranging from +150° or +100° C to −196° C with notched and unnotched specimens in a pendulum hydraulic testing machine. The specimens were strained slowly with the deformation rate maintained at about 0.5 to 1.0 percent reduction in area per minute during the deformation beyond initial yielding. The specimens, except those tested at room temperature, were strained to fracture while completely immersed in an appropriate bath maintained at the selected temperature. The specimens were immersed in the bath for a period of 30 min prior to the application of load. Simultaneous load and diameter (minimum diameter of unnotched specimens, diameter at base of the notch of the notched specimens) measurements were made throughout each tension test.

3. Results and Discussion

3.1. Impact Tests

The results obtained in the impact tests are summarized in figure 3. A transition temperature of about +110° C was indicated by the criteria of either (1) the steepest slope of the energy-temperature curve or (2) the mean value of the energy absorbed at the lowest temperature, and at the highest temperature at which complete fracture occurred. These impact data differed appreciably from those obtained previously [10] on another heat of commercially pure titanium with relatively small amounts of interstitials, which had a transition temperature about *40° C higher*, and a considerable degree of notch toughness (10 ft-lb, energy absorbed) at −196° C. This difference in the notched-bar impact behavior of these two heats of annealed commercially pure titanium may be attributed to the effects of the interstitial elements (carbon, nitrogen, oxygen, and hydrogen) as the other impurities did not vary significantly. The observed lower notch toughness (energy absorbed) at temperatures below the transition temperature range of the present heat of titanium with the higher interstitials, and thus with the higher hardness and strengths, conforms to the normal behavior for metals. However, the observed lower transition temperature for this heat of titanium is surprising, and no satisfactory explanation for this behavior can be given at the present time. As the grain size of the previous heat of titanium with low interstitials was slightly finer than that of the present heat, the difference in the transition temperatures cannot be readily attributed to a grain size effect.

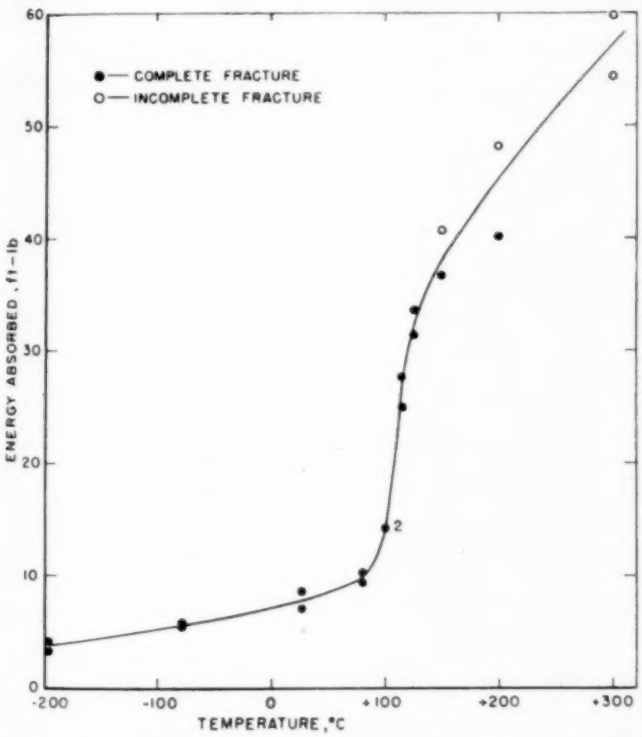

FIGURE 3. *Relation of temperature to the energy absorbed in fracturing the Charpy V-notch specimens.*

3.2. Tensile Tests

a. Flow Curves

The true stress-true strain relations obtained in tension tests on unnotched specimens at different temperatures are presented in figure 4. The true stress [5]-true strain [6] values that were obtained in duplicate tests at +100°, +25°, and −196° C were fairly consistent and showed only slight deviations from the curves representing the average values at each temperature. The marked effect of temperature on the strength of the titanium is shown by the increase in height of the true stress-true strain curves as the temperature is lowered. The initial resistance of the metal to plastic flow at −196° C is more than three times that at +150° C.

Logarithmic graphs of the true stress-true strain data (not shown) were sigmoidal. These data, like those obtained previously on another heat of titanium [10], and on other metals [13, 14], do not conform to the often postulated relationship, $\sigma = k\delta^m$, for tensile deformation, where σ and δ are the true stress and true strain, respectively, and k and m are constants.

The true stress-true strain relations obtained in tension tests at +100°, +25°, −78°, and −196° C on circumferentially notched specimens are presented

[5] True stress, σ, was determined by dividing the current load by the current minimum cross-sectional area of the specimen.

[6] True strain, δ, was determined as the natural logarithm of the ratio of the original minimum cross-sectional area of the specimen A_0, to the current minimum cross-sectional area, A.

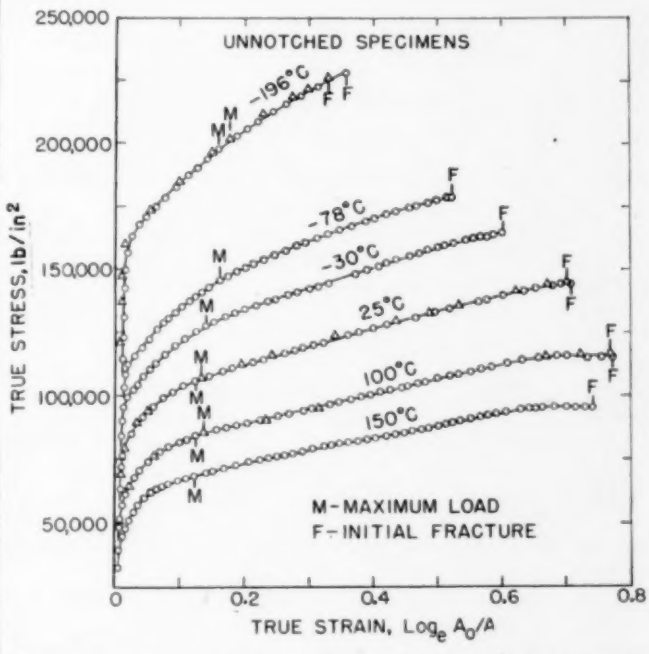

FIGURE 4. *True stress-true strain relations obtained in the tension tests at different temperatures on unnotched specimens.*

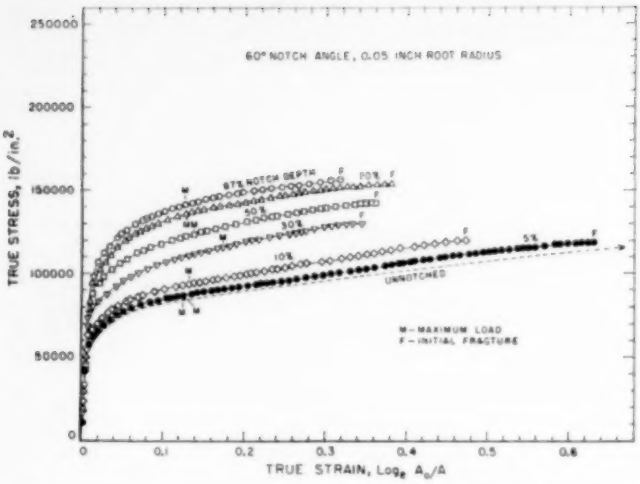

FIGURE 5. *True stress-true strain relations obtained in the tension tests at +100° C on notched specimens.*

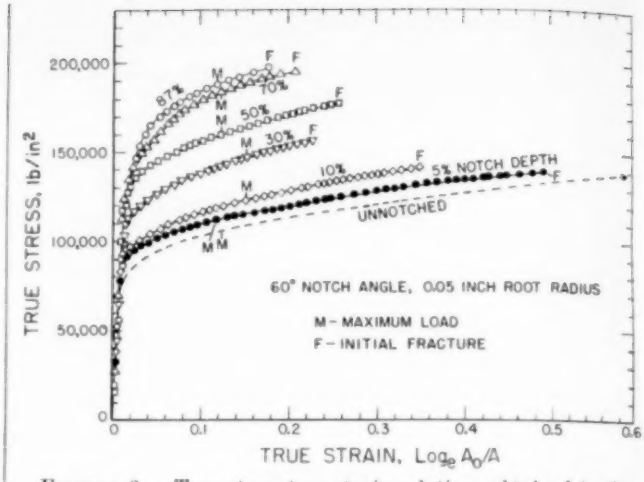

FIGURE 6. *True stress-true strain relations obtained in the tension tests at +25° C on notched specimens.*

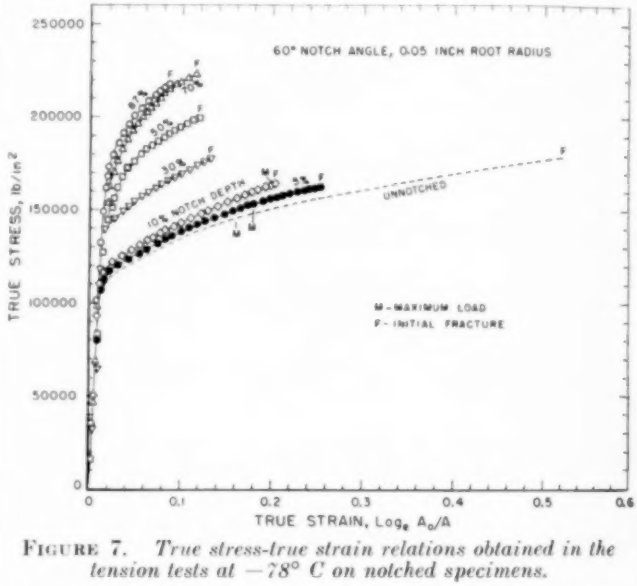

FIGURE 7. *True stress-true strain relations obtained in the tension tests at −78° C on notched specimens.*

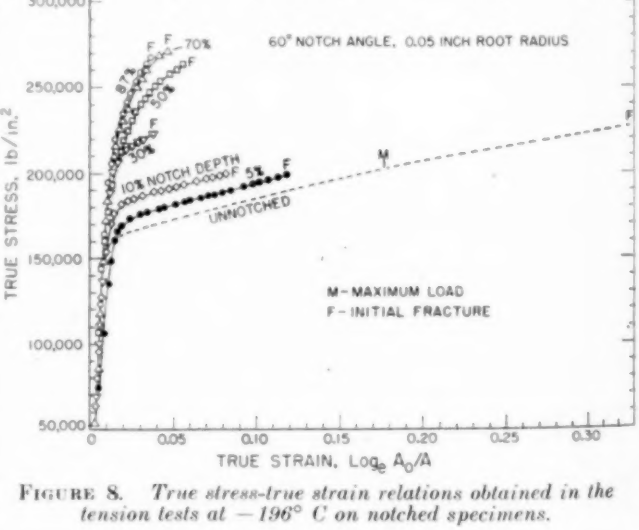

FIGURE 8. *True stress-true strain relations obtained in the tension tests at −196° C on notched specimens.*

in figures 5 to 8, respectively. Portions of the true stress-true strain curves for unnotched specimens are also included in these graphs. The resistance of the metal to flow, in general, increased with (1) decrease in temperature, (2) increase in the triaxiality accompanying increase in notch depth, and (3) increase in true strain. At each temperature, the increase in the resistance to flow with increase in notch depth became relatively small as the notch depth was increased above 70 percent. This is to be expected, because the increase in triaxiality was also relatively small as the depth was increased from 70 to 87 percent.

Both the stress concentration and the triaxiality induced in a notched specimen in a tensile test vary with the geometry of the notch. The variation of these factors with the notch depth for the titanium specimens of circular cross section containing a circumferential notch of 60° angle and 0.05-in. root radius, is shown in figure 9. The values for the stress concentration factor K_t, were derived from published stress concentration design charts [15]. The triaxiality, determined as the ratio S_t/S_l, where S_t and S_l are the transverse and longitudinal stresses, respectively, is based on the method proposed by Sachs and Lubahn [16]; that is, $S_t/S_l = 1-(1/R)$, where R is the ratio of notch strength [7] to the tensile strength. The triaxiality increases at a nearly constant rate with increase in notch depth to about 20 percent, and then increases at a continuously decreasing rate with further increase in notch depth. The stress concentration factor increases very rapidly with increase in notch depth to about 10 percent, less rapidly with increase in depth from 10 to 30 percent and then increases only slightly with further increase in the depth.

[7] Notch strength was determined by dividing the highest load attained on the notched tensile specimen by the original minimum cross-sectional area at the notch. In determining the values of R, the notch strength values are restricted to those in which the specimen had sufficient ductility to attain a normal maximum load condition, that is, the slope of the load-extension curves becomes zero.

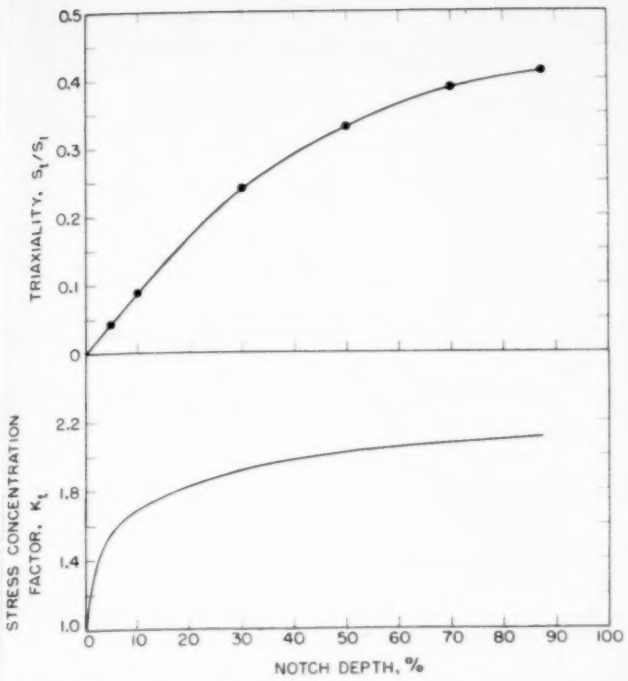

FIGURE 9. *Effect of notch depth on the stress concentration factor and the triaxiality of the tensile specimens used.*

(60° notch angle, 0.05-in. root radius, and 0.350-in. diameter at the base of the notch.)

b. Effects of Temperature and Notch Geometry

(1) *Strength Indices.* The results of the tensile tests on unnotched and notched specimens are summarized in tables 1 and 2, respectively. A determination of yield strength, as normally based on offset values from autographic load-extension curves, was not feasible with the equipment employed. However, an indication of the stresses at which appreciable yielding has taken place is given by the values of true stress at a true strain (elastic plus plastic) of 0.02. These "0.02 stress" values would be higher than the 0.2 percent offset yield strength values for unnotched specimens, particularly at the higher temperatures because the amount of elastic strain prior to yielding, in general, increased with lowering of temperature and with increase in notch depth.

The relations between the 0.02 stress of the titanium and the notch depth and temperature are represented by the surface delineated in figure 10. The 0.02 stress at each test temperature increased, at a slightly decreasing rate, with increase in notch depth; the values for the specimens with the deep notches (70 and 87% notch depths) were approximately one and one-half times those for unnotched specimens at corresponding temperatures. A relatively large increase in the 0.02 stress was observed for both the notched and unnotched specimens with decrease in temperature from +100° to −196° C; the strengths of the specimens at −196° C were greater than those of corresponding specimens at +100° C by factors of 2.5 for unnotched specimens and 2.7 to 2.2 for the notched specimens (table 3). No simple relation between 0.02 stress and temperature is indicated as the curves (fig. 10) representing the variation of the stress with temperature for specimens of the same notch depth have an inflection point near 0° C. The inflection point may be an indication of a significant increase in the number of active slip plane systems and accompanying decrease in the stress for activation of slip with increase in temperature above 0° C.

TABLE 1. *Tensile properties at +150°, +100°, +25°, −30°, −78°, and −196° C of unnotched specimens of initially annealed commercially pure titanium*

Specimen [a] designation	Temperature	Tensile strength	True stress			True strain [b]		Reduction of area	Elongation [c] in 2 in.
			At true strain of 0.02	At maximum load	At initial fracture	At maximum load	At initial fracture		
	° C	lb/in.²	lb/in.²	lb/in.²	lb/in.²			%	%
B10	+150	60,000	50,000	69,000	95,000	0.121	0.741	52	44
B8	+100	75,000	64,000	85,000	115,000	.123	.774	57	40
B6	+100	75,000	63,000	86,000	117,000	.137	.770	57	42
B1	+25	94,000	84,000	106,000	144,000	.123	.708	53	30
B9	+25	94,000	84,000	108,000	145,000	.136	.703	51	30
B5	−30	111,000	100,000	128,000	165,000	.140	.602	45	26
B2	−78	124,000	113,000	146,000	179,000	.160	.522	42	26
B7	−196	169,000	164,000	202,000	227,000	.176	.330	29	20
B4	−196	169,000	157,000	198,000	229,000	.159	.358	31	22

[a] All specimens were prepared from the same bar, B.
[b] Includes elastic and plastic deformation.
[c] Measurements based on punch marks in fillets. Specimens had a reduced section of 2.0 in. length.

The observed relations between the notch strength of the titanium and the notch depth and temperature are represented by the surface delineated in figure 11. The shape of this surface is nearly similar to that shown for the 0.02 stress (fig. 10). As shown in figure 12, the percentage increase in notch strength is approximately equal to the notch depth for depths up to 50 percent. However, nearly all of the values for notch depths of 70 and 87 percent lie considerably below the dotted line representing the above relationship. This deviation may be attributed partially to the relatively low rate of increase in triaxiality with increase in notch depths for depths greater than 50 percent (fig. 9). A considerable portion of the deviation of the values for the deep-notched specimens at −78° and −196° C may be attributed to the very small ductility of these specimens (table 2).

The combined effects of temperature and notch depth on the true stresses at maximum load and at initial fracture are illustrated by the two surfaces delineated in figure 13. These two surfaces coincide at temperatures of −78° C and below, for notch depths of 10 percent or greater, and for all notch depths at −196° C. This coincidence is associated with the fracture of these specimens while the loads were still increasing.

The true stresses at maximum load and at initial fracture increased greatly with decrease in temperature (fig. 13). However, the relative increase in these values with decrease in temperature from +25° to −78° or to −196° C (table 3) is significantly smaller

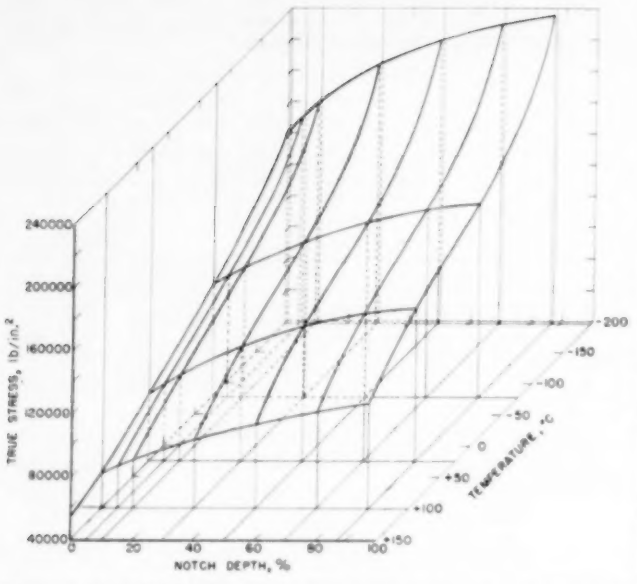

FIGURE 10. *Variation of the true stress at a true strain of 0.02 with notch depth and temperature of the tensile specimens.*

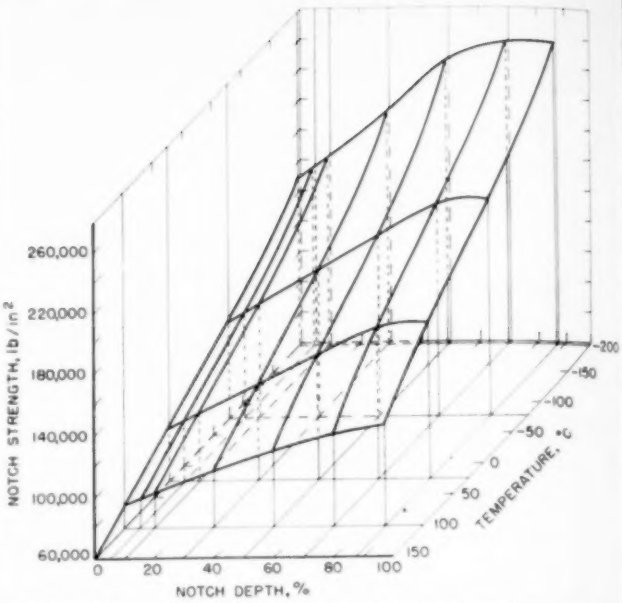

FIGURE 11. *Variation of the notch strength with the notch depth and temperature of the tensile specimens.*

TABLE 2. *Tensile properties at +100°, +25°, −78°, and −196° C of notched specimens (60° notch angle, 0.05-in. root radius) of initially annealed, commercially pure titanium*

Specimen [a] designation	Temperature	Notch depth	D [b]	d [c]	Notch strength [c]	Ratio of notch strength to tensile strength	True stress at—			Ratio of true stress of notched to unnotched specimens at—			True strain [f] at—		Ratio of true strain of notched to unnotched specimens at—		Reduction of area
							True strain of 0.02	Maximum load	Initial fracture	True strain of 0.02	Maximum load	Initial fracture	Maximum load	Initial fracture	Maximum load	Initial fracture	
	°C	$\frac{D}{d}$	*in.*	*in.*	*lb/in.²*		*lb/in.²*	*lb/in.²*	*lb/in.²*								$\frac{d_0}{d}$
G4	+100	5	0.360	0.350	77,000	1.03	65,000	87,000	119,000	1.02	1.02	1.03	0.124	0.631	0.95	0.82	49
G11	+100	10	.370	.350	81,000	1.08	64,000	93,000	121,000	1.01	1.09	1.04	.136	.534	1.05	.69	42
G2	+100	10	.370	.350	82,000	1.09	70,000	94,000	123,000	1.09	1.11	1.06	.132	.522	1.02	.68	40
G3	+100	30	.418	.350	98,000	1.30	83,000	116,000	130,000	1.30	1.36	1.12	.173	.363	1.33	.47	30
G1	+100	50	.495	.350	108,000	1.44	93,000	126,000	142,000	1.46	1.47	1.22	.154	.363	1.19	.47	30
J6	+100	50	.495	.350	109,000	1.45	91,000	129,000	142,000	1.43	1.51	1.22	.162	.332	1.25	.43	28
G5	+100	70	.639	.350	119,000	1.59	100,000	136,000	154,000	1.56	1.59	1.33	.135	.382	1.04	.50	32
J7	+100	70	.639	.350	120,000	1.60	101,000	138,000	154,000	1.58	1.61	1.33	.139	.359	1.07	.47	30
E11	+100	87	.990	.350	125,000	1.67	107,000	143,000	157,000	1.67	1.67	1.35	.135	.318	1.04	.41	29
D14	+25	5	.360	.350	99,000	1.05	92,000	112,000	140,000	1.10	1.05	0.97	.118	.488	0.91	.69	41
D15	+25	10	.370	.350	105,000	1.12	96,000	122,000	141,000	1.14	1.15	.98	.151	.348	1.17	.49	32
G6	+25	10	.370	.350	103,000	1.10	91,000	120,000	139,000	1.08	1.13	.96	.155	.341	1.20	.48	30
F5	+25	10	.370	.350	103,000	1.10	88,000	123,000	144,000	1.05	1.16	1.00	.172	.391	1.33	.55	33
D17	+25	30	.418	.350	125,000	1.33	114,000	146,000	156,000	1.36	1.37	1.08	.151	.226	1.17	.32	20
G12	+25	30	.418	.350	120,000	1.28	104,000	145,000	154,000	1.24	1.36	1.07	.192	.266	1.48	.38	24
F10	+25	30	.418	.350	123,000	1.31	106,000	148,000	156,000	1.26	1.39	1.08	.182	.250	1.41	.35	24
D4	+25	50	.495	.350	141,000	1.50	130,000	159,000	177,000	1.55	1.49	1.23	.122	.256	0.94	.36	23
J5	+25	50	.495	.350	140,000	1.49	120,000	164,000	172,000	1.43	1.54	1.19	.158	.218	1.22	.31	20
F20	+25	50	.495	.350	142,000	1.51	118,000	166,000	174,000	1.40	1.56	1.20	.158	.222	1.22	.31	23
D16	+25	70	.639	.350	162,000	1.72	138,000	183,000	195,000	1.64	1.72	1.35	.122	.207	0.94	.29	21
F21	+25	70	.639	.350	156,000	1.66	126,000	178,000	192,000	1.50	1.67	1.33	.130	.255	1.00	.36	24
D19	+25	87	.990	.350	167,000	1.78	135,000	188,000	198,000	1.61	1.77	1.37	.118	.183	0.91	.26	18
A3	+25	87	.990	.350	155,000	1.65	134,000	180,000	188,000	1.60	1.69	1.30	.146	.216	1.13	.31	20
N6	+25	87	.990	.350	160,000	1.70	132,000	181,000	195,000	1.57	1.70	1.35	.125	.222	0.97	.31	21
I5	−78	5	.360	.350	128,000	1.03	117,000	154,000	162,000	1.04	1.06	0.91	.178	.252	1.11	.48	24
I3	−78	10	.370	.350	134,000	1.08	120,000	164,000	164,000	1.06	1.12	.92	.203	.203	1.27	.39	19
I2	−78	30	.418	.350	156,000	1.26	142,000	[g]	177,000	1.26	.....	.99	[g]	.132	.....	.25	12
I1	−78	50	.495	.350	177,000	1.43	146,000	[g]	200,000	1.28	.....	1.12	[g]	.119	.....	.23	10
I4	−78	70	.639	.350	199,000	1.61	153,000	[g]	223,000	1.35	.....	1.25	[g]	.115	.....	.22	12
A12	−78	87	.990	.350	200,000	1.61	173,000	[g]	217,000	1.53	.....	1.21	[g]	.086	.....	.17	10
N7	−78	87	.990	.350	200,000	1.61	150,000	[g]	222,000	1.33	.....	1.24	[g]	.102	.....	.20	10
F1	−196	5	.360	.350	177,000	1.05	160,000	[g]	199,000	1.05	.....	0.87	[g]	.118	.....	.34	11
F2	−196	10	.370	.350	183,000	1.08	182,000	[g]	199,000	1.13	.....	.87	[g]	.081	.....	.24	8
F3	−196	30	.418	.350	213,000	1.26	210,000	[g]	221,000	1.31	.....	.97	[g]	.039	.....	.11	5
F17	−196	50	.495	.350	249,000	1.47	215,000	[g]	263,000	1.34	.....	1.15	[g]	.056	.....	.16	6
A11	−196	50	.495	.350	243,000	1.44	225,000	[g]	255,000	1.40	.....	1.12	[g]	.052	.....	.15	6
F4	−196	70	.639	.350	258,000	1.53	230,000	[g]	270,000	1.43	.....	1.18	[g]	.046	.....	.13	5
A9	−196	87	.990	.350	257,000	1.52	235,000	[g]	266,000	1.46	.....	1.17	[g]	.037	.....	.11	4
N8	−196	87	.990	.350	256,000	1.52	239,000	[g]	264,000	1.48	.....	1.16	[g]	.031	.....	.09	4

[a] All specimens prepared from the same bar are designated by the same letter.
[b] Diameter of cylindrical portion of the specimen adjacent to the notch.
[c] Diameter of specimen at the base of the notch.
[d] Determined by dividing the highest load attained by the original minimum cross-sectional area.
[f] Includes elastic and plastic deformation.
[g] Fractured before the slope of the load-extension curves became zero.

TABLE 3. *Effect of test temperature and notch depth on relative values of some strength indices for initially annealed commercially pure titanium*

Notch depth	$\frac{\sigma_{l=0.02} \text{ at } T_2}{\sigma_{l=0.02} \text{ at } T_1}$				$\frac{\sigma_{\text{Maximum load}} \text{ at } T_2}{\sigma_{\text{Maximum load}} \text{ at } T_1}$				$\frac{\sigma_{\text{fracture}} \text{ at } T_2}{\sigma_{\text{fracture}} \text{ at } T_1}$				$\frac{\text{Notch strength at } T_2}{\text{Notch strength at } T_1}$			
T_1, ° C	+25	+25	+25	+100	+25	+25	+25	+100	+25	+25	+25	+100	+25	+25	+25	+100
T_2, ° C	+100	−78	−196	−196	+100	−78	−196	−196	+100	−78	−196	−196	+100	−78	−196	−196
%																
0	0.76	1.35	1.91	2.53	0.80	1.36	1.87	2.34	0.80	1.24	1.58	1.97	[a] 0.80	[a] 1.32	[a] 1.80	[a] 2.25
5	.71	1.27	1.84	2.60	.78	1.38	1.78	2.29	.85	1.16	1.42	1.67	.78	1.29	1.79	2.30
10	.73	1.31	1.99	2.72	.77	1.35	1.64	2.13	.86	1.16	1.41	1.63	.78	1.29	1.76	2.24
30	.77	1.31	1.94	2.53	.79	[b]	[b]	[b]	.84	1.14	1.42	1.70	.80	1.27	1.73	2.17
50	.75	1.19	1.79	2.39	.78	[b]	[b]	[b]	.81	1.15	1.49	1.82	.77	1.26	1.74	2.27
70	.76	1.16	1.74	2.29	.76	[b]	[b]	[b]	.80	1.15	1.40	1.75	.75	1.25	1.62	2.16
87	.80	1.21	1.77	2.21	.78	[b]	[b]	[b]	.81	1.13	1.37	1.69	.78	1.24	1.59	2.05

[a] Ratio of tensile strengths.
[b] Fractured at −78° and −196° C before the slope of the load-extension curves became zero.

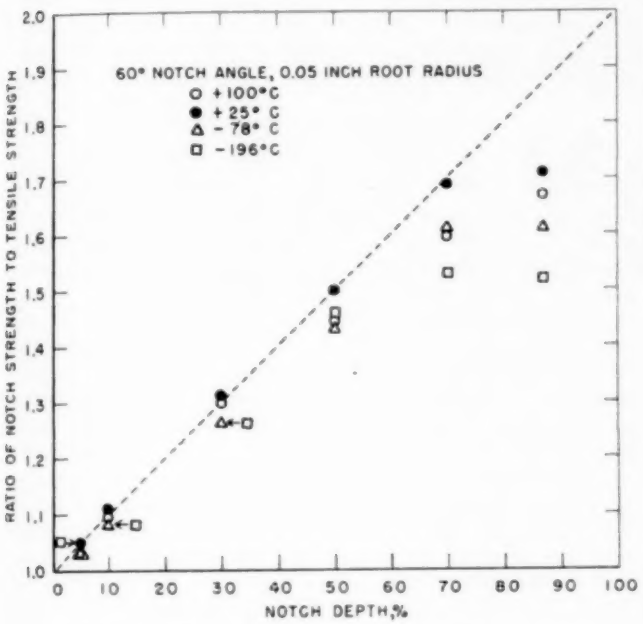

FIGURE 12. *Effect of the notch depth of tensile specimens on the ratio of notch strength to tensile strength.*

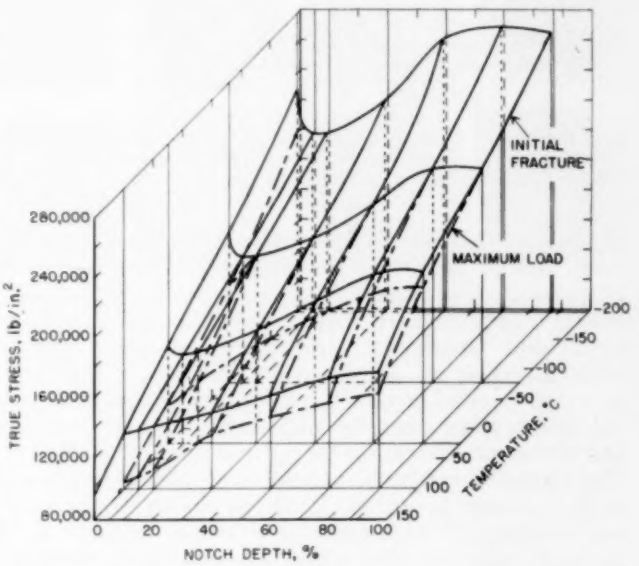

FIGURE 13. *Variation of the true stresses at maximum load and at initial fracture with the notch depth and temperature of tensile specimens.*

than the corresponding relative increase in the 0.02 stress values; this feature can also be attributed mainly to the decrease in ductility of the specimens with decrease in temperature.

The true stress at initial fracture at temperatures of +25° C and below, decreased with increase in notch depth up to 10 percent, then increased with increase in depth through the range of 10 to 70 percent, and thereafter changed only slightly with further increase in depth to 87 percent. The decrease for 5 and 10 percent depths can be attributed directly to the decrease in the true strain at initial fracture associated with the stress concentration at the root of the notch. The decrease in the true stress at fracture due to this factor is greater than the small increase in the true stress associated with the induced triaxiality for these shallow notches. For notch depths of 30 percent and greater, the relative effect of the above two factors is reversed, and the triaxiality is the predominant one, as the stress concentration factor and the ductility of the specimens changed only slightly, whereas the triaxiality and flow stress increased considerably, with the increase in notch depth.

(2) *Ductility.* The effects of temperature and notch depth on the true strains at maximum load and at initial fracture are shown in figure 14. The true strains at maximum load for the specimens that attained a normal maximum load condition did not vary significantly either with temperature or notch depth. A slight, although probably insignificant, maximum is exhibited in the curves showing the effect of notch depth on the true strain at maximum load at temperatures of +25° and +100° C. The true strain at initial fracture decreased continuously with decrease in temperature below +100° C.

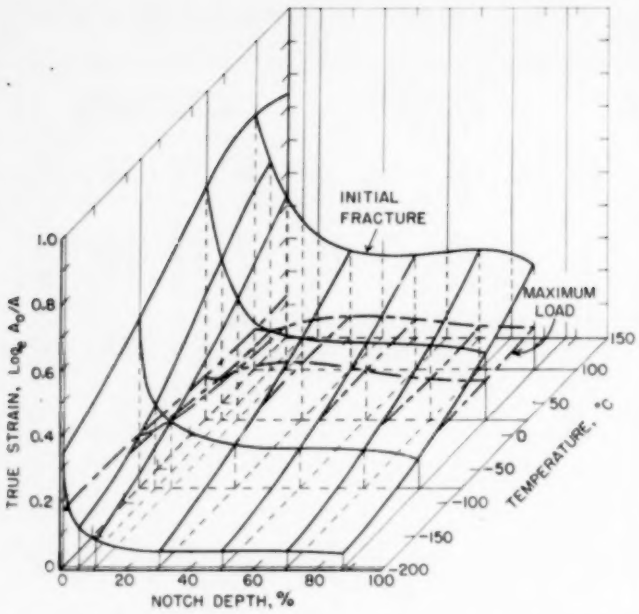

FIGURE 14. *Variation of the true strains at maximum load and at initial fracture with the notch depth and temperature of the tensile specimens.*

Moreover, the true strain at initial fracture decreased very rapidly with increase in notch depth to about 10 percent, less rapidly with increase to 30 percent, changed only slightly with further increase in depths to 50 and 70 percent, and then decreased slightly with increase in depth to 87 percent. The pronounced dependence of the ductility of this metal on the notch depth can be attributed to variations in the stress concentration factor and triaxiality (fig. 9). The stress concentration factor increases very rapidly with increase in notch depth to about 10 percent, and less rapidly with increase in depth from 10 to 30 percent, whereas the triaxiality for these shallow-notched specimens is relatively small. Therefore, it can be postulated that the large decrease in ductility of these titanium specimens (fig. 14) with increase in notch depth to 5, 10, and 30 percent is due mainly to the detrimental effect of the stress concentration and accompanying stress and strain gradients in the region near the base of the notch. The triaxiality of the stress system also reduces the ductility of specimens but its effect for these shallow-notched specimens is relatively small. However, for the deep-notched specimens, the effect of the relatively large triaxiality on the ductility is significant as is shown in figure 14 by an appreciable decrease in the true strain at initial fracture at temperatures of +100°, +25°, and −78° C as the notch depth is increased from 70 to 87 percent; the change in the stress concentration factor with notch depth in this range is very small, and the triaxiality apparently is the predominant factor involved in the initiation of the fracture at these temperatures of the specimens with notch depths of 70 and 87 percent.

Some corroboratory evidence in support of the above views is provided in the photographs of the fracture surfaces of the notched specimens presented in figure 15. The fractures at +100°, +25°, and −78° C of specimens with notch depths of 5, 10, 30, and 50 percent, and the fractures of all the notched specimens at −196° C were initiated at points of high-stress concentration at, or near, the root of the notch. Conversely, the fractures at +100°, +25°, and −78° C of specimens with notch depths of 70 and 87 percent were initiated in the region of high triaxial stresses near the axis. The total deformation of the deep-notched specimens at these temperatures was considerable; it apparently was great enough to reduce the stress concentration near the root of the notch so that the effect of the high triaxial stresses was the predominant factor in the initiation of these fractures. At −196° C, the total deformation of the deep-notched specimens was very small. It was not great enough to reduce, to any significant extent, the stress concentration near the root of the notch, and the stress concentration remained as the predominant factor in the initiation of the fractures.

c. Work Hardening Characteristics

The rate of work hardening,[8] $d\sigma/d\delta$, of the titanium was affected by the temperature and notch depth. This is indicated qualitatively in figures 4 to 8 by an increase in the slopes of the curves at a given true strain with either a decrease in temperature or an increase in notch depth.

The relations observed between the rates of work hardening and true strain of unnotched specimens of the titanium at different temperatures are summarized in figure 16. The rates of work hardening at constant true strains, except at the small true strains in the region of initial yielding, increased continuously with decrease in temperature over the range of +150° to −196° C. The rates of work hardening of the specimens decreased greatly with increase in true strains for strains less than those at the maximum loads. The decrease in the rate of work hardening with increase in strain, above that at maximum load was still considerable at the lower temperatures, but it was very slight at +100° and +150° C.

The effect of notch depth and the accompanying induced triaxiality on the rate of work hardening of the titanium is illustrated quantitatively in figure 17 for the tension tests at +25° C. The rate of work hardening of the metal increased with increase in the notch depth and decreased with increase in true strain; the rate of decrease was relatively small with strains in excess of about 0.3. Similar results (not shown) were observed for the tests at +100°, −78°, and −196° C; however, at −78° and −196° C the true strain range was much smaller due to the limited ductility of the notched specimens at these temperatures. In the tests at +100° C, considerable scatter was observed in the rates of work hardening of the notched specimens at strains

[8] The rate of work hardening, determined as $d\sigma/d\delta$, at any true strain is the slope of the true stress-true strain curve at that strain. For strains of an unnotched specimen beyond that at maximum load, the increase in the flow stress resulting from the triaxiality induced by the necking of the specimen is included in the value of $d\sigma/d\delta$.

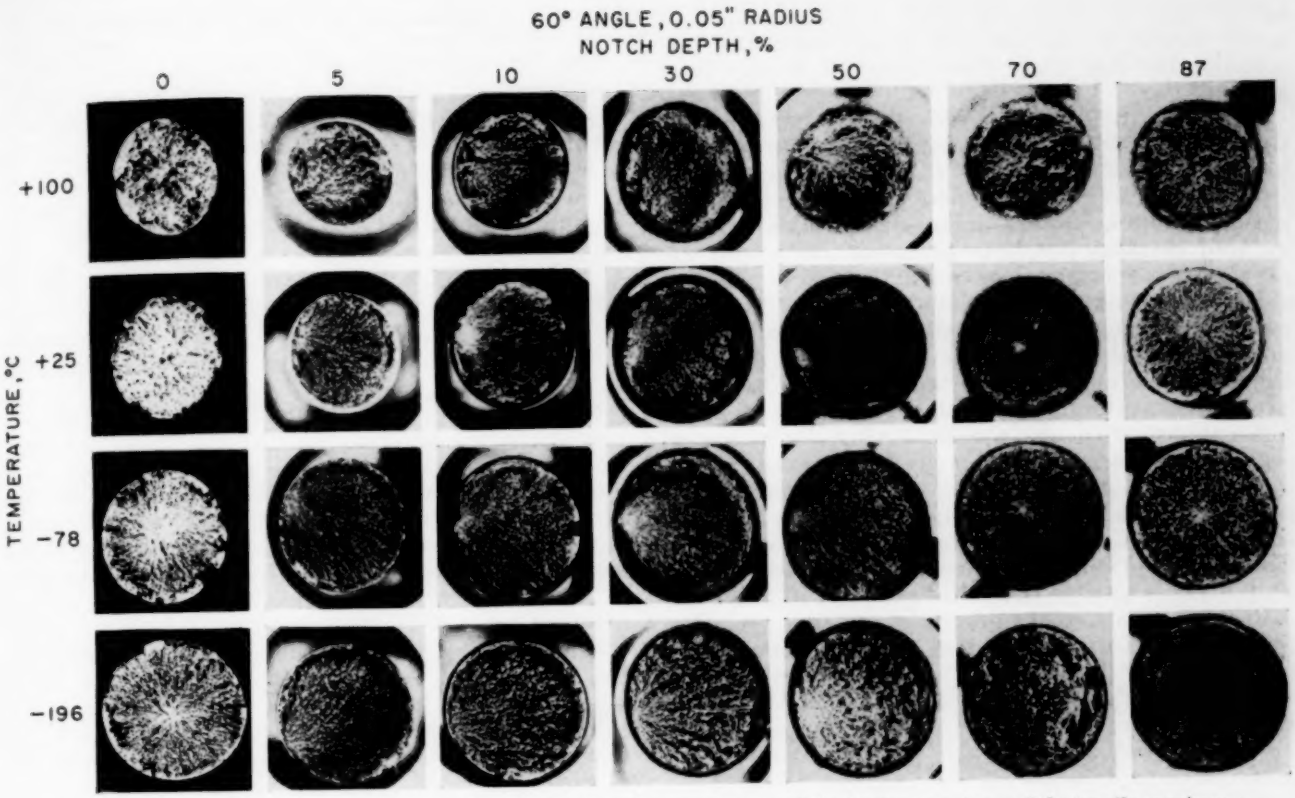

FIGURE 15. *Effect of test temperature and notch depth on the appearance of the fracture surfaces of the tensile specimens.*
Photographs, X 2.

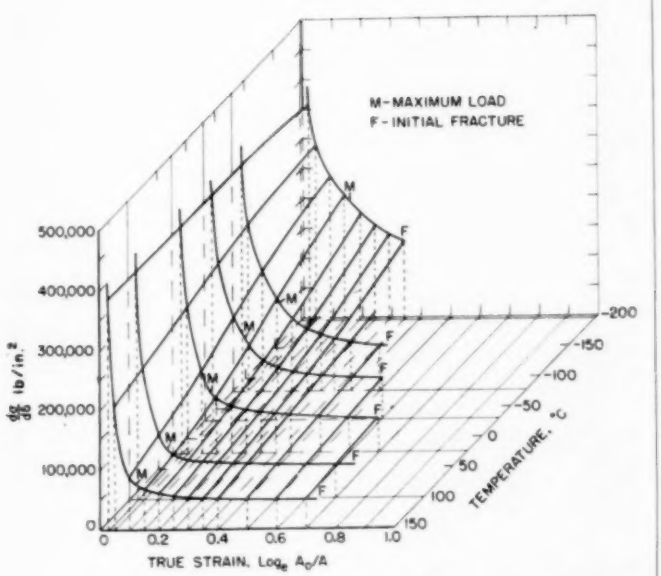

FIGURE 16. *Relation between the rate of work hardening and true strain of unnotched tensile specimens at different temperatures.*

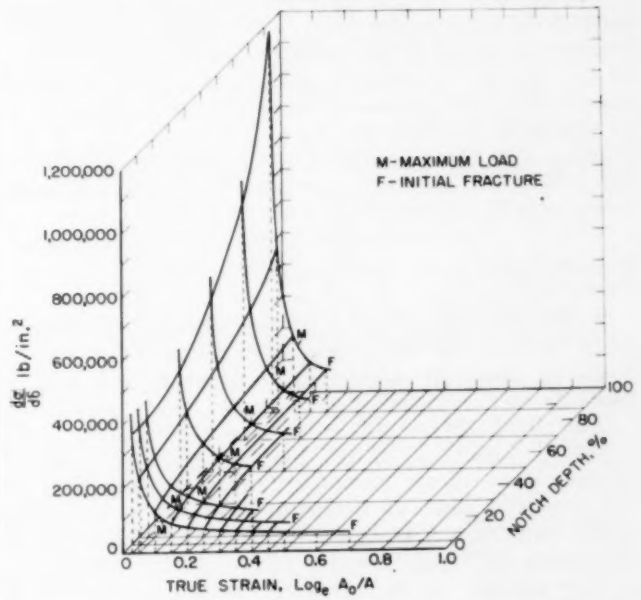

FIGURE 17. *Relation between the rate of work hardening and true strain of tensile specimens of different notch depths at +25° C.*

above that at maximum load, and the effect of notch depth on the rates of work hardening was considerably less than that observed in the tests at +25° C.

The dependence of the rates of work hardening of the titanium on the stress system may be explained by the hypothesis, suggested in a previous paper [10], as follows: Deformation in tension under a multiaxial stress system, such as the triaxial stresses induced in these notched specimens, occurs by the movement of dislocations on a greater number of slip planes within the individual crystals of the polycrystalline specimen than is the case for deformation under uniaxial tension, and more duplex or cross slip will also occur with deformation under the multiaxial stress system. The number of intersections of dislocations, with the accompanying formation of jogs in the dislocations and point defects in the metal, increases with increase in the triaxiality and accompanying increase in cross slip. Energy is required to move one dislocation across another dislocation. Moreover, the energy required to move a dislocation with a jog is greater than that required to move the dislocation prior to the formation of the jog. The point defects formed may also act as barriers to the movement of dislocations. These factors tend to increase the rate of work hardening of the metal [17, 18, 19].

d. Some Effects of Interstitials

Recent investigations [20, 21, 22] have shown that the mechanical properties of high-purity alpha titanium are affected greatly by the interstitial elements (carbon, nitrogen, oxygen, and hydrogen). Carbon, nitrogen, and oxygen strengthen the metal and also tend to decrease its ductility. Hydrogen is generally believed to be one of the main causes of embrittlement of the metal. The main difference in the chemical composition of the present heat of titanium and that of the heat used in the previous study [10] at the Bureau is in the amounts of the interstitial elements; the interstitial contents (percent by weight) of these two heats of the titanium were as follows:

	Carbon	*Oxygen*	*Nitrogen*	*Hydrogen*
Previous heat	0.02	0.07	0.02	0.006
Present heat	.04	.21	.04	.012

A comparison of some of the strength and ductility indices of unnotched specimens of the two heats of titanium studied at the Bureau is given in table 4.

The 0.02 stress at +100°, +25°, −78°, and −196° C (table 4) of the present heat of titanium ranged from 12 to 30 percent greater than that of the previous heat of titanium with its lower interstitial contents. It may be postulated that this difference in the 0.02 stress values of the two heats is due mainly to the greater density of "Cottrell clouds" (clusters of interstitial atoms around the dislocations) [17] in the annealed metal with the higher interstitial contents; more energy is required for the initiation of the movement of a dislocation with a surrounding cluster of interstitial atoms than for that of a similar dislocation not partially anchored by interstitial atoms. The binding effect of the surrounding interstitial atoms on a dislocation increases with decrease in the rates of diffusion of the interstitial atoms such as accompanies a decrease in temperature of the metal. This feature is indicated in table 4 by the significantly higher ratio of the 0.02 stresses at −196° and +25° C, respectively, for the present heat of titanium with its higher interstitial contents.

TABLE 4. *Some comparative strength and ductility values of the unnotched tensile specimens of the present and previous heats [10] of initially annealed, commercially pure titanium*

Temperature	+100° C	+25° C	−78° C	−196° C
Ratio of true stress at a true strain of 0.02 for the present heat to that for the previous heat	1.12	1.22	1.27	1.30
Ratio of true stress at a true strain of 0.15 to that at 0.02 (Present heat)	1.32	1.39	1.27	1.26
Ratio of true stress at a true strain of 0.15 to that at 0.02 (Previous heat)	1.31	1.32	1.31	1.29
Ratio of true strain at initial fracture for the present heat to that for the previous heat	1.25	1.03	0.70	0.44
Ratio of true stress at a true strain of 0.02 at −196° to that at +25° C (Present heat)	1.90			
Ratio of true stress at a true strain of 0.02 at −196° to that at +25° C (Previous heat)	1.75			

The interstitial atoms also greatly affect the resistance of the metal to the continued movement of dislocations and thus affects its work hardening characteristics. Evidence of this effect is provided indirectly in table 4 by the ratios of the true stresses at true strains of 0.15 and 0.02, respectively, for these two heats of titanium.[9] These ratios, which may be considered as measures of the relative work hardening during this range of deformation, are nearly the same for both heats of the metal. However, as the 0.02 stress was greater for the heat with the higher interstitial contents, the increase in the resistance to flow during the deformation of these specimens was greater than that of specimens of the other heat of titanium. The slight increase exhibited in these ratios for both heats of titanium as the temperature was increased may also be interpreted as indirect evidence of slip along more prismatic planes, and including some pyramidal planes and possibly basal planes at the higher temperatures. This would be accompanied by an increase in the amount of cross slip and the number of intersections of dislocations, thereby increasing the work hardening of the metal.

The effect of the interstitials on the embrittlement of the titanium at low temperatures is indicated in table 4 by the ratios of the true strain at initial fracture of the specimens. The ductility at room temperature of specimens of both heats was about the same. However, the low temperature embrittlement of the titanium by the interstitials was very pronounced as shown by the large decrease in these ratios as the temperature was lowered to −78° and −196° C.

[9] The upper range of the strain for these ratios was limited to 0.15 in order to eliminate any effects that might be attributed to triaxiality accompanying the necking of the specimens.

4. Summary and Conclusions

A study was made of the behavior at low temperatures of unnotched and notched tensile specimens (60° notch angle, 0.05-in. root radius, 0.35-in. diameter at root of notch, and selected notch depths) and Charpy V-notch impact specimens of a heat of annealed commercially pure titanium.

The transition from ductile to brittle behavior in the Charpy impact tests occurred within the range of +125° to +80° C; only a small amount of notch toughness (3 to 4 ft-lb energy absorbed) was retained by the metal at −196° C.

The resistance to deformation of unnotched and notched tensile specimens increased continuously as the temperature was lowered within the range of +150° to −196° C. The strength of the titanium was also affected greatly by the stress system induced by a notch; strength indices, such as true stress at a true strain of 0.02 notch strength, and true stresses at maximum load and at initial fracture, increased greatly with increase in the induced triaxiality accompanying an increase in the notch depth.

The ability of the titanium to deform under uniaxial stress apparently was not affected greatly by lowering of temperature, as the true strain at maximum load in the tension tests on unnotched specimens increased only slightly as the temperature was lowered within the range of +150° to −196° C.

The ductility of the titanium under multiaxial stresses, however, was very dependent on temperature. The true strain at initial fracture of notched specimens of constant notch depth decreased continuously with lowering of temperature. Moreover, the ductility of notched specimens decreased very rapidly at all test temperatures with increase in notch depth to 10 percent, decreased less rapidly with increase in depth to 30 percent, changed very little with further increase in depth to 70 percent and then decreased slightly with increase in depth to 87 percent. The stress concentration factor increases very rapidly with increase in notch depth to about 10 percent, less rapidly with increase in depth from 10 to 30 percent, and then rather slowly with further increase in notch depth, whereas, the induced triaxiality is relatively small for the shallow-notched specimens but increases to a fairly large value for the deep notch specimens. Thus, it may be concluded that the decrease in tensile ductility of the notched specimens apparently depends mainly on the stress and strain gradients accompanying the stress concentration near the root of the notch, and only to a minor extent, except perhaps for very deep notches, on the induced triaxiality. This conclusion, however, should be considered as tentative, as the change in notch geometry in this study was limited to a variation of the notch depth of notches with constant notch angle, root radius, and minimum diameter at the root of the notch. Additional experimental data involving other variations in the geometry of the notch, such as notch angle and root radius, are needed to definitely establish the relative effect of the stress concentration factor and triaxiality on the ductility of the titanium.

The rates of work hardening of the titanium specimens under tension depended on the temperature and the stress system; the rate of work hardening increased with decrease in temperature and with increase in the triaxiality of the stress system.

A comparison of the tensile data obtained previously on another heat of annealed commercially pure titanium of low interstitial contents, with those obtained in the present investigation shows that the strength and work hardening increase and the ductility at temperatures below +25° C decreases with increase in the interstitial contents of titanium.

5. References

[1] F. D. Rosi, F. C. Perkins, and L. L. Seigle, Mechanism of plastic flow in titanium at low and high temperatures, Trans. Am. Inst. Mining Met. Engrs. **206,** 115 (1956).

[2] E. A. Anderson, D. C. Jillson, and S. R. Dunbar, Deformation mechanisms in alpha titanium, Trans. Am. Inst. Mining Met. Engrs. **197,** 1191 (1953).

[3] C. J. McHargue and J. P. Hammond, Deformation mechanisms in titanium at elevated temperatures, Acta Metallurgica **1,** 700 (1953).

[4] A. T. Churchman, The slip modes of titanium and the effects of purity on their occurrence during tensile deformation of single crystals, Proc. Royal Soc. (London) [A] **226,** 216 (1954).

[5] A. T. Churchman, The yield phenomena, kink bands and geometric softening in titanium crystals, Acta Metallurgica **3,** 22 (1955).

[6] J. W. Spretnak, M. G. Fontana, and H. E. Brooks, Notched and unnotched tensile and fatigue properties of ten engineering alloys at 25° C and −196° C, Trans. Am. Soc. Metals **43,** 547 (1951).

[7] S. M. Bishop, J. W. Spretnak, and M. G. Fontana, Mechanical properties, including fatigue of titanium base alloys RC130B and Ti75A at very low temperatures, Trans. Am. Soc. Metals **45,** 993 (1953).

[8] H. R. Ogden, F. C. Holden, and R. I. Jaffee, The effect of microstructure on the mechanical properties of titanium alloys—Properties of titanium alloys as affected by temperature and notches, Fifth Interim Report (Contract No. DA-33-019 ORD-1397) Battelle Memorial Institute to Watertown Arsenal (Jan. 3, 1955).

[9] F. R. Brotzen, E. L. Harmon, Jr., and A. R. Troiano, How notch sensitive are titanium alloys?, Iron Age **174,** 52 (Dec. 30, 1954).

[10] G. W. Geil and N. L. Carwile, Effect of low temperatures on the mechanical properties of a commercially pure titanium, J. Research NBS **54,** 91 (1955) RP2569.

[11] D. I. Walter, Determination of oxygen in titanium, Anal. Chem. **22,** 297 (1950).

[12] G. W. Geil and N. L. Carwile, A reduction of area gage for use at low temperatures, J. Research NBS **43,** 527 (1949) RP2044.

[13] G. W. Geil and N. L. Carwile, Tensile properties of ingot iron at low temperatures, J. Research NBS **45,** 129 (1950) RP2119.

[14] G. W. Geil and N. L. Carwile, Tensile properties of copper, nickel and some copper-nickel alloys at low temperatures, NBS Circular 520, 67 (1952).

[15] R. E. Peterson, Stress concentration design factors (John Wiley & Sons, Inc., New York, N. Y., 1953).

[16] G. Sachs and J. D. Lubahn, The effect of triaxiality on the technical cohesive strength of steels, Trans. ASME 67, A240 (1945).

[17] A. H. Cottrell, Dislocations and plastic flow in crystals (Oxford at the Clarendon Press, London, 1953).

[18] W. T. Read, Jr., Dislocations in crystals (McGraw-Hill Book Co., Inc., New York, N. Y., 1953).

[19] E. R. Parker and J. Washburn, Effect of impurities and imperfections on mechanical properties, Impurities and imperfections, Am. Soc. Metals (1955).
[20] W. L. Finley and J. A. Snyder, Effect of three interstitial solutes (nitrogen, oxygen and carbon) on the mechanical properties of high-purity alpha titanium, Trans, Am. Inst. Mining Met. Engrs. **188,** 277 (1950).
[21] R. I. Jaffee, H. R. Ogden, and D. J. Maykuth, Alloys of titanium with carbon, oxygen and nitrogen, Trans. Am. Inst. Mining Met. Engrs. **188,** 1261 (1950).
[22] G. A. Lenning, C. M. Craighead, and R. I. Jaffee, Constitution and mechanical properties of titanium-hydrogen alloys, Trans. Am. Inst. Mining Met. Engrs. **200,** 367 (1954).

Washington, February 4, 1957.

Journal of Research of the National Bureau of Standards Vol. 59, No. 3, September 1957 Research Paper 2791

Determination and Use of the Sag Point as a Reference Point in the Heating of Glasses

Sam Spinner, Given W. Cleek, and Edgar H. Hamilton

Glasses, when heated, undergo a gradual continuous change from solids to liquids over a rather wide temperature range. As a consequence, it has been found necessary to define certain temperature reference points in this transition range so that different glasses may be compared with each other. These points are chosen to correspond to established stages in the annealing or forming process. A new reference point, designated as the sag point, is described. The experimental determination of this point is rapid and simple. Also, it gives useful information concerning the annealing temperatures and ease of formation of glasses of widely varying compositions.

The sag point is defined as the temperature at which a glass fiber 0.5 to 0.8 millimeter in diameter, horizontally supported at ½-inch intervals, will sag under its own weight in 25 ±5 minutes.

1. General

One of the more widely accepted definitions of glass is that it is a material that has cooled from the liquid state without undergoing a change in phase [1].[1] Though glass may be regarded either as a supercooled liquid or an amorphous solid, the latter designation is more appropriate to stress the fact that ostensibly glass behaves like a solid, i. e., it retains its shape and reacts elastically to shear and tensile stresses. The process of transition from liquid to glass on cooling or from glass to liquid on heating is a continuous one. There is no sharply defined temperature, corresponding to the melting point of a crystal, at which it can be said that glass melts. Glass technologists have found it necessary, therefore, as a practical matter, to define certain reference points in the heating or cooling process so that reasonable comparisons can be made between glasses of different compositions, similar to the comparison of crystals by their melting points. Because the reference points for glass are not sharply defined, their selection is, in a sense, arbitrary. Their choice, however, is governed by established procedures in the annealing, forming, or other stages in the production process.

Glasses of different compositions have different temperature-viscosity relationships. Hence, glasses whose reference points might correspond in one temperature region, such as the annealing range, will, in all probability, not have corresponding points in another region such as the forming range. Considerations of this nature show why more than one reference point is necessary.

Littleton and Roberts [2] and Littleton [3] made the original contributions to the establishment of reference points by defining successively the annealing and softening points. Significant refinements and additions have been made by Lillie [4]. The American Society for Testing Materials [5] defines several such points now in use. These points are usually defined in terms of a specific phenomenon associated with a set of experimental operations, and also in terms of the viscosity of the glass at the temperature of this phenomenon. For instance, the deformation point is defined as "the temperature observed during the measurement of expansivity by the interferometer method at which viscous flow exactly counteracts thermal expansion. The deformation point generally corresponds to a viscosity in the range from 10^{11} to 10^{12} poises." The point defined by an operational procedure is preferable because the experimental procedure can usually be reproduced more accurately than the viscosity can either be calculated from the experimental conditions, or measured at the same temperature by some independent method. Furthermore, the viscosity frequently is not the only determining parameter. In the case of the softening point, for instance, the density of the glass must also be considered. The kinematic viscosity, then, would be the relevant factor. The situation is further complicated by the fact that at a lower temperature a considerable time may be required before the glass comes to the equilibrium viscosity for that temperature [6, 7]. This fact has led Lillie to regard the strain point, which occurs in such a low temperature region, to be of limited significance [4b]. It may also be mentioned, in this connection, that Adams, in his well-known paper on the annealing of glass [8], doubted whether the viscosity, which is designated as a megoscopic property, was really related to the release of stress, which involves only microscopic processes.

In the Bureau's Glass Section laboratory, it became necessary to devise a reference point that would serve as a reliable guide for annealing a large number of glasses of widely varying compositions. In order to be serviceable, it was also necessary for the determination of this point to be rapid and reproducible.

It seems desirable to summarize some of the requirements, which a good reference point should satisfy, as follows:

(1) The apparatus and procedure should be simple so that they may be easily duplicated by other laboratories. Methods that require elaborate specimen preparation, for instance, would be undesirable. In general, the fewer qualifying specifications that need be made, the better.

[1] Figures in brackets indicate the literature references at the end of this paper.

(2) The method should yield reproducible results. In order to fulfill this most important requirement, the effect sought for should vary sharply with temperature and, conversely, should be relatively insensitive to extraneous factors. If, for instance, the specimen measured is in the fiber form, the thickness of the fiber should not be critical.

(3) The determination should be rapid. This condition is especially important when the specimen is used as a control test for some portion of the manufacturing process.

(4) The value of such a point is obviously enhanced, if significant additional information is obtained.

A reference point satisfying these requirements was suggested by C. A. Faick, formerly of this Bureau, in 1948, and has been utilized successfully ever since. This point is hereinafter designated as the sag point. It is about 40° C higher than the deformation point, usually regarded as the upper limit of the annealing region. In the technique of determining the sag point, it was found that additional significant information could be gained as to the feasibility of making sizable melts of hitherto untried compositions. This will be discussed later.

It is the purpose of this paper to define the sag point, to describe the experimental equipment and procedure for its determination, and to show some typical results with glasses of different compositions. The sag points are compared with the deformation and softening points.

2. Experimental Technique

The technique about to be described for determining the sag point bears some similarity to that originated by Silverman [9] and refined by Grauer and Hamilton [10] for measuring the liquidus temperatures of glasses.

2.1. Equipment

The basic equipment consists of a temperature gradient furnace, shown in figure 1, and a platinum specimen holder, figure 2. The platinum holder is 6 in. long with supports for the fibers spaced approximately ½ in. apart.

The furnace is essentially the same as that described by Grauer and Hamilton [10] except that the heating coils are of Nichrome rather than platinum wire. Figure 3 shows a typical curve of the temperature distribution along the length of the furnace. The temperature range, as well as the gradient, can be altered considerably by proper adjustment of the power controls.

2.2. Procedure

A specimen is drawn in the form of a fiber, 0.5 to 0.8 mm in diameter. Suitable fibers can be prepared by drawing from the lip of the crucible in which the glass was melted. This is a convenient method of obtaining fibers directly from the melt, even in those cases where the glasses devitrify readily. The specimen is placed lengthwise on the holder (see fig. 2A) and the holder is inserted into the core of the furnace. After 25 min the holder is withdrawn. If the furnace has been properly adjusted, that section of the fiber that was in the hotter region will have sagged between the supports, whereas the section of fiber that remained in the cooler region will not have sagged. The temperature at the first compartment, measured from the open end of the furnace, in which the glass sagged between the supports (fig. 2B) is the temperature of the sag point.

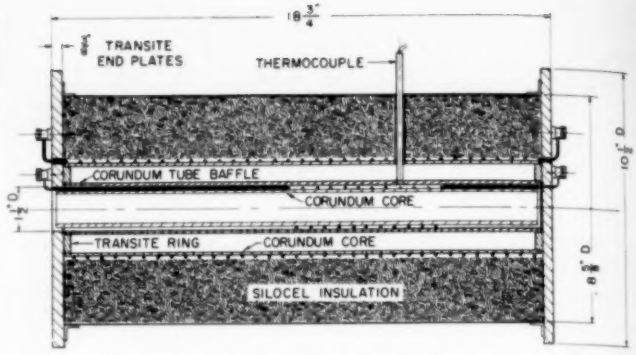

FIGURE 1. *Temperature gradient furnace.*

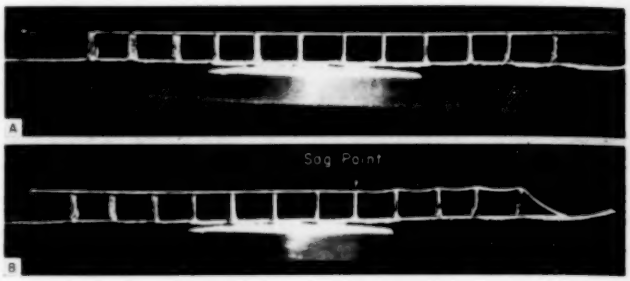

FIGURE 2. *Platinum holder with glass fiber specimen.*
A, Before insertion in furnace; B, after withdrawal from furnace.

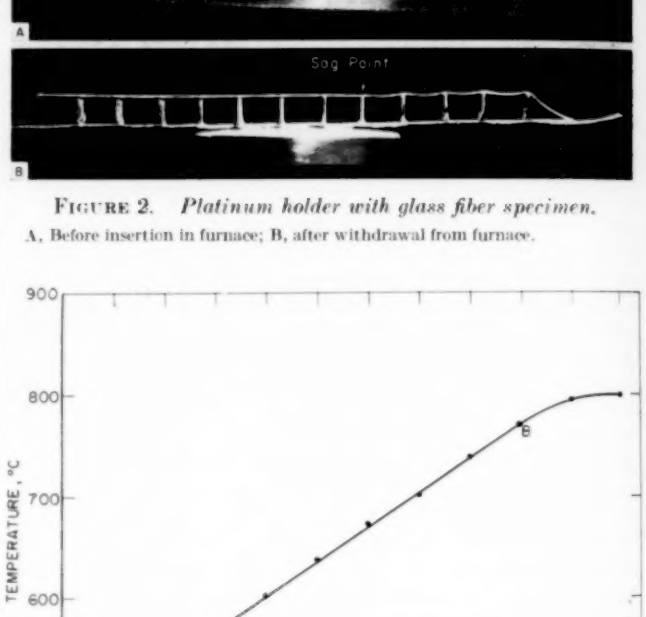

FIGURE 3. *Typical temperature distribution curve along length of gradient furnace.*

The furnace is properly adjusted when the sag point occurs in the linear gradient region of the temperature distribution curve, shown between points A and B in figure 3. A probe thermocouple is then inserted into the furnace up to this sag point distance and the temperature is measured.

2.3. Definition

Following the above procedure, the sag point is defined as the temperature at which a fiber, 0.5 to 0.8 mm in diameter, horizontally supported at ½-in. intervals, will sag under its own weight in 25 ±5 min.

2.4. Precision of Results

a. General Considerations

Under the conditions given in figure 3, repeated measurements with different specimens of the same glasses, but with the position of the holder varied slightly in the furnace, indicated a reproducibility of the order of ±7° C. This is the limiting precision for the determination of the sag point and follows from the condition that ½ in. of furnace length corresponds to a temperature change of about 15° C. Increased precision of results may be obtained by decreasing the over-all temperature gradient and hence the gradient per compartment. In this case, the following factors must be given greater consideration: Maintenance of a uniform distance between supports of the holder, the fiber diameter, and measurement of the temperature. It may also be noted here that it was not found necessary to reinsert the platinum holder in the furnace when measuring the temperature of the sag point with the probe thermocouple. Within the experimental precision of the measurement, no difference was observed whether the holder was in or out of the furnace. The apparatus and method described here were found to give the speed, convenience, and precision sufficient for the purpose of the determination.

b. Effect of Fiber Diameter

As might be expected, the temperature of the sag point was found to increase somewhat with increased fiber diameter. Within the precision used here, no significant variation was found within the given fiber diameter tolerance. The following table for one glass, BSC 517, shows typical data relating fiber diameter to sag point.

Diameter	Sag point
mm	° *C*
0.50 to 0.84	650
.52 to .69	650
.50 to .60	657
.55 to .70	657
.62 to .76	650

It may also be noted that the diameter for any single fiber may vary over the specified range without affecting the reproducibility of the result.

c. Effect of Time

The sag point was found to be relatively insensitive to time in the furnace within rather broad limits. Although longer times may be used safely, less than 20 min may not give reproducible results. The time is not critical within the specified 25 ±5 min. One of the conveniences of the method consists in the fact that it is not necessary for the operator to observe the specimen during the time of test, as is usually the case with other reference point determinations [11].

3. Use of Sag Point in Problems Pertaining to Glass Formation

As was mentioned earlier, significant information could be obtained in the process of determining the sag point as to the feasibility of cooling sizable melts of new compositions to form glasses. In considering the problem of the glass-forming possibilities of a melt of a new composition, one is interested not only in whether the melt will cool as a glass, but whether glass will form in sufficiently large quantity so that sizable articles can be fabricated from it. Once the glass has formed, one is further concerned if such articles can be annealed without danger of devitrifying. It is necessary to recall that the liquidus temperature is the temperature above which crystals cannot form. The temperature of maximum rate of crystal growth is usually 50 to 100° C below the liquidus temperature [10]. This region of maximum crystal growth is of the greatest concern in the practical problem of cooling a melt to glass. As the temperature is decreased below this region, the rate of crystal growth decreases rapidly because the increased viscosity associated with lower temperatures counteracts the tendency toward crystal growth. For practical purposes, this rate becomes zero at sufficiently low temperatures. Many compositions that will form glasses in small quantities, or when the melt is poured on a cold plate, will devitrify to a considerable extent when an attempt is made to make these same compositions in large quantities for melts of about 500 g or more, because the center of the cooling piece must remain at temperatures in this region of maximum crystal growth for considerable periods of time. Thus, when specifying whether a particular composition will form a glass, the experimental conditions under which glass formation occurs must be specified [12].

In the technique of determining the sag point, a portion of the specimen is usually held in the temperature region where crystal growth may occur. The presence of crystals on withdrawal from the furnace, and their relation to the sag point, gives an indication of the tendency of the particular glass to devitrify in this critical region. As a consequence, the feasibility of cooling large melts of a given composition as glass can be predicted.

The one extreme would be a specimen that emerges without the sag point having developed, and yet shows the presence of crystals along the section that

was in the hotter region of the furnace. Such a composition would present the least favorable condition for glass formation. The opposite, and most favorable condition for glass formation, would be a specimen that emerges with a well-defined sag point and shows no evidence of crystallization anywhere along the fiber.

The fact that crystals do not form in the temperature region above the sag point does not necessarily indicate that the temperature of maximum crystallization is higher than the hottest portion of the specimen. It may indicate that the rate of crystallization is so slow that crystals do not form in the time that the fiber was in the furnace. This shows that the melt can be held for considerable time in this dangerous region with little fear of devitrification.

In general, the difficulty of glass formation increases as crystals appear closer to the sag point. If crystals form on the cold side of the sag point, it indicates that even if glasses are formed, the problem of crystallization during the process of annealing would still remain.

If a glass crystallizes in the annealing temperature range, the difficulties involved are not necessarily insurmountable. Fused silica, for instance, crystallizes in the annealing region, the crystal growth being initiated at the surface. It would appear, however, that if the criterion suggested by this procedure, and by what has been said before, is adopted, then fused silica is far from being the ideal glass it is frequently described to be. If a glass is regarded as the opposite of a crystal, then those glasses that devitrify least readily come closest to being "ideal" from a theoretical as well as a practical point of view. Thus, glasses that contain "network modifiers" and "intermediates" in addition to the so-called basic silica network, but which crystallize fairly slowly in the region of maximum crystal growth, come closer to being "ideal" than does pure silica. On the other hand, pure B_2O_3 can be crystallized only with the greatest difficulty and is more nearly an ideal glass in spite of certain (usually) undesirable properties (i. e., high hygroscopicity, low melting point, high coefficient of expansion).

4. Results

Table 1 lists several optical glasses [2] comparing the temperatures of the deformation point, sag point, and softening point. The fiber diameter chosen for the sag point determination (0.50 to 0.80 mm) is practically the same as that used for the softening point (0.55 to 0.75 mm) [14] so that no correction for this dimension is necessary in comparing these two points. The last two columns give successively the difference between the softening point and deformation point, and the difference between the sag point and the deformation point. For the various glasses, these reference points vary, the differences between them vary, and the sag points lie between the deformation and the softening points. This is an example of the fact, mentioned earlier, that the temperature-viscosity relations of glasses of different compositions can vary widely, and consequently of the necessity for using several points to specify more fully the change in properties of different glasses as they are heated. The particular reference point chosen is governed by its ease of determination and proximity to the temperature range of the particular process involved.

[2] The compositions as well as the meaning of the symbols designating these glasses may be found in reference [13].

TABLE 1. *Temperatures of reference points of several optical glasses*

Glass type [a]	Temperature of—			$b-a$	$c-a$
	Deformation point [b] (a)	Sag point (b)	Softening point [b, c] (c)		
	°C	°C	°C		
BSC 511	580	655	701	75	121
BSC 517	604	653	729	49	125
LC 523	590	629	702	39	112
BaC 541	640	650	737	10	97
BaC 5725	664	697	753	33	89
BaC 574	670	718	752	48	82
BaC 617	692	731	785	39	93
CF 529	495	546	641	51	146
F 620	477	515	592	38	115

[a] Compositions are given in [13], Leo Shartsis and Sam Spinner, Viscosity and density of molten optical glasses, J. Research NBS **46**, 176–194 (1951) RP2190.
[b] ASTM Standards, Standard definitions of terms relating to glass and glass products, C162–52 (1955).
[c] ASTM Standards, Tentative method of test for softening point of glass, C338–54T (1955).

The sag point is not offered to replace either the deformation or the softening point. The deformation point is obtained from the determination of the thermal expansion by the interferometric method and is part of the data that are essential to establishing the correct temperature to use for the fine annealing of optical glasses. The sag point is determined in a matter of minutes as compared with a day or more for the deformation point, and can be used to establish a maximum temperature for the comparable annealing of experimental glasses. The temperature of the sag point is nearer to the annealing range than is the softening point and hence devitrification troubles encountered in the latter determination are avoided.

5. Summary

(1) A new reference point, the sag point, in the heating (or cooling) of glasses has been defined and the method for experimentally determining this point described. The determination is rapid and simple.

(2) The sag point has proved itself to be of considerable value in determining the maximum annealing temperature of new glasses of widely varying compositions.

(3) A method is also shown for obtaining additional information concerning the devitrification tendencies of experimental melts and the feasibility of cooling them as homogeneous glasses.

(4) Data have been presented in which the sag point is compared to previously defined reference points in the heating of glasses.

6. References

[1] George W. Morey, Properties of glass, Reinhold Publishing Corp., 330 West 42d St., New York 18, N. Y., 2d ed., 24–28 (1954).

[2] J. T. Littleton and E. H. Roberts, A method for determining the annealing temperature of glass, J. Opt. Soc. Amer. **4,** 224–29 (1920).

[3] (a) J. T. Littleton, A method for measuring the softening temperature of glasses, J. Am. Ceram. Soc. **10,** 259–63 (1927); (b) J. T. Littleton, The softening point of glass, J. Soc. Glass Technol. **24,** 176 (1940).

[4] (a) H. R. Lillie, Viscosity of glass between the strain point and melting temperature, J. Am. Ceram. Soc. **14,** 502–11 (1931); (b) H. R. Lillie, A method for measuring the flow point of glass, J. Am. Ceram. Soc. **35,** 149–55 (1952); (c) H. R. Lillie, Re-evaluation of glass viscosities at annealing and strain points, J. Am. Ceram. Soc. **37,** 111–17 (1954).

[5] Am. Soc. Testing Materials, Standards, Standard definitions of terms relating to glass and glass products, C 162–52 (1955).

[6] V. H. Stott, E. Irvine, and D. Turner, Viscosity measurements with glass, Proc. Roy. Soc. London [A] **108,** 154 (1925).

[7] H. R. Lillie, Viscosity-time-temperature relations in glass at annealing temperatures, J. Am. Ceram. Soc. **16,** 619 (1933).

[8] L. H. Adams, The annealing of glass as a physical problem, J. Franklin Inst. **216,** 39–71 (July 1933).

[9] W. B. Silverman, Effect of alumina on devitrification of soda-lime-silica glasses, J. Am. Ceram. Soc. **22,** 378 (1939).

[10] O. H. Grauer and E. H. Hamilton, An improved apparatus for the determination of liquidus temperatures and rates of crystal growth in glasses, J. Research NBS **44,** 495–502 (1950) RP2096.

[11] L. K. Kowalew and R. L. Shuster, Determination of the softening temperature of glass, Vestnik Akad. Nauk Kazakh. S. S. R. **1,** 81–5 (1953); Glastech. Ber. **28,** 313 (1955).

[12] Given W. Cleek and Edgar H. Hamilton, Properties of barium titanium silicate glasses, J. Research NBS **37,** 317–323 (1956) RP2720.

[13] Leo Shartsis and Sam Spinner, Viscosity and density of molten optical glasses, J. Research NBS **46,** 176–194 (1951) RP2190.

[14] Am. Soc. Testing Materials, Standards, Tentative method of test for softening point of glass, C 338–54T (1955).

WASHINGTON, February 15, 1957.

THE NATIONAL BUREAU OF STANDARDS

The scope of activities of the National Bureau of Standards at its headquarters in Washington, D. C., and its major field laboratories in Boulder, Colorado, is suggested in the following listing of the divisions and sections engaged in technical work. In general, each section carries out specialized research, development, and engineering in the field indicated by its title. A brief description of the activities, and of the resultant publications, appears on the inside of the front cover.

WASHINGTON, D. C.

Electricity and Electronics. Resistance and Reactance. Electron Devices. Electrical Instruments. Magnetic Measurements. Dielectrics. Engineering Electronics. Electronic Instrumentation. Electrochemistry.

Optics and Metrology. Photometry and Colorimetry. Optical Instruments. Photographic Technology. Length. Engineering Metrology.

Heat. Temperature Physics. Thermodynamics. Cryogenic Physics. Rheology. Engine Fuels. Free Radicals Research.

Atomic and Radiation Physics. Spectroscopy. Radiometry. Mass Spectrometry. Solid State Physics. Electron Physics. Atomic Physics. Neutron Physics. Nuclear Physics. Radioactivity. X-rays. Betatron. Nucleonic Instrumentation. Radiological Equipment. AEC Radiation Instruments.

Chemistry. Organic Coatings. Surface Chemistry. Organic Chemistry. Analytical Chemistry. Inorganic Chemistry. Electrodeposition. Molecular Structure and Properties of Gases. Physical Chemistry. Thermochemistry. Spectrochemistry. Pure Substances.

Mechanics. Sound. Mechanical Instruments. Fluid Mechanics. Engineering Mechanics. Mass and Scale. Capacity, Density, and Fluid Meters. Combustion Controls.

Organic and Fibrous Materials. Rubber. Textiles. Paper. Leather. Testing and Specifications. Polymer Structure. Plastics. Dental Research.

Metallurgy. Thermal Metallurgy. Chemical Metallurgy. Mechanical Metallurgy. Corrosion. Metal Physics.

Mineral Products. Engineering Ceramics. Glass. Refractories. Enameled Metals. Concreting Materials. Constitution and Microstructure.

Building Technology. Structural Engineering. Fire Protection. Air Conditioning, Heating, and Refrigeration. Floor, Roof, and Wall Coverings. Codes and Specifications. Heat Transfer.

Applied Mathematics. Numerical Analysis. Computation. Statistical Engineering. Mathematical Physics.

Data Processing Systems. SEAC Engineering Group. Components and Techniques. Digital Circuitry. Digital Systems. Analog Systems. Application Engineering.

• Office of Basic Instrumentation.

• Office of Weights and Measures.

BOULDER, COLORADO

Cryogenic Engineering. Cryogenic Equipment. Cryogenic Processes. Properties of Materials. Gas Liquefaction.

Radio Propagation Physics. Upper Atmosphere Research. Ionospheric Research. Regular Propagation Services. Sun-Earth Relationships.

Radio Propagation Engineering. Data Reduction Instrumentation. Modulation Systems. Navigation Systems. Radio Noise. Tropospheric Measurements. Tropospheric Analysis. Radio Systems Application Engineering.

Radio Standards. High Frequency Electrical Standards. Radio Broadcast Service. High Frequency Impedance Standards. Calibration Center. Microwave Physics. Microwave Circuit Standards.

Recent Publications of the National Bureau of Standards

Journal of Research of the National Bureau of Standards, Volume 59, No. 1, July 1957 (RP2768 to RP2772 incl.). 60 cents. Annual subscription $4.00.

Technical News Bulletin, Volume 41, No. 7, July 1957. 10 cents. Annual subscription $1.00.

Basic Radio Propagation Predictions for October 1957. Three months in advance. CRPL–D 155. Issued July 1957. 10 cents. Annual subscription $1.00.

Applied Mathematics Series

AMS48. Fractional factorial experiment designs for factors at two levels. 50 cents.

Building Materials and Structures Report

BMS150. Methods of testing small fire extinguishers. 15 cents.

Circulars

C579. Underground corrosion. (Buckram bound) $3.00.

Available from the Superintendent of Documents, U. S. Government Printing Office, Washington 25, D. C. (foreign postage, 25% additional).

UNITED STATES
GOVERNMENT PRINTING OFFICE
DIVISION OF PUBLIC DOCUMENTS
WASHINGTON 25, D. C.

OFFICIAL BUSINESS

PENALTY FOR PRIVATE USE TO AVOID PAYMENT OF POSTAGE, $300 (GPO)

Journal of Research of the National Bureau of Standards Vol. 59, No. 3 September 1957

Contents

	Page
A computation of cyclic cubic units. Harvey Cohn and Saul Gorn. RP2783	155
Estimation of the frequencies of thin elastic plates with free edges. Tosio Kato, Hiroshi Fujita, Yoshimoto Nakata, and Morris Newman. RP2784	169
A thermochemical study of the reaction of calcium hydroxide, silica gel, and water. Edwin S. Newman. RP2785	187
On some expansions for Bessel integral functions. F. Oberhettinger. RP2786	197
Table of the first moment of ranked extremes. Julius Lieblein and Herbert E. Salzer. RP2787	203
An approximate expression for gamma-ray degradation spectra. U. Fano and Ann T. Nelms. RP2788	207
Some infrared bands of deuterium sulfide. Harry C. Allen, Jr., Earle K. Plyler, and L. R. Blaine. RP2789	211
Some effects of low temperatures and notch depth on the mechanical behavior of an annealed commercially pure titanium. Glenn W. Geil and Nesbit L. Carwile. RP2790	215
Determination and use of the sag point as a reference point in the heating of glasses. Sam Spinner, Given W. Cleek, and Edgar H. Hamilton. RP2791	227

[A list of recent NBS publications is given on page 3 of the cover.]

For sale by the Superintendent of Documents, U. S. Government Printing Office, Washington 25, D. C. Price 60 cents (single copy). Subscription price: $4.00 a year; $1.25 additional for foreign mailing.

UNITED STATES GOVERNMENT PRINTING OFFICE, WASHINGTON : 1957